UAS-BASED HIGH-THROUGHPUT PHENOTYPING FOR ESTIMATING ALFALFA (*Medicago sativa* L.) YIELD, PLANT HEIGHT, AND FORAGE QUALITY

by

RENELIZA D. CEJALVO

(Under the Direction of Ali Mekki Missaoui)

ABSTRACT

Breeding alfalfa (*Medicago sativa* L.) presents challenges due to its perennial characteristics. Its biomass yield needs to be characterized several times annually. However, conventional techniques in characterizing plants are a bottleneck in plant breeding. This study explores the potential of UAS-based sensors for phenotyping to estimate alfalfa biomass, plant height, and forage quality. Plant height is considered a surrogate for biomass yield. We correlated ground-based measurements with UAS-based spectral and structural data from RGB, multispectral, and LiDAR sensors. Integrating RGB, multispectral, and plant height data yielded more accurate biomass predictions. Machine learning models showed that combining RGB and LiDAR data improved plant height predictions. For forage quality, vegetation indices from the dual multispectral sensor showed strong correlations with ADF and NDF, while single bands from the sensor are highly correlated with CP. These findings highlight the potential of UAS-based HTP for efficiently and accurately characterizing alfalfa traits.

INDEX WORDS: Remote sensing, Vegetation indices, LiDAR, Multispectral, RGB, Structure from Motion, Machine learning

UAS-BASED HIGH-THROUGHPUT PHENOTYPING FOR ESTIMATING ALFALFA (*Medicago sativa* L.) YIELD, PLANT HEIGHT, AND FORAGE QUALITY

by

RENELIZA D. CEJALVO

BS, University of the Philippines Los Baños, 2017

A Thesis Submitted to the Graduate Faculty of The University of Georgia in Partial Fulfillment of the Requirements for the Degree

MASTER OF SCIENCE

ATHENS, GEORGIA

2025

UAS-BASED HIGH-THROUGHPUT PHENOTYPING FOR ESTIMATING

ALFALFA (*Medicago sativa* L.) YIELD, PLANT HEIGHT, AND FORAGE QUALITY

by

RENELIZA D. CEJALVO

Major Professor:	Ali Mekki Missaoui
Committee:	Leonardo Bastos
	Sergio Bernardes
	Francesco Marinello

Electronic Version Approved:

Ron Walcott
Vice Provost for Graduate Education and Dean of the Graduate School
The University of Georgia
December 2025

DEDICATION

To our little one, growing quietly within me, your presence has been my light, a silent rhythm of hope and strength, beating beneath each step of this journey.

To my dearest Shawn, my confidant, my constant, thank you for your patience, your sacrifices, and the steady love that held me through every long night and uncertain day.

This chapter closes with gratitude, and the next begins with you both.

ACKNOWLEDGEMENTS

I would like to express my heartfelt gratitude to my advisor, Dr. Ali Missaoui, for his invaluable guidance, unwavering support, and enduring patience throughout my research journey. I am also deeply grateful to my committee members, Dr. Leonardo Bastos, Dr. Sergio Bernardes, and Dr. Francesco Marinello, for their time, insightful feedback, and expertise.

I gratefully acknowledge the support and encouragement provided by Dr. Miguel Cabrera, Dr. Nicola Dal Ferro, Dr. Francesco Morari, and Dr. George Vellidis during my dual degree program between the University of Padua and the University of Georgia.

My sincere thanks go to my colleagues and lab members in the Forage Breeding Lab — Shiva, Jazib, Holly, Chloe, Kim, Andy, Anita, Razi, Angel, Kendall, Jonathan, and Min — for their camaraderie and assistance. The memories we created in the field and the lab will always hold a special place in my heart.

Finally, I would like to thank the small but close-knit community of Pinoy graduate students at UGA, as well as the friends I've met along the way, for making my time in Athens feel like home. Your friendship and support meant so much to me, and I am truly grateful for the experiences we shared.

TABLE OF CONTENTS

Page

LIST OF TABLES

Page

LIST OF FIGURES

Page

CHAPTER 1

INTRODUCTION AND LITERATURE REVIEW

Alfalfa (*Medicago sativa* L.) is a perennial forage crop belonging to the Fabaceae Family. It is native to the Mediterranean, Western Siberia, and Iran, primarily thriving in temperate regions (POWO,2023). Alfalfa, also called Lucerne, is a preferred feed for livestock due to its high protein content and easily digestible fiber (Samac et al., 2006; Ruckle et al., 2017; Hojilla-Evangelista et al., 2016). Alfalfa enhances soil health by enhancing nitrogen (Creech et al., 2019) and sequestering large amounts of carbon in the soil (Cates et al., 2016).

Alfalfa plays a role in sustainable agriculture and livestock production (Wang and Brummer, 2012; Kingston-Smith et al., 2013). In 2024, alfalfa ranked fourth among the most economically valuable field crops in the United States, behind corn, soybean, and wheat (USDA, 2025). The national estimated value of alfalfa hay and haylage in the United States was approximately $9.5 billion. The country's average alfalfa yield was 8,450 kilograms per hectare. With the increasing global demand for animal products, optimizing the production, quality, and management of perennial forage crops becomes increasingly vital (Capstaff and Miller, 2018).

Breeding alfalfa presents challenges due to its perennial characteristics. Furthermore, it has a longer life cycle than annual crops, making breeding programs more complex. With multiple harvests per year, their biomass yield and other phenotypic and physiological features must be characterized and evaluated several times annually (Surault et al., 2021). With the large number

of experimental plots in plant breeding programs, the measurement of traits in alfalfa, such as biomass, plant height, and forage quality, is time-consuming and labor-intensive.

Plant phenotyping is a crucial component of plant breeding programs, providing insights into genotypic expression, the influence of the environment, and the interplay between genotype and environment (Fasuola, 2020). However, the use of conventional phenotyping, involving manual techniques for measuring and observing plant morphological and physiological traits, is considered a bottleneck in developing novel and improved crop varieties (Chawade et al., 2019; Ninomiya, 2022). The conventional method of characterizing plants is impractical for large-scale data analysis and experiments since the process is laborious and time-consuming, and the results are subject to human bias (Qiu et al., 2018). To alleviate this bottleneck in plant breeding, research on high-throughput phenotyping (HTP) intensified in the last decade (Costa et al., 2019).

HTP uses automated, non-destructive technologies to collect large amounts of phenotypic data from plants rapidly and accurately. Advances in HTP were assisted by the improvements of unmanned aerial systems (UAS) and developments in sensors such as red-green-blue (RGB), hyperspectral, multispectral, thermal, and light detection and ranging (LiDAR) systems (Zhao et al., 2019; Guo et al., 2021). UAS-based HTP has become a critical tool for accurate phenotypic assessment and selection of a large number of populations and rapid advancement of genetic gain in breeding programs (Fu, 2015).

Increasing and optimizing the biomass yield is the primary objective of most breeding programs. Early estimation of biomass is beneficial for the management and utilization of forage crops (Singh et al., 2023). For alfalfa, biomass yield is quantified through its dry weight. RGB, multispectral, and LiDAR sensors have been employed to assess and enhance crop yield. Using

UAS-mounted RGB and multispectral sensors, researchers have successfully measured and predicted the yield of major crops like corn (*Zea mays* L.) (Barzin et al., 2020), rice (*Oryza sativa* L.) (Duan et al., 2019), and sugarcane (*Saccharum officinarum* L.) (Khuimphukhieo et al., 2023). Using UAS-based hyperspectral imagery and machine learning methods, Wang et al. (2021) developed a method to estimate the yield of rice (Oryza sativa subsp. japonica).

Plant height is an important yield component of most crops, as taller plants generally have higher dry matter yield. Manually, plant height is measured using a ruler or a meter stick from the soil surface to the tip of the stem (Michel, 2021). Many studies include plant height as a factor in developing a machine learning model for predicting yield (Tao et al., 2020; Ji et al., 2022). Moreover, UAS-based studies aiming to assess and predict yield incorporate plant height and dry matter yield as key factors (Li et al., 2020). Khuimphukhieo et al. (2023) investigated the direct and indirect effects of canopy features on cane yield of sugarcane (*Saccharum officinarum* L.), and their RGB imagery shows that canopy height and NDVI has the strongest correlation on tons of cane per hectare.

Breeding targets for forage crops also include forage nutritive quality such as neutral detergent Fiber (NDF), acid detergent fiber (ADF), and crude protein (CP), as they determine forage digestibility, energy availability, intake quantity, and protein content, which are essential for animal growth. Forage quality is extensively studied using near-infrared spectroscopy (Rushing et al., 2016; Pittman et al., 2016). Even using near-infrared spectroscopy, the process is still destructive and resource-consuming. Plant samples would have to be harvested in the field, then dried and ground before being analyzed using the machine.

Despite the advancements in UAS-based HTP, research examining and optimizing HTP methods for yield, plant height, and forage quality remains limited for alfalfa. Hence, this study will explore and evaluate the potential of UAS for conducting HTP methods in alfalfa using RGB, multispectral, and LiDAR sensors.

Objectives

This study aims to evaluate the use of UAS-based HTP for measuring aboveground biomass (AGB), plant height, and forage quality of alfalfa. The specific objectives are as follows:

1. Determine the AGB, plant height, and forage quality of various varieties of alfalfa using ground-based or laboratory-based measurements.

2. Utilize UAS-based remote sensors such as red, green, and blue (RGB), multispectral (XS), and light detection and ranging (LiDAR) data to calculate vegetation indices and obtain structural or point cloud data, which will be compared with AGB, plant height, and forage quality parameters.

3. Investigate the relationships between the UAS-based remote sensing data and field data, and identify the key wavelengths and metrics that are strongly associated with each parameter.

4. Develop and evaluate predictive models for estimating AGB, plant height, and forage quality in alfalfa.

Sensors Used in UAS-based HTP

High-Throughput Phenotyping (HTP) provides non-destructive and rapid measurements of various plant traits. Remote sensing technologies use active sensors like LiDAR, and passive sensors such as RGB, multispectral, hyperspectral cameras, and thermal cameras to capture data

of large plant populations. In contrast, proximal sensors are used for small-scale phenotyping and placed within two meters of the target object, thus providing finer spatial resolutions (Viscarra Rossel et al., 2011). The captured data can then be processed and analyzed using various computer software, including Agisoft Metashape (Agisoft LLCC, St. Petersburg, Russia), Global Mapper (Blue Marble Geographics, Hallowell, ME, USA), Pix4Dmapper (Pix4D, Prilly, Switzerland) for generating orthomosaics, as well as R and RStudio (RStudio, PBC, Boston, MA, USA), and ArcGIS Pro (Esri, Redlands, CA, USA) for extracting vegetation indices that can be correlated with field data.

Applications of RGB Sensors in HTP

Red-green-blue (RGB) sensors capture red, green, and blue channels of light to produce two-dimensional (2D) images. RGB imaging has been widely used to quantify various plant traits, such as yield, plant height, leaf area, and canopy cover (Niu et al., 2019; Lu et al., 2021). Singh et al. (2023) utilized a structure from motion (SfM) technique on a UAS-based RGB data and an Unmanned Ground Vehicle (UGV) equipped with an ultrasound sensor to estimate dry biomass yield (DBY) from crop height (CH) for the tall fescue forage crop in a two-acre paddock. While their results indicated a lower correlation of UAS-based CH with DBY (r-squared = 0.47) compared to UGV-based CH with DBY (r-squared = 0.66), they concluded that UAS-based results are more accurate due to lower Root Mean Square Error (RMSE) and standard deviation. Additionally, they suggested that increasing the number of data points in the UGV-based method could lead to higher accuracy in CH estimation and, consequently, DBY prediction. Similarly, Volpato et al. (2021) used SfM techniques and utilized point clouds to generate crop surface models to estimate the plant height of wheat (*Triticum* sp.). Their results presented high Spearman rank correlations (0.47-0.91) and R2 (0.63-0.95) of adjusted and predicted UAS-based RGB

imagery measurements against field data measurements of wheat. In alfalfa, Surault et al. (2021) used RGB cameras to measure crop height, suggesting a high correlation between UAS-based crop height and dry matter.

De Swaef et al. (2021) employed a UAS mounted with RGB and thermal sensors, deriving 35 indices from the RGB camera and two indices from the thermal sensor. Correlating these indices with breeder scores for drought evaluation in three common forage types (*Festuca arundinacea,* diploid *Lolium perenne,* and tetraploid *Lolium perenne*), they identified H (Hue), NDLab (Normalized Difference CIELab Index), and VARI (Visible Atmospherically Resistant Index) with r values of 0.84, 0.82, and 0.79, respectively, as proxies for breeder scores. Visual-based indices were deemed more useful as complementary to breeder scores than thermal-based indices. Their study also highlighted the superior drought tolerance of *F. arundinacea* compared to *L. perenne.*

RGB imaging has been successfully applied to estimate crop emergence rates, with a study on potato (*Solanum tuberosum* L.) reporting a high coefficient of correlation (0.96) with ground-truth data (Li et al., 2019). Additionally, research has shown that canopy cover, canopy volume, and excessive greenness index (ExG) derived from RGB images can accurately predict tomato (*Solanum lycopersicon* L.) yields at the field level (Chang et al., 2021).

Applications of Multispectral Sensors in HTP

Multispectral sensors capture light in several bands of the electromagnetic spectrum, typically fewer than ten bands. Calculated vegetation indices (VIs) from multispectral cameras have been utilized to monitor coffee (*Coffea* sp.) vigor, crop status, and phenology (Manzano et al., 2020) and to predict corn (*Zea mays* L.) yields (Barzin et al., 2020). Multispectral imaging has been employed in high-throughput phenotyping (HTP) to detect plant stress caused by nutrient

deficiencies, water deficits, pests, pathogens, and insects (Thorp et al., 2018; Xia et al., 2022). In addition, Patrick et al. (2017) used VIs to screen peanut genotypes for resistance to tomato spotted wilt virus, demonstrating that image-based phenotyping can rank genotype resistance as early as 93 days after sowing.

Multispectral imagery has also been used to select alfalfa with optimal herbage accumulation (HA). Cazenave et al. (2019) utilized multispectral sensors to create a UAS-based Normalized Difference Vegetation Index (NDVI) for alfalfa. The ground coverage data of alfalfa germplasm revealed significant correlations, ranging from 0.88 to 0.91, between the model-based dry weight values and manually harvested dry weight across all four harvests. Biswas et al. (2021) assessed the effectiveness of UAS-based multispectral imagery and spatial analysis for selecting alfalfa with optimal HA, revealing Pearson correlations exceeding 0.71 between HA and various vegetation indices (NDVI, Green Normalized Difference Vegetation Index (GNDVI), Normalized Difference Red Edge (NDRE), and Green-Red Vegetation Index (GRVI)). across four harvesting periods. Tang et al. (2023) utilized UAS-based multispectral images to develop a fully automated segmentation pipeline for extracting features from alfalfa plots. Their regression model, including canopy area, plant height, NDRE, and NGRDI (Normalized Green–Red Difference Index), demonstrated an accuracy range of 0.5–0.7 (R2) in predicting plot biomass. Sapkota et al. (2023) used UAS-mounted multispectral and thermal sensors to calculate eight vegetation indices and a crop water stress index for fall-harvested alfalfa. Contrary to expectations, their findings indicated that incorporating inputs related to canopy temperature did not enhance the predictive power of the yield models.

Applications of Hyperspectral Sensors in HTP

Hyperspectral sensors capture light in many narrow spectral bands, providing higher spectral resolution than multispectral sensors. In HTP, hyperspectral imaging has been used to detect plant stress caused by diseases, pests, and abiotic stresses (de Castro et al., 2015; Genangeli et al., 2023). Using UAS-based hyperspectral imagery and machine learning methods, Wang et al. (2021) developed a method to estimate the yield of rice (*Oryza sativa* subsp. *japonica)* while Fan et al. (2022) established a formula to estimate the yield and flowering time in maize.

Pittman et al. (2016) concluded that the prediction of Crude Protein (CP) using hyperspectral data is accurate enough for reporting forage CP in bermudagrass, with seasonally dependent accuracy for tall fescue and wheat. The predicted CP from hyperspectral data regressed with those measured by near-infrared spectroscopy (NIRS) in a laboratory produced $R2 = 0.80$.

Applications of LiDAR Sensors in HTP

Light Detection and Ranging (LiDAR) is an active sensor that uses laser pulses to collect data, which is then used to create high-resolution 3D models of objects and surfaces. In the context of plant phenotyping, LiDAR sensors can accurately measure various plant traits, including plant height, canopy cover, plant biomass, leaf area index (LAI), and canopy volume. Li et al. (2020) demonstrated the potential of LiDAR technology in plant phenotyping by using UAS-based LiDAR and multispectral sensors to measure plant height, perimeter, and biomass yield in field-grown switchgrass (Panicum virgatum L.). Their results showed that UAS-based plant height and perimeter measurements were highly correlated and consistent with manual measurements ($r = 0.93$, $p < 0.001$). This study highlighted the accuracy and efficiency of LiDAR technology in estimating bioenergy traits and its potential applications in plant breeding and crop monitoring.

Schaefer and Lamb (2016) utilized a ground-based LiDAR sensor and an active optical sensor to measure pasture height and NDVI of tall fescue, respectively. The combination of NDVI and height measurements was observed to be more accurate in assessing total biomass than using only NDVI (RMSEP ≈ 846.51 kg/ha) or height (RMSEP ≈ 708.13 kg/ha) individually. NDVI (R^2 = 0.56) and LiDAR canopy height (R^2 = 0.61) showed a low correlation with ground-measured Green Dry Matter (GDM), but the correlation increased to R^2 = 0.76 when LiDAR canopy height and NDVI were combined.

Ground-based LiDAR sensors have also been used to measure alfalfa traits, such as canopy height. Sheffield et al. (2021) employed a ground-based LiDAR sensor to measure the canopy height of alfalfa. By utilizing the 95th percentile of the LiDAR-measured canopy height, they attained an R^2 of 0.90 and an RMSE of 4.5 cm.

UAS-based studies have demonstrated significant potential for measuring alfalfa traits, including yield, height, and biomass. Given its high nutritional and economic value, considerable research efforts focus on enhancing alfalfa yield. However, despite the growing body of research on UAS-based High-Throughput Phenotyping (HTP) in alfalfa, a knowledge gap remains in exploring alfalfa traits using HTP.

CHAPTER 2

MATERIALS AND METHODS

Study Site

The experimental plots for forage breeding of alfalfa were established at the West Unit of the J. Phil Campbell Sr. Research and Education Center, located in Watkinsville, Georgia, at coordinates 33° 52' N and 83° 26' W. The predominant soil type on the farm is Cecil sandy loam (Soil Survey Staff, Natural Resources Conservation Service, and United States Department of Agriculture). The alfalfa yield trial experiment was conducted using a randomized complete block design with five replicates. The trial was established in 2023 and consists of 17 entries (Table 1). Each plot measures 1.5 m x 3 m and is managed under rainfed conditions.

Table 1. Alfalfa entries included in the yield trial.

Entry ID	Entry name
1	GAMS1403FSH
2	GAMS1405FSH
3	GAMS1406FSH
4	GAMS1433
5	GAMS1434
6	GAMS1406A35
7	GAMS1438
8	GAMS1439
9	GAMS1548
10	GAMS19100
11	Bulldog 505
12	Bulldog805

13	GAMS1402FSH
14	GAMS1401A35
15	Alfagraze 600 RR
16	GAMS1404FSH
17	GAMS1436

Field Data Collection for Aboveground Biomass

Field data for the aboveground biomass (AGB) of alfalfa were acquired through destructive manual measurements at the harvest stage. Field data collection was done within two days of the UAS flight dates. AGB was obtained by harvesting plants per row and was measured on a dry-weight basis. Approximately 200 – 400 g of fresh samples were obtained per plot upon harvesting. After sampling, the harvester collects the entire plot, and the fresh weight is recorded. The samples were then weighed and subjected to oven-drying at 60°C for 72 hours or until a constant weight was achieved. The dry weight of the samples was obtained, and the dry matter content was then calculated. The field data measurements of alfalfa for AGB were compared to the spatial data collected by UAS-mounted RGB and multispectral sensors.

Field Data Collection for Plant Height

Field data for plant height were collected within two days after the flight dates. Plant height was obtained by measuring the plant from the base of the stem to the tip of the plant using a meter stick. For each plot, five random plants were taken to ensure a representative sample of the entire plot. These measurements were then used as a field reference to evaluate the performance of RGB and LiDAR metrics in estimating the plant height of alfalfa.

Forage Quality Analysis Using a Near-Infrared Spectroscopy

Forage quality parameters, including Acid Detergent Fiber (ADF), Neutral Detergent Fiber (NDF), and Crude Protein (CP), were measured. The concentrations of ADF, NDF, and CP were

determined on a percent dry weight basis using a near-infrared (NIR) spectroscopic analyzer (Asay et al., 2002; Noland et al., 2018). To prepare plant samples for analysis, they were oven-dried at 60°C for 72 hours, then ground to pass through a 1 mm screen size. The Perten DA7250 SD (PerkinElmer®, USA), a NIR spectroscopic analyzer, was employed to examine the ground samples. The resulting ADF, NDF, and CP data were compared with the spatial data collected by the UAS-mounted multispectral sensor, enabling the evaluation of relationships between forage quality and spectral reflectance.

UAS-Based Data Collection

Pre-Flight Preparations

Flights were scheduled on the same day as, or one to two days before, field data collection (Table 2). They were done within solar noon on clear, sunny days with low wind speeds and gusts to minimize image distortions and reduce the strain on the UAS. A flight plan was prepared, outlining UAS routes and specifying flight parameters such as image overlap, flight speed, and altitude.

As the accuracy of global positioning system (GPS) location measurements influences the quality of UAS-based results, a Real Time Kinematic (RTK) System with Global Navigation Satellite System (GNSS) was set up on-site. Temporary ground control points (GCPs) were strategically positioned at the four corners of the field to accurately determine plot geolocations. These GCPs were measured using an Emlid RS2 and M2 GNSS Receivers.

Table 2. Remote sensing and field data collection dates.

Flight Dates	Harvest/Sampling Date	Plant Height	Forage Quality
11-Jun	11-Jun	11-Jun	No dual XS data
11-Jul	11-Jul	11-Jul	Analyzed
20-Aug	21-Aug	21-Aug	Analyzed
23-Sep	Not harvested	24-Sep	No dual XS data

Platforms and Sensors

Multiple multirotor UAS, each equipped with either RGB, XS, and LiDAR sensors, were deployed for data acquisition. For LiDAR data, a Freefly Systems Alta X (Woodinville, WA, USA) mounted with a LiDAR sensor (LiDAR USA Revolution 120) for high-resolution 3D mapping was used. The RGB and XS camera of the DJI Mavic 3M (Shenzhen, Guangdong, China) was used to obtain RGB and XS data, respectively. A DJI Matrice 600 Pro (SZ DJI Technology Co., Ltd., Shenzhen, Guangdong, China) with a multispectral sensor, specifically MicaSense RedEdge-P Dual Camera (AgEagle, Wichita, KS, USA) for capturing spectral data. The central wavelength and the bandwidth of the bands from the 4-band multispectral sensor and the 10-band multispectral sensor are shown in Tables 3 and 4, respectively. A pre-flight checklist was reviewed for each UAS platform. Furthermore, the images from the multispectral sensor were calibrated using calibration panels to ensure that the sensors are accurately collecting data on the reflectance values of the forage crops.

Table 3. Characteristics of the bands from the 4-band multispectral camera.

Band name	ID	Center Wavelength (nm)	Bandwidth (nm)
Green	G	560	16
Red	R	650	16
Red Edge	RE	730	16
Near Infrared	NIR	860	26

Table 4. Characteristics of the bands from the 10-band multispectral camera.

Band name	ID	Center Wavelength (nm)	Bandwidth (nm)
Blue	B	475	32
Green	G	560	27
Red	R	668	14
Red Edge	RE	717	12
Near Infrared	NIR	842	57
Coastal Blue	B 444	444	28
Green	G 531	531	14
Red	R 650	650	16
Red Edge	RE 705	705	10
Red Edge	RE 740	740	18

Image Processing and Analysis

RGB and Multispectral Data Processing

Photogrammetric processing of RGB and multispectral data was performed using AgiSoft Metashape Professional Version 2.2.1 software (AgiSoft LLC, St. Petersburg, Russia) and Pix4D Mapper (Pix4D SA, Lausanne, Switzerland) to produce orthomosaics of the plots. This process involved aligning photos, eliminating noise, incorporating GPS coordinates from the ground control points, constructing a dense point cloud, and generating a Digital Surface Model (DSM).

The result of merging multiple overlapping aerial images is a high-resolution georeferenced image known as an orthomosaic.

Vegetation index (VI) Generation

Vegetation indices were generated in ArcGIS Pro version 3.4 (ESRI, Redlands, California, USA) using the RGB and multispectral orthomosaics produced in Agisoft Metashape and Pix4D Mapper. Field boundary, plot, and subplot shapefiles were imported to delineate the study area. A subplot was created using a shapefile within a plot to exclude the boundary effects. Furthermore, the remote sensing data was extracted from the subplot. The RGB and multispectral orthomosaics were loaded into the software. To exclude soil pixels, the Image Classification Wizard in ArcGIS Pro was used to perform supervised classification. Training samples were manually created by digitizing polygons around soil and vegetation pixels. A Support Vector Machine (SVM) classifier was employed, and the classified raster was then reclassified to isolate vegetation pixels, effectively masking out soil pixels. Subsequently, several vegetation indices were calculated from RGB and multispectral data. The vegetation indices from RGB, 4-band multispectral, and 10-band dual multispectral sensors are shown in Tables 5, 6, and 7. VI metrics were then extracted for each plot and each collecting date

Table 5. Vegetation indices extracted from the RGB sensor.

Index	Formula	Source
Green Red Vegetation Index (GRVI)	$GRVI = \frac{(Green - Red)}{(Green + Red)}$	Yin et al. (2022)
Visible Atmospherically Resistance Index (VARI)	$VARI = \frac{(Green - Red)}{(Green + Red - Blue)}$	Gitelson et al. (2002)

Green Leaf Index (GLI)	$GLI = \frac{(2x\ Green - Red - Blue)}{(2x\ Green + Red + Blue)}$	Louhaichi et al. (2001)
Excessive Green Index (ExG)	$ExG = 2x\ Green - Red - Blue$	Woebbecke et al. (1995)

Table 6. Vegetation indices extracted from the multispectral sensor.

Index	Formula	Source
Green Red Vegetation Index (GRVI)	$GRVI = \frac{(Green - Red)}{(Green + Red)}$	Yin et al. (2022)
Normalized Difference Red Edge Index (NDRE)	$NDRE = \frac{(NIR - Red\ Edge)}{(NIR + Red\ Edge)}$	Rodriguez et al. (2006)
Normalized Difference Vegetation Index (NDVI)	$NDVI = \frac{(NIR - Red)}{(NIR + Red)}$	Rouse et al. (1974)
Simple Ratio Index (SR)	$SR = \frac{(NIR)}{(Red)}$	Jordan (1969)

Table 7. Vegetation indices extracted from the dual multispectral 10-band sensor.

Index	Formula	Source
Normalized Difference Vegetation Index (NDVI 1)	$NDVI\ 1 = \frac{(NIR - Red)}{(NIR + Red)}$	Rouse et al. (1974)
NDVI 2	$NDVI\ 2 = \frac{(NIR - Red\ 650)}{(NIR + Red\ 650)}$	

Normalized Difference Red Edge Index (NDRE 1)	$NDRE\ 1 = \frac{(NIR - Red\ Edge)}{(NIR + Red\ Edge)}$	Rodriguez et al. (2006)
NDRE 2	$NDRE\ 2 = \frac{(NIR - Red\ Edge\ 705)}{(NIR + Red\ Edge\ 705)}$	
NDRE 3	$NDRE\ 3 = \frac{(NIR - Red\ Edge\ 740)}{(NIR + Red\ Edge\ 740)}$	
Green Normalized Difference Vegetation Index (GNDVI 1)	$GNDVI\ 1 = \frac{(NIR - Green)}{(NIR + Green)}$	Gitelson et al (1996)
GNDVI 2	$GNDVI\ 2 = \frac{(NIR - Green\ 531)}{(NIR + Green\ 531)}$	
(Chlorophyll Red Edge Index) CHLRE 1	$CHLRE\ 1 = \frac{(NIR)}{(Red\ Edge)} - 1$	Gitelson et al (2006)
CHLRE 2	$CHLRE\ 2 = \frac{(NIR)}{(Red\ Edge\ 705)} - 1$	
CHLRE 3	$CHLRE\ 3 = \frac{(NIR)}{(Red\ Edge\ 740)} - 1$	
Simple Ratio Index (SR 1)	$SR\ 1 = \frac{(NIR)}{(Red)}$	Jordan (1969)
SR 2	$SR\ 2 = \frac{(NIR)}{(Red\ 650)}$	
MERIS Terrestrial Chlorophyll Index (MTCI 1)	$\text{MTCI}\ 1 = \frac{(NIR - Red\ Edge)}{(Red\ Edge - Red)}$	Dash and Curran (2004)
MTCI 2	$\text{MTCI}\ 2 = \frac{(NIR - Red\ Edge)}{(Red\ Edge - Red\ 650)}$	

MTCI 3	$\text{MTCI } 3 = \frac{(NIR - Red\ Edge\ 705)}{(Red\ Edge\ 705 - Red)}$
MTCI 4	$\text{MTCI } 4 = \frac{(NIR - Red\ Edge\ 740)}{(Red\ Edge\ 740 - Red)}$
MTCI 5	$\text{MTCI } 5 = \frac{(NIR - Red\ Edge\ 705)}{(Red\ Edge\ 705 - Red\ 650)}$
MTCI 6	$\text{MTCI } 6 = \frac{(NIR - Red\ Edge\ 740)}{(Red\ Edge\ 740 - Red\ 650)}$

Canopy Height Model (CHM) Generation

A canopy height model (CHM) was generated for each RGB and LiDAR data using Global Mapper software version 25.0 (Blue Marble Geographics, Hallowell, ME, USA). The process involved importing point cloud (.laz) files and classifying points into noise, ground, and vegetation categories. A Digital Terrain Model (DTM) and Digital Surface Model (DSM) were then generated by creating elevation grids. Finally, the CHM was produced by combining the terrain models, calculated as the difference between the DSM and DTM.

RGB and LiDAR Metrics Extraction from CHM

RGB and LiDAR metrics were extracted by importing CHM layers generated from both RGB and LiDAR data. Statistical summaries, including maximum, mean, median, and percentile values from the 80^{th} to 99^{th} percentile, were calculated for each plot. These metrics were then extracted to individual plot boundaries, enabling plot-level analysis of canopy height characteristics.

Data Analysis

R version 4.3.2 with RStudio integrated development environment (IDE) was used as the software tool for data analysis. Packages, libraries, and extensions were utilized for statistical analysis, data visualization, and modeling.

Analysis of Variance (ANOVA)

A linear mixed-effects model was used to analyze the manually measured plant height and yield, accounting for the fixed effects of variety and harvest date, as well as their interaction. The model included a random effect of block and an autoregressive order 1 (AR1) covariance structure to account for repeated measures over time. The analysis was conducted using R software version 4.3.2 with R Studio IDE with the nlme package.

Pearson Correlation Analysis

To investigate the relationships between manually measured yield, plant height, and forage quality, and the UAS-derived metrics, Pearson correlation coefficients were calculated using the R software.

Pearson Correlation Analysis for Yield and Forage Quality

Correlation analysis was conducted between yield and bands and vegetation indices derived from each sensor, including RGB and 4-band multispectral. The relationship between forage quality and the bands and vegetation indices derived from the three sensors, RGB, multispectral, and 10-band dual multispectral, was calculated using the Pearson correlation coefficient.

Pearson Correlation Metrics for Plant Height

The RGB metrics included both Structure-from-Motion (SfM) derived plant height features, such as maximum (Max), Mean, Median, 80^{th} percentile (P80), 85^{th} percentile (P85), 90^{th} percentile (P90), 95^{th} percentile (P95), and 99^{th} percentile (P99), and RGB-based vegetation

indices, including GRVI, VARI, GLI, and ExG. The LiDAR metrics consisted of features derived from LiDAR point clouds, including Max, Mean, Median, P80, P85, P90, P95, and P99 of LiDAR-derived plant height.

Predictive Models for Yield, Plant Height, and Forage Quality

Predictive models were developed for yield, plant height, and forage quality estimation. Each dataset was divided into a 70% training set and a 30% validation set to facilitate model development and evaluation. Hyperparameter tuning was performed for each model using grid search or cross-validation to optimize key parameters. Model performance was evaluated on a test dataset using Root Mean Squared Error (RMSE) and R-squared (R^2) metrics, comparing predicted values to field data measurements to assess accuracy. Additionally, variable importance was calculated for each model to identify the most influential predictors.

Machine Learning Models and Data Types for Yield and Forage Quality Estimation

Two machine learning models, random forest (RF) and extreme gradient boosting (XGBoost), were evaluated for the estimation of alfalfa yield and forage quality. For yield estimation, six data types and nine different data type combinations were used:

- RGB: Seven variables, including bands and vegetation indices derived from the RGB sensor.
- RGB + PH: Eight variables of manually-measured plant height data and RGB-derived bands and vegetation indices.
- XS: Eight variables, including bands and vegetation indices derived from the 4-band multispectral sensor.
- XS + PH: Nine variables, including manually-measured plant height data and multispectral-derived bands and vegetation indices.

- RGB + XS: Fifteen (15) variables, including bands and vegetation indices derived from the RGB and multispectral sensors.
- RGB + XS + PH: Sixteen variables, including manually-plant height data and the bands and vegetation indices derived from the RGB and multispectral sensors.

For each forage quality metric (ADF, NDF, and CP), three data types were used:

- RGB: Seven variables, including bands and vegetation indices derived from the RGB sensor.
- XS: Eight variables, including bands and vegetation indices derived from the 4-band multispectral sensor.
- Dual XS: Twenty-eight (28) variables, including bands and vegetation indices derived from the 10-band multispectral sensor.

Machine Learning Models and Data Types for Plant Height Estimation

Four machine learning models, including Conditional Inference Trees (CIT), Elastic Net, Extreme Gradient Boosting (XGBoost), and Random Forest (RF), were developed in R software to predict plant height based on combinations of RGB and/or LiDAR metrics.

To compare the effects of different combinations of input features, five distinct datasets were used:

- SfM RGB: Eight variables, including only SfM-derived structural metrics of plant height (Max, Mean, Median, P80, P85, P90, P95, and P99).
- RGB (SfM RGB plus vegetation indices): Twelve (12) variables including SfM-derived structural metrics combined with RGB-based vegetation indices (GRVI, VARI, GLI, and ExG).

- LiDAR: Eight variables, including LiDAR-derived structural metrics of plant height (Max, Mean, Median, P80, P85, P90, P95, and P99).
- SfM RGB plus LiDAR: Sixteen (16) variables, including a combination of SfM-derived structural metrics with LiDAR-derived structural metrics.
- RGB plus LiDAR: Twenty variables, including all RGB metrics (SfM-derived structural metrics and vegetation indices) combined with LiDAR-derived structural metrics.

CHAPTER 3

RESULTS

Biomass Yield

Manually Measured Alfalfa Yield across Harvests

The alfalfa yield in Table 8 varied significantly across the three harvest dates, with mean yields of 6452 kg/ha on June 11 (D1), 1322 kg/ha on July 11 (D2), and 2900 kg/ha on August 20 (D3). Yield in D1 produced the highest yield, while the D2 harvest had the lowest. The coefficients of variation were 19%, 22%, and 12% for D1, D2, and D3, respectively, indicating relatively low variability in yield within each harvest date, with the least variability observed in the August harvest. The higher yield in D3 in comparison to D2 can be attributed to the larger gap in the harvesting date.

Table 8. Statistical summary of alfalfa yield across three harvest periods.

Collection date	ID	Mean yield (kg/ha)	Minimum	Maximum	Standard deviation	Coefficient of variation (%)
June 11	D1	6452	4038	9215	1197	19
July 11	D2	1322	792	1933	289	22
August 20	D3	2900	1860	3610	352	12

Analysis of Variance (ANOVA) for Yield

The analysis shown in Table 9 reveals significant effects of Entry, Collection date, and their interaction on the alfalfa biomass yield (< 2.2e-16 and 3.095e-12). This suggests that

differences between entries change over collection dates, and the interaction between these factors all contribute substantially to variations in yield.

Table 9. The analysis of variance (Type III tests) table for alfalfa yield.

Source of Variation	χ^2 (Chisq)	DF	p-value
Entry	169.42	16	<2.2e-16 ***
Collection date	121.50	2	<2.2e-16 ***
Entry x Collection date	120.79	32	3.095e12 ***

Significance codes: *** p < 0.001, ** p < 0.01, * p < 0.05, . p < 0.1

The boxplot of alfalfa yield across three harvest dates (D1, D2, D3) revealed significant differences in yield performance (Figure 1). D1 harvest date shows statistically higher yield than the two harvest dates, while D2 shows the lowest yield. The average yield of each entry per harvest date is shown in Appendices A and B.

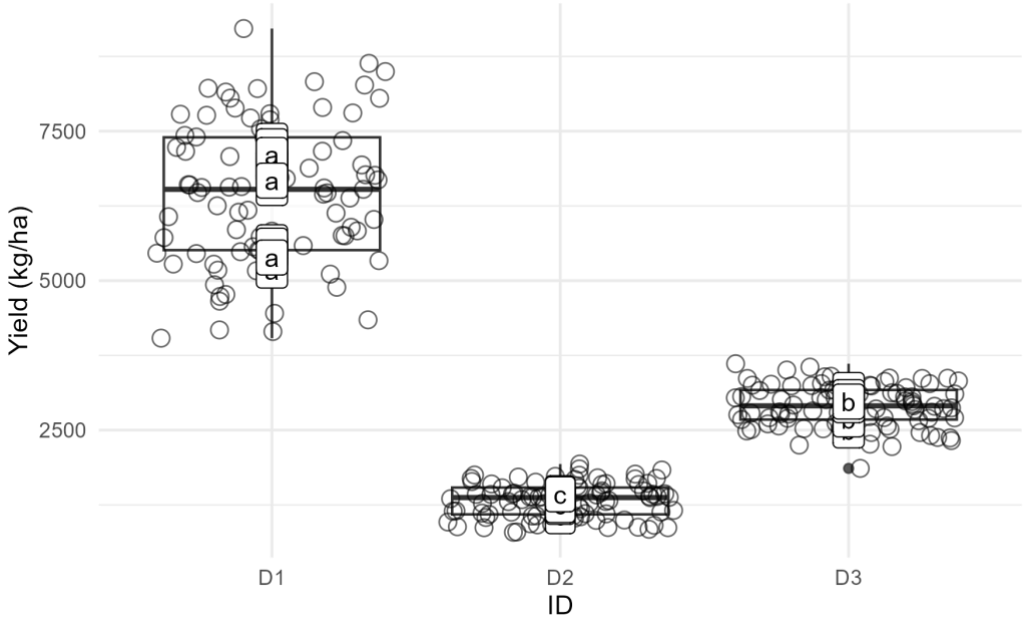

Figure 1. Alfalfa yields across three harvest dates. Boxplots followed by the same letter are not statistically different at alpha = 0.05.

Relationship of RGB-Based Bands and Vegetation Indices with Yield

The correlation matrix (Figure 2) shows the overall relationships between RGB bands from the Mavic 3M camera, vegetation indices, and alfalfa yield. Table 4 also shows the correlation between alfalfa yield and various RGB-based bands and vegetation indices across different alfalfa entries. The green (r = 0.57) and red (r = 0.53) bands show moderate correlations with yield. In contrast, the blue (r = -0.56) band shows a moderate negative correlation with yield. Vegetation indices, such as GLI (r = 0.67) and ExG (r = 0.67), exhibit high positive correlations. Whereas GRVI (r = 0.31) and VARI (r = 0.21) have weak positive correlations with alfalfa yield.

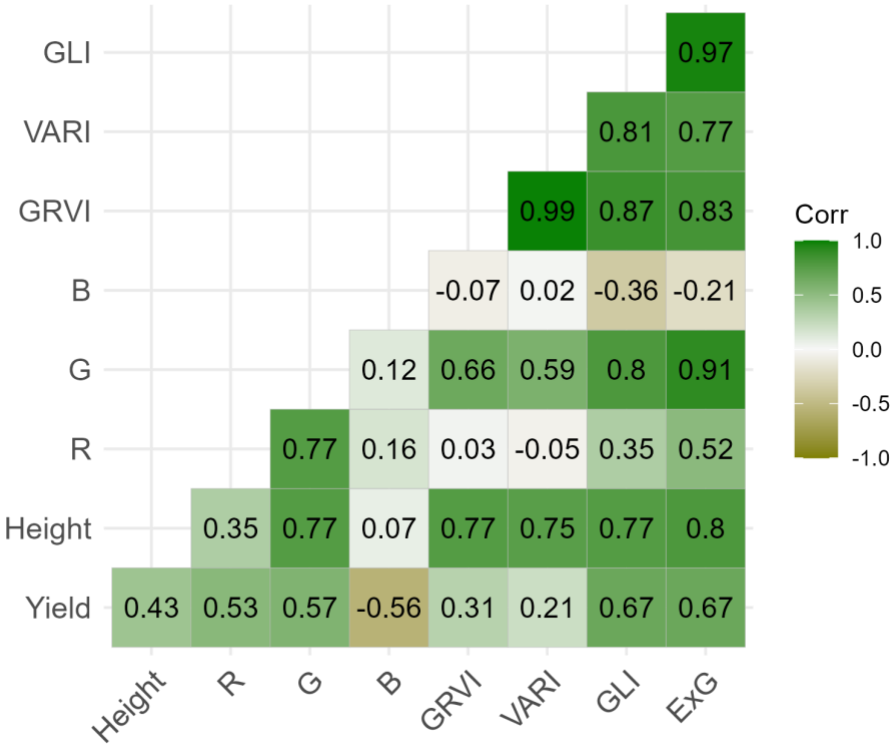

Figure 2. Correlation matrix showing the relationships between yield and RGB-based bands and vegetation indices. R = Red. G = Green. B = Blue. GRVI = Green Red Vegetation Index. VARI = Visible Atmospherically Resistance Inde . GLI = Green Leaf Index. ExG = Excessive Green Index.

Relationship of Multispectral (XS)-Based Bands and Vegetation Indices with Yield

The correlation matrix shown in Figure 3 displays the relationships between XS-derived spectral data and alfalfa yield. Table 5 shows the correlation between alfalfa yield and various XS-based bands and vegetation indices for different alfalfa entries. The green band and GRVI exhibit strong positive correlations with yield, with correlation values of 0.91 and 0.86, respectively. NDVI (r = 0.31), SR (r = 0.22), and RE (r = 0.17) have low correlations with biomass yield. Negative correlations with yield resulted from the red band, NDRE, and NIR band.

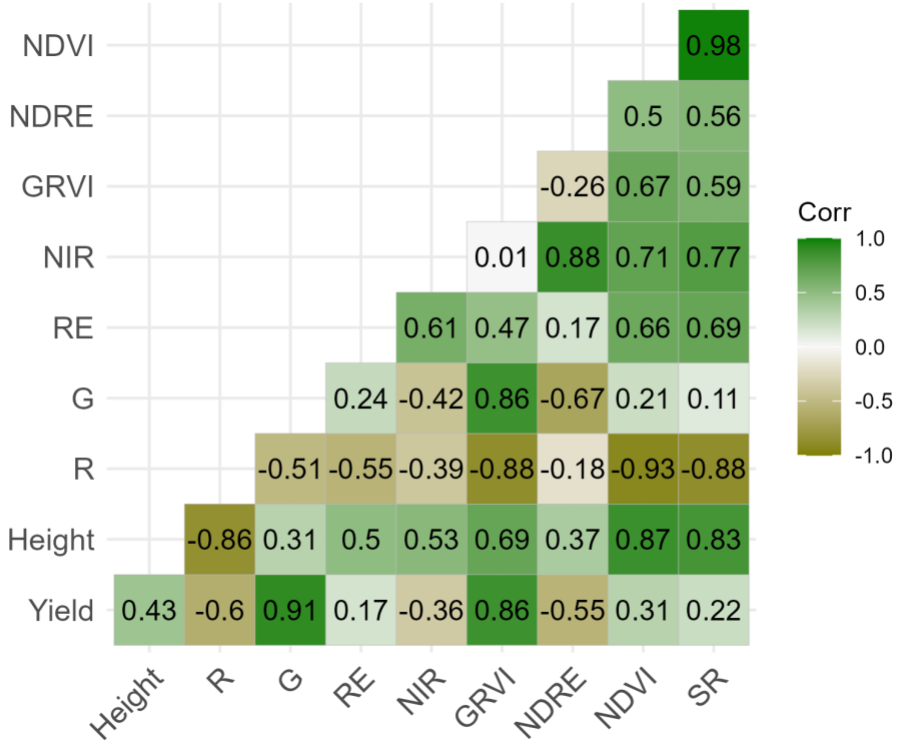

Figure 3. Correlation matrix showing the relationships between yield and multispectral-derived bands and vegetation indices. R = Red. G = Green. RE = Red Edge. NIR = Near Infrared. GRVI = Greed Red Vegetation Index. NDRE = Normalized Difference Red Edge Index. NDVI = Normalized Difference Vegetation Index. SR = Simple Ratio.

Machine Learning Models

The results show that the RF model outperforms the XGBoost model in predicting alfalfa yield, with generally lower RMSE values and higher R2 values across most data type combinations (Figure 4). The integration of red, green, blue (RGB), multispectral (XS), and manually-measured plant height (PH) (RGB + XS + PH) data resulted in the lowest RMSE value for both RF (RMSE = 774.21) and XGBoost (RMSE = 768.2) models. While RGB only data has the highest RMSE and lowest R2 in both models, and addition of plant height data type to the RGB data (RGB + PH) improved the prediction accuracy of both models based on decreased RMSE and increased R2. Similarly, adding plant height to XS data (XS + PH) increased the accuracy of the RF and XGBoost models with decreased RMSE and increased R2. The combination of RGB and XS data (RGB + XS) has better performance than RGB and RGB + PH data types, but displays inferior performance than XS and XS + PH data types. In terms of feature importance, the key predictor for data types with XS variables is the green band. While for RGB and RGB + PH data types, the top important variables are GLI and the blue band.

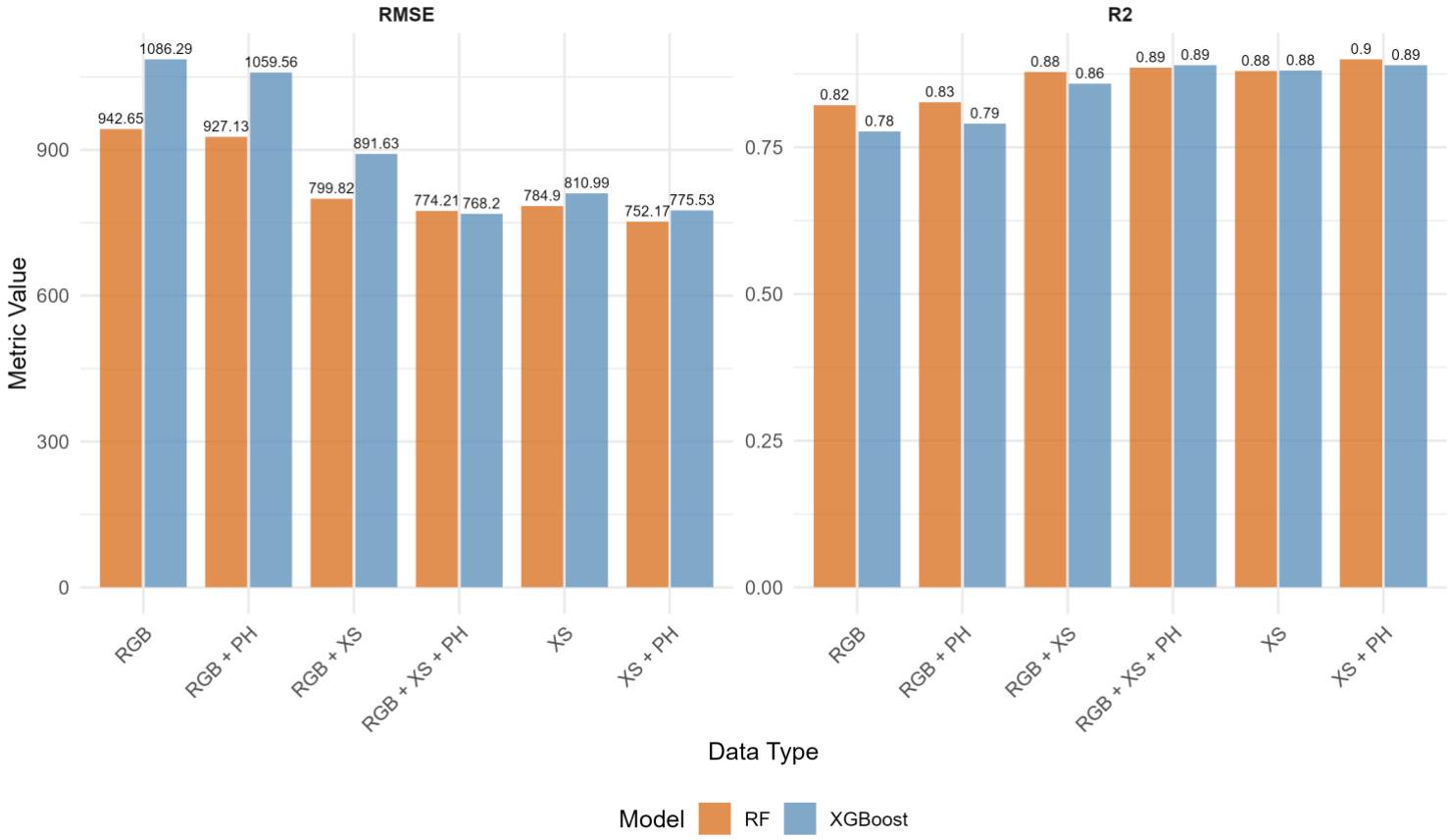

Figure 4. Comparison of random forest and XGBoost models for predicting alfalfa yield. RMSE = Root Mean Square Error. R2 = Coefficient of Determination. RF = Random Forest. XGBoost = Extreme Gradient Boosting. RGB = Red, Green, Blue. PH = Manually-measured plant height. XS = Multispectral.

Table 10. Correlation of yield and RGB-based bands and vegetation for each alfalfa entry.

Entry	Entry Name	PH	R	G	B	GRVI	VARI	GLI	ExG
1	GAMS1403FSH	0.53	0.32	0.6	-0.91	0.61	0.51	0.82	0.76
2	GAMS1405FSH	0.26	0.78	0.75	-0.38	0.37	0.22	0.77	0.77
3	GAMS1406FSH	0.41	0.58	0.52	-0.41	0.16	0.07	0.56	0.55
4	GAMS1433	0.34	0.69	0.69	-0.54	0.28	0.07	0.86	0.84
5	GAMS1434	0.5	0.59	0.64	-0.8	0.34	0.24	0.72	0.72
6	GAMS1406A35	0.5	0.63	0.53	-0.42	0.2	0.13	0.53	0.53
7	GAMS1438	0.38	0.7	0.63	-0.44	0.3	0.21	0.66	0.66
8	GAMS1439	0.54	0.64	0.67	-0.6	0.34	0.24	0.69	0.7
9	GAMS1548	0.59	0.4	0.6	-0.88	0.43	0.34	0.73	0.73
10	GAMS19100	0.42	0.49	0.5	-0.7	0.38	0.24	0.75	0.68
11	Bulldog 505	0.48	0.64	0.51	-0.66	0.27	0.16	0.69	0.64
12	Bulldog805	0.46	0.22	0.38	-0.89	0.22	0.13	0.6	0.58
13	GAMS1402FSH	0.31	0.82	0.7	-0.5	0.24	0.12	0.74	0.74
14	GAMS1401A35	0.44	0.8	0.69	-0.36	0.29	0.2	0.67	0.69
15	Alfagraze 600 RR	0.15	0.55	0.63	-0.68	0.5	0.37	0.83	0.79
16	GAMS1404FSH	0.28	0.63	0.64	-0.14	0.32	0.24	0.67	0.69
17	GAMS1436	0.58	0.67	0.59	-0.43	0.3	0.18	0.69	0.67

Table 11. Correlation of yield and multispectral-based bands and vegetation indices for each alfalfa entry.

Entry	Entry Name	PH	R	G	B	GRVI	VARI	GLI	ExG	Entry
1	GAMS1403FSH	0.53	-0.72	0.92	0.49	-0.14	0.89	-0.51	0.52	0.43
2	GAMS1405FSH	0.26	-0.59	0.94	0.33	-0.36	0.92	-0.54	0.3	0.2
3	GAMS1406FSH	0.41	-0.52	0.94	-0.04	-0.42	0.85	-0.55	0.16	0.06
4	GAMS1433	0.34	-0.59	0.94	0.31	-0.41	0.92	-0.66	0.18	0.07
5	GAMS1434	0.5	-0.62	0.96	0.25	-0.39	0.88	-0.58	0.34	0.21
6	GAMS1406A35	0.5	-0.57	0.93	0.15	-0.35	0.83	-0.54	0.23	0.15
7	GAMS1438	0.38	-0.51	0.98	0.22	-0.32	0.87	-0.55	0.24	0.12
8	GAMS1439	0.54	-0.59	0.94	0.47	-0.38	0.88	-0.59	0.3	0.22
9	GAMS1548	0.59	-0.67	0.92	0.63	-0.33	0.9	-0.54	0.48	0.4
10	GAMS19100	0.42	-0.68	0.96	0.11	-0.36	0.9	-0.58	0.36	0.27
11	Bulldog 505	0.48	-0.62	0.95	0	-0.41	0.87	-0.55	0.32	0.2
12	Bulldog805	0.46	-0.61	0.92	-0.13	-0.43	0.83	-0.49	0.34	0.21
13	GAMS1402FSH	0.31	-0.66	0.94	-0.01	-0.4	0.91	-0.62	0.28	0.17
14	GAMS1401A35	0.44	-0.57	0.96	0.27	-0.33	0.89	-0.59	0.29	0.18
15	Alfagraze 600 RR	0.15	-0.68	0.94	0.56	-0.42	0.92	-0.62	0.39	0.29
16	GAMS1404FSH	0.28	-0.73	0.9	0.08	-0.38	0.9	-0.47	0.42	0.38
17	GAMS1436	0.58	-0.72	0.9	-0.03	-0.46	0.9	-0.56	0.41	0.33

Plant Height

Manually Measured Alfalfa Plant Height across Harvests

The height of alfalfa plants showed considerable variations across different harvesting dates (Table 12). The tallest height was recorded on the third date, D3 (August 20, 72.30 cm), while the shortest height was recorded on D4 (September 23, 22.80 cm). Standard deviation values range from 4.74 cm at D3 to 10.58 cm at D1. The coefficient of variation is lowest at D3 (7 %), indicating that plant heights are mostly uniform. In contrast, D4 exhibits the highest CV (23%), demonstrating greater variability compared to the mean.

Table 12. Statistical summary of plant height (cm) across four harvest periods.

Collection date	Entry	Mean (cm)	Minimum	Maximum	Standard deviation	Coefficient of variation (%)
June 11	D1	58.81	41.20	81.60	10.58	18
July 11	D2	35.45	23.20	46.40	5.28	15
August 20	D3	72.30	59.00	85.40	4.74	7
September 23	D4	22.80	12.40	36.58	5.19	23

Effect of Entry and Collection Date on Plant Height

The results indicate significant effects of entry or variety ($\chi^2 = 106.66$, df = 16, $p < 0.001$), collection date ($\chi^2 = 196.04$, df = 3, $p < 0.001$), and their interaction ($\chi^2 = 99.72$, df = 48, $p < 0.001$) on plant height field data (Table 13). The significant interaction between entry and collection date ($\chi^2 = 99.718$, p = 1.733e-05) suggests that the effect of treatment on plant height depends on the collection date. This interaction effect highlights the importance of considering the temporal dynamics of plant growth when evaluating treatment effects.

Table 13. Analysis of deviance (Type III tests) for plant height field data.

Source of Variation	χ^2 (Chisq)	DF	p-value
Entry	106.664	16	1.925e-15 ***
Collection date	196.042	3	< 2.2e-16 ***
Entry: Collection date	99.718	48	1.733e-05 ***

Signif. codes: 0 '***' 0.001 '**' 0.01 '*' 0.05 '.' 0.1 ' ' 1

Relationships between Alfalfa Plant Height and UAS-Based RGB and Lidar Metrics

Figure 5 illustrates the relationships using Pearson's correlation coefficient between alfalfa plant height and UAS-based RGB and LiDAR-derived metrics. For the RGB-derived metrics, plant height showed positive correlations with several percentile-based height measures and vegetation indices. The 95th percentile has the highest correlation (r = 0.88) with plant height, followed by 90th percentile (P90, r = 0.85), 85th percentile (P85, r = 0.82), and 80th percentile (P80, r = 0.79). Correlations with vegetation indices, including Green-Red Vegetation Index (GRVI, r = 0.80), Green Leaf Index (GLI, r = 0.79), and Visible Atmospherically Resistant Index (VARI, r = 0.78), were also strong. Median RGB height, however, showed moderate correlation (r = 0.70).

In comparison, LiDAR-derived metrics demonstrated moderate correlations with plant height. The highest correlations were observed with the 99th percentile (P99, r = 0.45), followed by 95th percentile (P95, r = 0.44), 90th percentile (P90, r = 0.41), 85th percentile (P85, r = 0.38), and 80th percentile (P80, r = 0.35).

Overall, the RGB-derived metrics have higher correlations with plant height than the LiDAR-derived metrics. Notably, the 95th percentile values consistently showed the strongest correlation with measured plant height in both sensor types.

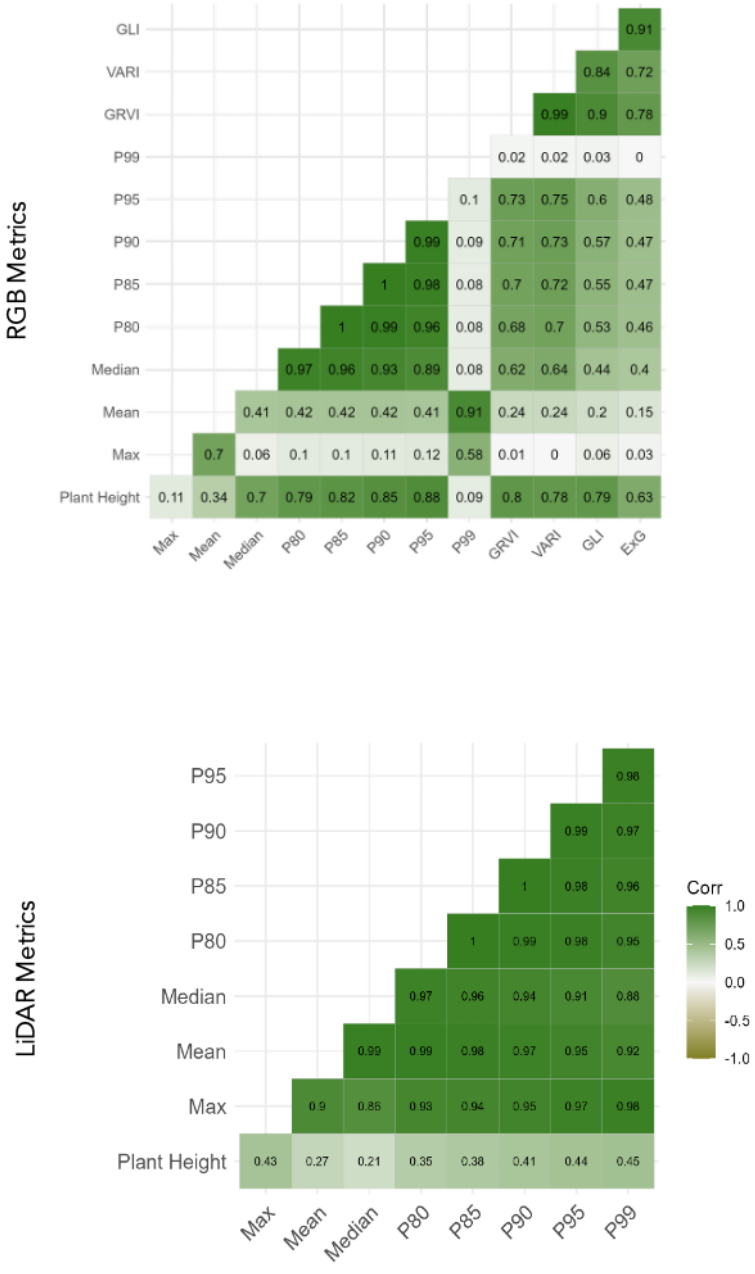

Figure 5. Correlation matrices illustrating the relationships between alfalfa plant height and UAS-based RGB and LiDAR metrics, analyzed using the Pearson correlation coefficient. P = Percentile.

Correlation Between Plant Height and Lidar Metrics for Each Alfalfa Entry

The Pearson correlation coefficient was calculated between manually measured plant height and LiDAR metrics for each of the 17 alfalfa entries (Table 8). This analysis aimed to determine if LiDAR data could distinguish between different entries and to show the relationship between manually measured plant height and LiDAR metrics for each entry.

The results in Table 8 reveal that the relationships between plant height and LiDAR metrics vary across the 17 entries. Entry 9 (GAMS1548) demonstrated moderate correlations across all LiDAR metrics, with the strongest correlation observed at the 99th percentile (P99 = 0.6051). Entries 1, 3, 5, 6, and 12 exhibited moderate correlations across most LiDAR metrics, except for Mean and Median. In contrast, entries 2, 4, 13, 15, and 16 displayed low to negatively low correlations across all metrics, indicating a weaker relationship between plant height and LiDAR metrics for these entries.

The maximum LiDAR metric (Max) and higher percentile metrics (P90, P95, and P99) showed moderate correlations for most entries, while the Mean and Median LiDAR metrics exhibited the lowest correlations with plant height, with some entries displaying negative correlations. These findings suggest that LiDAR metrics, particularly the higher percentile values, can be useful in estimating plant height for certain alfalfa entries, but the strength of the association varies across genotypes.

Correlation Between Plant Height and RGB Metrics for Each Alfalfa Entry

The Pearson correlation coefficient between plant height and RGB metrics is presented in Table 9. The results reveal that Mean and percentile metrics (P80 to P95) generally exhibit high to very high correlations with plant height across all 17 alfalfa entries. In contrast, Max and P99

metrics show very high correlations in most entries, but exhibit low correlations in specific entries, such as Entry 3 for P99 (0.3348) and Entries 3 (0.3348), 7 (0.1296), and 12 (0.3359) for Max.

The vegetation indices derived from RGB images also demonstrate notable correlations with plant height. GRVI, VARI, and GLI exhibit moderate to very high correlations. Specifically, GRVI shows strong correlations, ranging from 0.6196 to 0.9281, while VARI and GLI display similar trends. In contrast, ExG shows varied correlations across the 17 alfalfa entries, ranging from moderate (0.4579) to high (0.7669).

Relationships of Plant Height on First Collecting Date (D1)

Figure 7 illustrates the relationships between manually measured plant height and RGB and LiDAR metrics across different collecting dates (D1-D4). Notably, during the first collection date (D1), the P80 to P95 of both RGB and LiDAR metrics exhibited very high correlations ($r \geq 0.80$) with plant height. Mean ($r = 0.83$) and median ($r = 0.81$) LiDAR values also showed a very high correlation with plant height. High correlations were observed with the maximum LiDAR, and the P95 and P99 of LiDAR with r values of 0.7, 0.78, and 0.72, respectively. In contrast, RGB-based vegetation indices, including GRVI, VARI, GLI, and ExG, demonstrated very low correlations ($r < 0.19$) with plant height in D1.

Relationships of Plant Height in the Second Collecting Date (D2)

In the second collecting date (D2), LiDAR metrics, including mean, median P80, P85, P90, and P95, showed high correlations ($0.6 \leq r \leq 0.79$) while P99 ($r = 0.58$) showed a moderate correlation with plant height.

For RGB metrics in D2, RGB-based vegetation indices have higher correlations with plant height than in D1. They also have a comparatively better correlation than the structure-from-motion derived RGB metrics in D2. The maximum RGB, P95, P99, GRVI, VARI, and GLI have

high correlation with plant height with r values of 0.6, 0.6, 0.67, 0.63, 0.62, and 0.61, respectively. While mean RGB (r = 0.55) and ExG (r = 0.48) have a moderate correlation with plant height.

Performance of Machine Learning Models with Various Data Types

In comparison of different data types (Figure 6), data type 5 (RGB + LiDAR) has the lowest RMSE and the highest R2 among the three machine learning models, RF (RMSE = 4.22, R2 = 0.96), XGBoost (RMSE = 4.55, R2 = 0.95), and Elastic Net (RMSE = 6.23, R2 = 0.91). The metric values for data types 2 (RGB) and 4 (SfM RGB + LiDAR) are comparable to data type 5. In CIT, data type 4 has the lowest RMSE (4.93) and the highest R2 (0.94).

It can also be observed that the data type 2 has better model performance as shown by the lower RMSE (4.6) and higher R2 (0.95) compared to the data type 1 (SfM RGB), which has RMSE and R2 values of 6.15 and 0.91, respectively.

The results notably show that data type 3 (LiDAR), which includes the LiDAR-derived metrics, has the highest RMSE and lowest R2 values across all of the machine learning models. Additionally, the highest RMSE (15.76) and lowest R2 (0.41) of data type 3 were observed in the elastic net model.

Variable Importance in Different Machine Learning Models

Figure 8 shows the variable importance across four machine learning models, CIT, ElasticNet, RF, and XGBoost. In the CIT model, the 95th percentile height from SfM-derived RGB data (pct95_rgb) is the most important variable, followed by the 80th percentile of LiDAR data (pct80_lidar) and maximum plant height from RGB data (max_rgb). In the ElasticNet model, the top positive contributors from SfM-derived RGB metrics are pct95_rgb, followed by the 80th percentile of RGB data (pct80_rgb) and 90th percentile of LiDAR data (pct90_lidar). While GRVI and ExG have negative contributions and GLI and VARI have positive contributions. The RF and

XGBoost have similar trends, with the max_rgb being the most important feature, followed by pct99_rgb. Also, in both models, RGB-based vegetation indices such as GRVI, VARI, and ExG have lower importance than the metrics derived from SfM RGB and LiDAR point clouds.

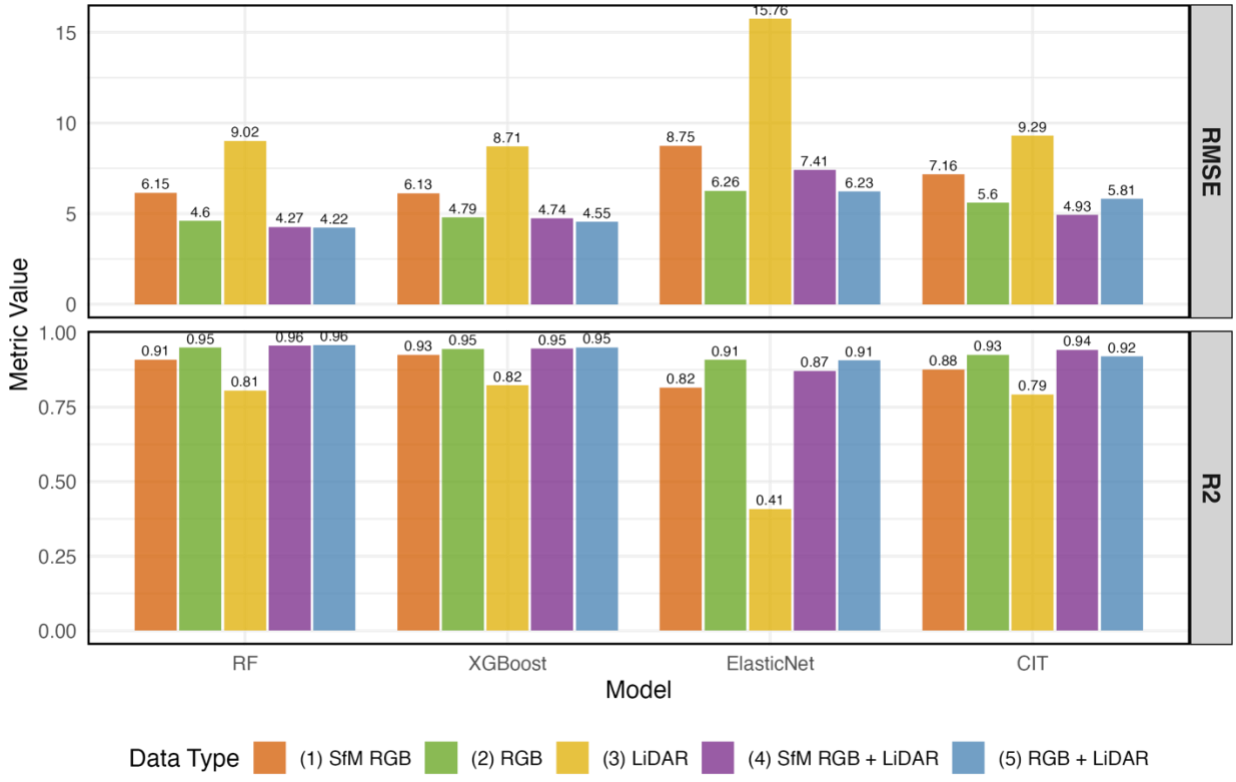

Figure 6. Performance of machine learning models for alfalfa height estimation using UAS-derived RGB and LiDAR data. RMSE = Root Mean Square Error. R2 = Coefficient of Determination. RF = Random Forest. XGBoost = Extreme Gradient Boosting. CIT = Conditional Inference Tree. SfM = Structure from Motion. RGB = Red, Green, Blue. LiDAR = Light Detection and Ranging.

Table 14. Correlation of plant height and LiDAR metrics for each alfalfa entry.

Entry	Entry Name	Max	Mean	Median	P80	P85	P90	P95	P99
1	GAMS1403FSH	0.5026	0.2792	0.1902	0.4001	0.4287	0.4566	0.4483	0.4778
2	GAMS1405FSH	0.2975	0.0565	-0.0224	0.1348	0.1593	0.2101	0.2542	0.2858
3	GAMS1406FSH	0.4857	0.3449	0.295	0.4193	0.4569	0.475	0.5089	0.5293
4	GAMS1433	0.3127	0.1982	0.1169	0.3026	0.3347	0.37	0.3699	0.333
5	GAMS1434	0.5036	0.3469	0.2889	0.4075	0.4489	0.4872	0.4973	0.4894
6	GAMS1406A35	0.5647	0.3789	0.3137	0.4606	0.477	0.4956	0.5128	0.5166
7	GAMS1438	0.4694	0.2673	0.2027	0.3447	0.3713	0.3993	0.4472	0.4529
8	GAMS1439	0.4874	0.3229	0.2684	0.3918	0.4149	0.439	0.5067	0.5241
9	GAMS1548	0.5828	0.4531	0.4142	0.5162	0.5384	0.5605	0.581	0.6051
10	GAMS19100	0.3717	0.1932	0.1162	0.3011	0.352	0.3651	0.4155	0.427
11	Bulldog 505	0.391	0.2976	0.2622	0.3886	0.404	0.416	0.4298	0.4146
12	Bulldog805	0.4198	0.3822	0.3532	0.4708	0.495	0.4978	0.5038	0.492
13	GAMS1402FSH	0.2225	-0.0467	-0.1162	0.0764	0.0961	0.1333	0.1993	0.2259
14	GAMS1401A35	0.438	0.2119	0.1265	0.3104	0.3513	0.3964	0.426	0.4746
15	Alfagraze 600 RR	0.1676	0.1408	0.1271	0.2207	0.2252	0.2548	0.2531	0.2435
16	GAMS1404FSH	0.3371	0.0546	-0.014	0.1789	0.2077	0.2376	0.2978	0.3315
17	GAMS1436	0.4732	0.2231	0.1376	0.3354	0.3627	0.3909	0.4429	0.4868

P = Percentile

Table 15. Correlation of plant height and RGB metrics for each alfalfa entry.

Entry	Entry Name	Max	Mean	Median	P80	P85	P90	P95	P99	GRVI	VARI	GLI	ExG
1	GAMS1403FSH	0.9335	0.7406	0.6678	0.7411	0.7702	0.8062	0.8398	0.8744	0.9281	0.9258	0.8744	0.7008
2	GAMS1405FSH	0.9527	0.8026	0.7685	0.8362	0.8492	0.8551	0.8635	0.8949	0.8198	0.792	0.7644	0.5938
3	GAMS1406FSH	0.3348	0.3984	0.7809	0.8465	0.8595	0.8771	0.9056	0.3348	0.7476	0.7354	0.7586	0.5154
4	GAMS1433	0.8955	0.6973	0.6378	0.7483	0.7674	0.7837	0.8057	0.8636	0.8416	0.809	0.7045	0.5041
5	GAMS1434	0.9751	0.7779	0.7112	0.8297	0.8508	0.8746	0.9168	0.9671	0.8376	0.8178	0.8642	0.7357
6	GAMS1406A35	0.9501	0.7596	0.6905	0.8184	0.8413	0.869	0.9033	0.9322	0.8044	0.7806	0.8902	0.7381
7	GAMS1438	0.1296	0.3735	0.747	0.8218	0.8399	0.8639	0.8937	0.9352	0.8435	0.826	0.8523	0.6138
8	GAMS1439	0.7184	0.7094	0.6349	0.7718	0.8101	0.8526	0.8914	0.919	0.7865	0.7633	0.8238	0.6362
9	GAMS1548	0.9634	0.7783	0.725	0.8444	0.8611	0.8776	0.8988	0.9523	0.8946	0.8753	0.8931	0.7142
10	GAMS19100	0.9009	0.6877	0.6387	0.7284	0.762	0.8145	0.8707	0.9197	0.8301	0.8206	0.7904	0.6504
11	Bulldog 505	0.9333	0.7152	0.626	0.7547	0.7949	0.8529	0.9227	0.9514	0.8246	0.8075	0.8374	0.6695
12	Bulldog805	0.3359	0.8059	0.7819	0.8281	0.8518	0.8817	0.9167	0.9561	0.8708	0.8642	0.8629	0.7669
13	GAMS1402FSH	0.9162	0.8061	0.7604	0.8179	0.8283	0.836	0.8457	0.9063	0.8674	0.8576	0.7795	0.6164
14	GAMS1401A35	0.9378	0.7313	0.6525	0.7996	0.8264	0.8581	0.8903	0.9492	0.7844	0.7597	0.8439	0.6123
15	Alfagraze 600 RR	0.9305	0.7809	0.7353	0.8031	0.819	0.8236	0.8329	0.8663	0.8048	0.8041	0.6928	0.4625
16	GAMS1404FSH	0.9329	0.8407	0.8156	0.834	0.8441	0.8609	0.8695	0.8922	0.6196	0.6215	0.5779	0.4579
17	GAMS1436	0.9602	0.7332	0.6766	0.7592	0.7922	0.8222	0.854	0.9206	0.8119	0.7945	0.8106	0.5689

Date ID	RGB	LiDAR
D1		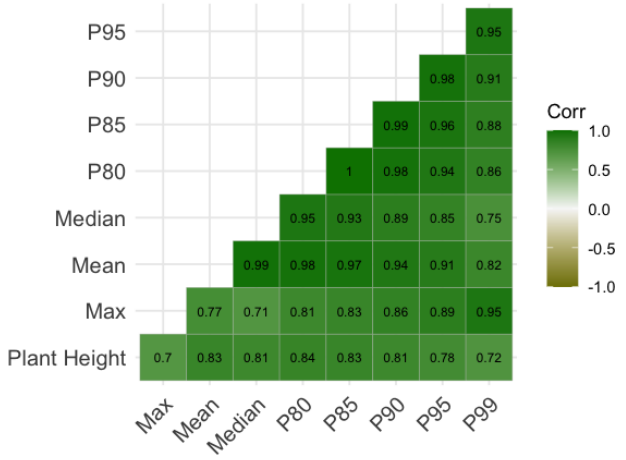
D2	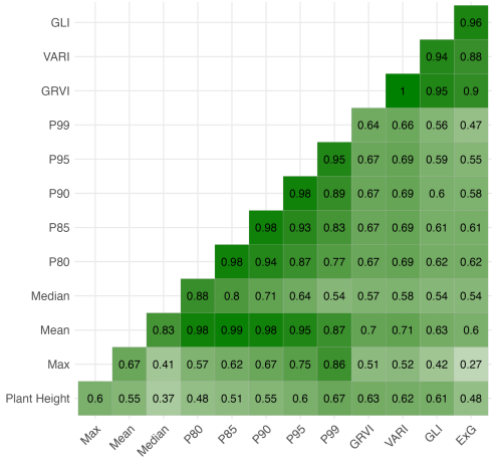	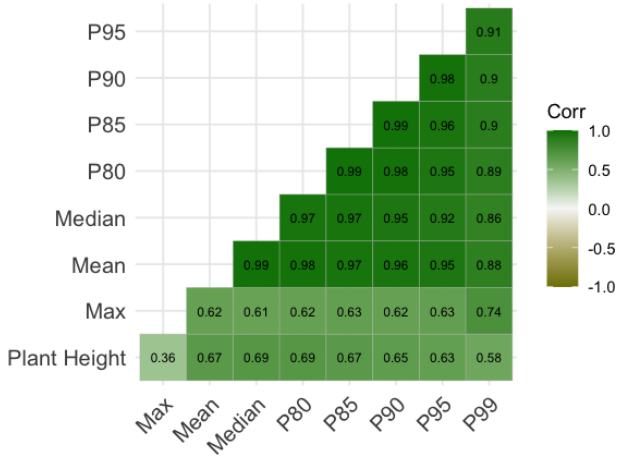

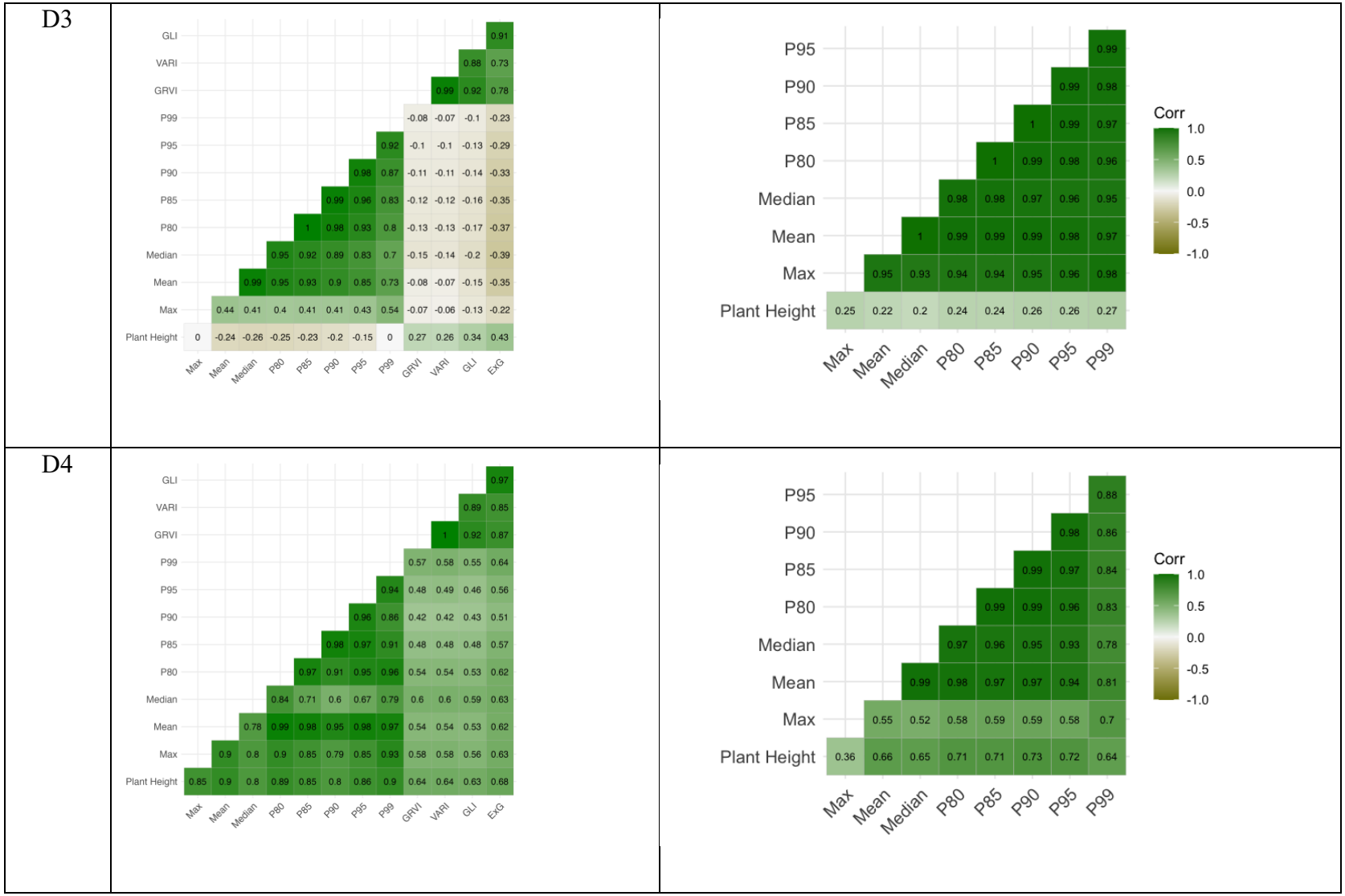

Figure 7. Correlation matrices showing the relationships between manually measured plant heights and various RGB and LiDAR metrics across different collection dates (D3 and D4).

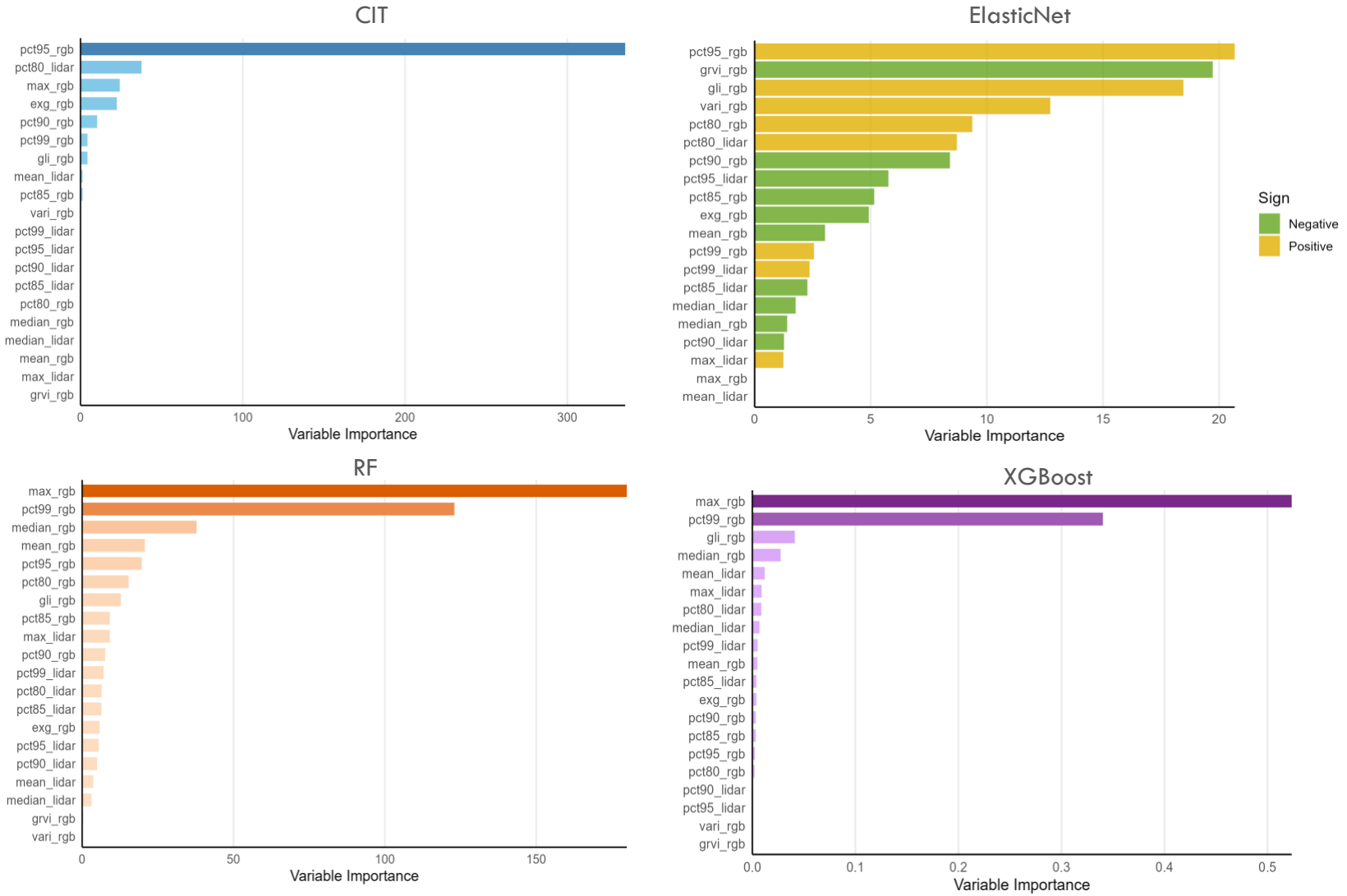

Figure 8. Variable importance in different machine learning models. CIT = Conditional Inference Tree. RF = Random Forest. XGBoost = Extreme Gradient Boosting.

Forage Quality: Acid Detergent Fiber (ADF)

Summary Statistics

The summary statistics for acid detergent fiber (ADF) of alfalfa across two collecting dates, D2 and D3, revealed varying levels of mean (Table 16). ADF values in D2 and D3 showed low variability, with CV values of 0.06 and 0.05, and SD values of 1.44 and 1.74, respectively. The mean ADF values also differed between collection dates, with D2 having a lower mean value of 25.61 compared to 32.62 for D3. These results suggest that ADF values are stable and consistent on both collecting dates.

Table 16. Summary statistics of acid detergent fiber of alfalfa obtained from a near-infrared spectroscopic analyzer.

Collecting date	Date	Mean	Coefficent of Varition	Standard Deviation	Minimum	Maximum
D2	July 11	25.61	6 %	1.44	22.42	29.17
D3	August 20	32.62	5 %	1.74	29.04	38.05

Pearson Correlation Coefficient Between ADF and RGB variables

The correlation matrix in Figure (9) shows the relationships between ADF and RGB-derived bands and vegetation indices across all collecting dates. Pearson correlation coefficient (r) values reveal that ADF has high to very high positive correlations with vegetation indices such as ExG (r = 0.86), GLI (r = 0.83), and GRVI (r = 0.81). VARI (r = 0.799). Also, the green band (r = 0.86) has very high correlations with ADF. The red band (r = 0.49) and blue band (r = 0.48) have moderate positive correlations with ADF.

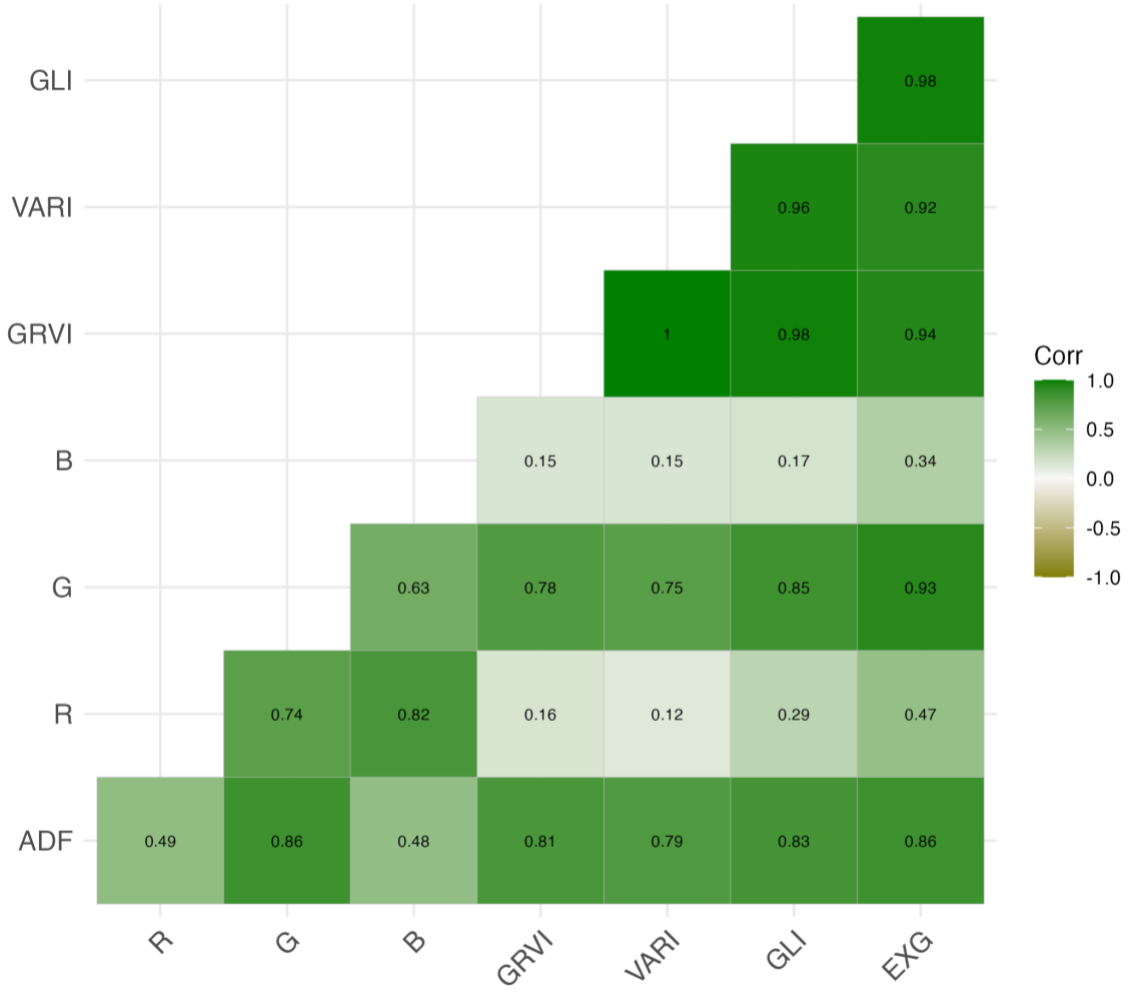

Figure 9. Relationships between Acide Detergent Fiber (ADF) and RGB-derived bands and vegetation indices. R = Red. G = Gree. B = Blue. GRVI = Greed Red Vegetaion Index. VARI = Visible Atmospherically Resistance Index. GLI = Green Lead Index. ExG = Excessive Green Index.

Pearson Correlation Coefficient Between ADF and XS variables

The relationships between ADF and bands and vegetation indices derived from multispectral cameras show that vegetation indices such as GRVI (r = 0.88), NDVI (r = 0.87), SR (r = 0.84), and NDRE (r = 0.83) have very high positive correlations with ADF (Figure 10). For single bands, the green (r = 0.69) and NIR (r = 0.77) bands have high correlations, while the RE (r

= 0.58) band has a moderate correlation. Notably, the red band (r = -0.89) has a very high negative correlation with ADF.

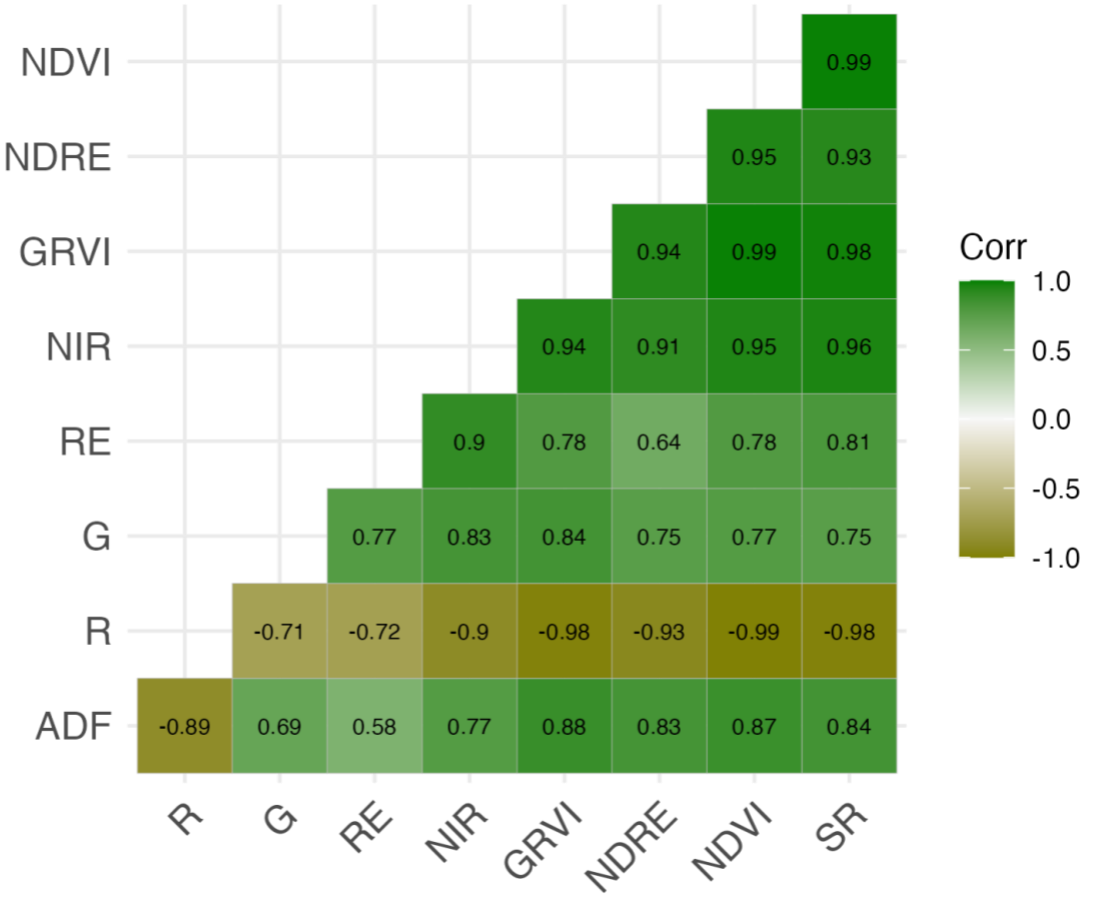

Figure 10. Relationships between Acid Detergent Fiber (ADF) and multispectral bands and vegetation indices. R = Red. G = Green. RE = Red Edge. NIR = Near Infrared. GRVI = Green Red Vegeation Index. NDRE = Normalized Difference Red Edge. NDVI = Normalized Difference Vegetation Index. SR = Simple Ratio.

Pearson Correlation Coefficient Between ADF and Dual XS Variables

The relationships between ADF and single bands (Figure 11) derived from dual multispectral cameras, red and blue, show that the single bands from the red camera, blue (475 nm), green (560 nm), red (668 nm), and red-edge (717 nm), and the single bands from the blue

camera, blue (444 nm), green (531 nm), red (650 nm), red-edge (705 nm), red-edge (740 nm), have moderate to very high negative correlations with ADF. Notably, the NIR band (842 nm) is the only band that has a positive correlation with ADF, but it has a weak relationship with ADF.

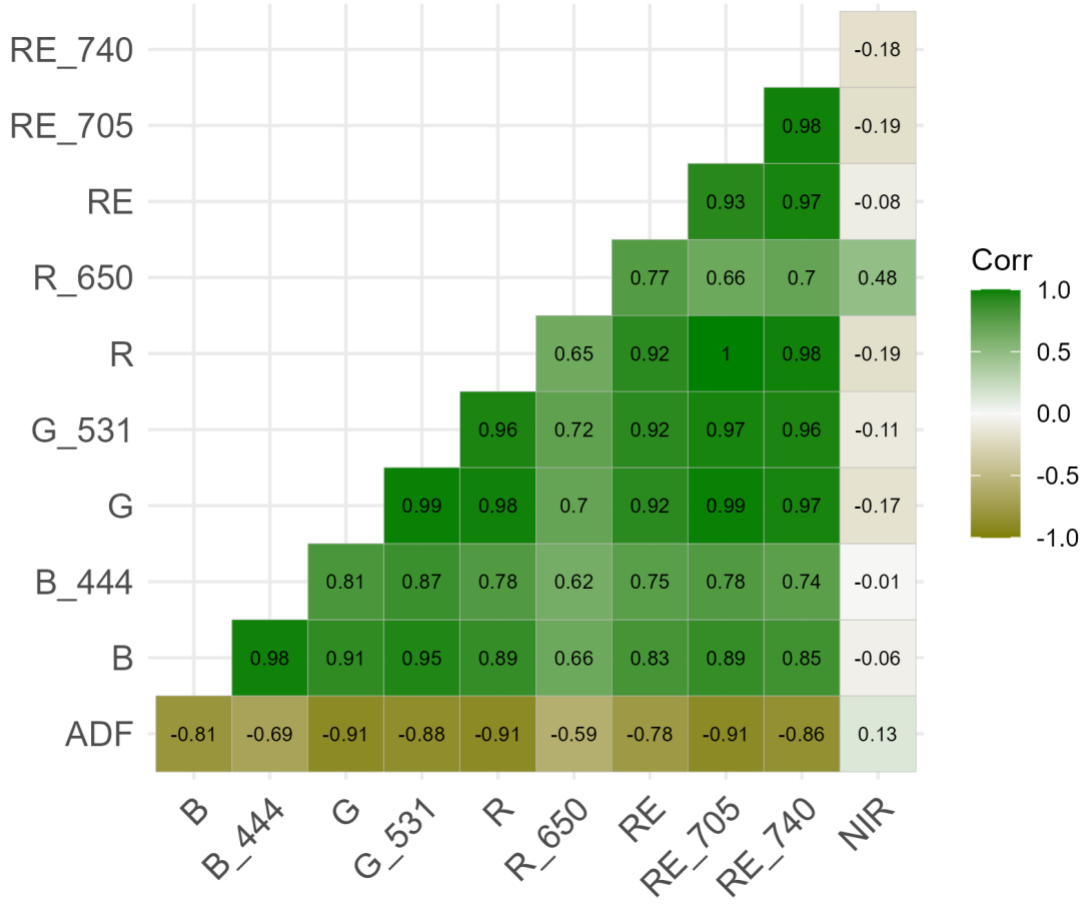

Figure 11. Correlation matrix showing the relationship between Acid Detergent Fiber (ADF) and various multispectral bands. B = Blue. G = Green. R = Red. RE = Red Edge. NIR = Near Infrared.

The vegetation indices based on the combinations of the 10 bands from the dual multispectral sensor (Figure 12) reveal that normalized difference vegetation index (NDVI 1,2), normalized difference red-edge index (NDRE 1,2,3), green normalized difference vegetation index (GNDVI 1,2), red edge chlorophyll index (CHLRE 1,2,3), and simple ratio (SR 1,2) have high to very high correlations with ADF. The MERIS Terrestrial Chlorophyll Indices (MTCI) 1 and 4

have low to very low correlations with ADF, with r values of 0.33 and 0.16, respectively. MTCI 5,2, and 6 have very low negative correlation, and MTCI 3 has a high negative correlation with ADF.

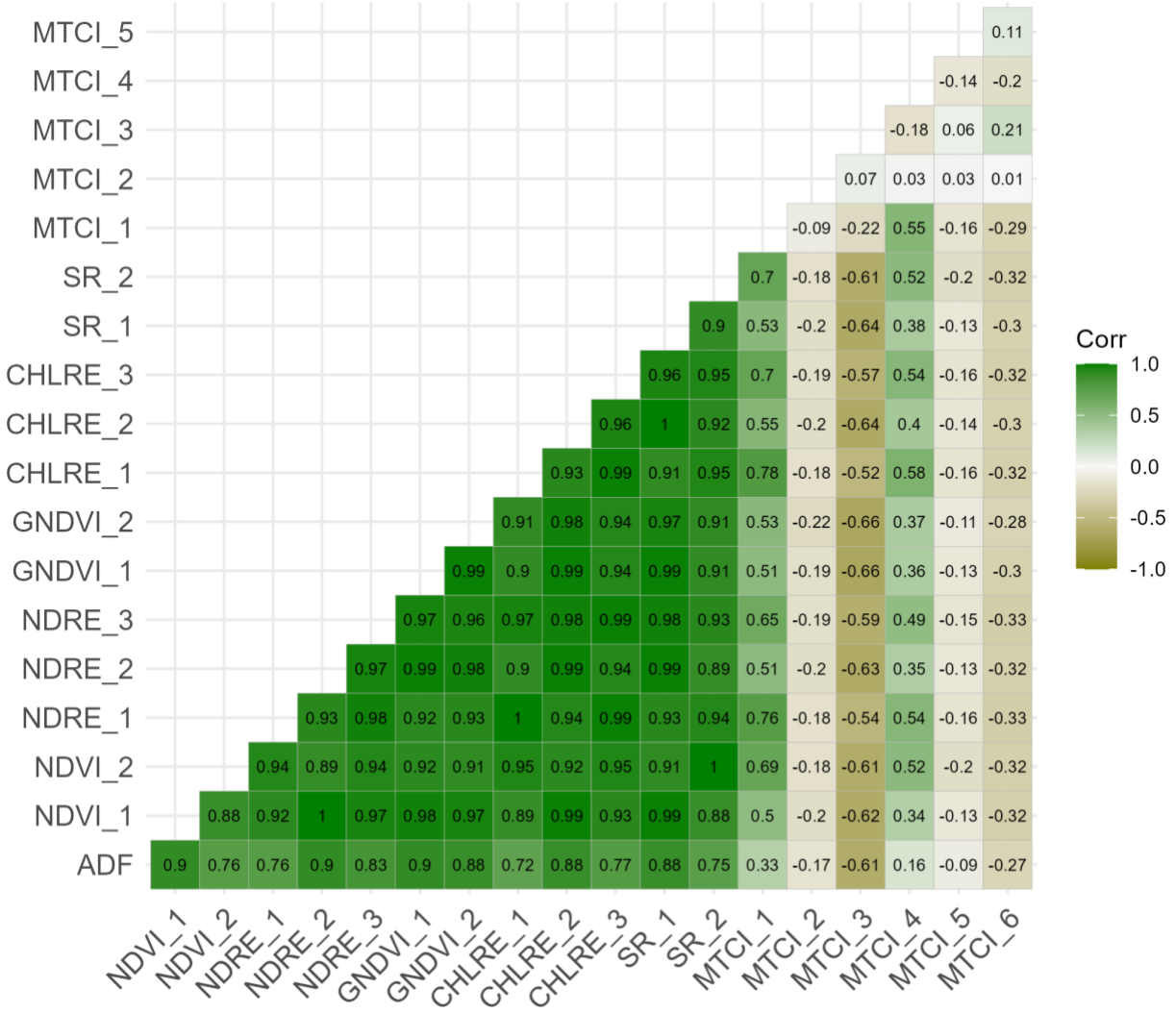

Figure 12. The correlation matrix shows the relationship between Acid Detergent Fiber (ADF) and various vegetation indices from dual multispectral cameras. NDVI = Normalized Difference Vegetation Index. NDRE = Normalized Difference Red Edge Index. GNDVI = Green Normalized Difference Vegetation Index. CHLRE = Chlorophyll Red Edge Index. SR = Simple Ratio. MTCI = MERIS Terrestrial Chlorophyll Index.

The model performance of random forest (RF) and extreme gradient boosting (XGBoost) in predicting ADF across three data types derived from three sensors, RGB, XS, and dual XS, is shown in Figure (13). The comparison is based on RMSE and R2 metrics. The dual XS data type showed the best performance when compared to RGB and XS data types, with the lowest RMSE and highest R2 values in both RF (RMSE = 1.3, R2 = 0.88) and XGBoost (RMSE = 1.41, 0.86) models. Moreover, the RF model performed better than the XGBoost model with the dual XS data type. RGB data type performed better than XS data type with lower RMSE and higher R2 in both models.

Additionally, the variable importance in the RF model with the dual XS data type shows that GNDVI 2 is the key variable in predicting ADF, followed by single bands such as B, RED 740, G 531, and G. Predominantly, the blue band (B) is the most important variable in the XGBoost model, followed by NDVI 2, RE 740, MTCI 3, and CHLRE 3.

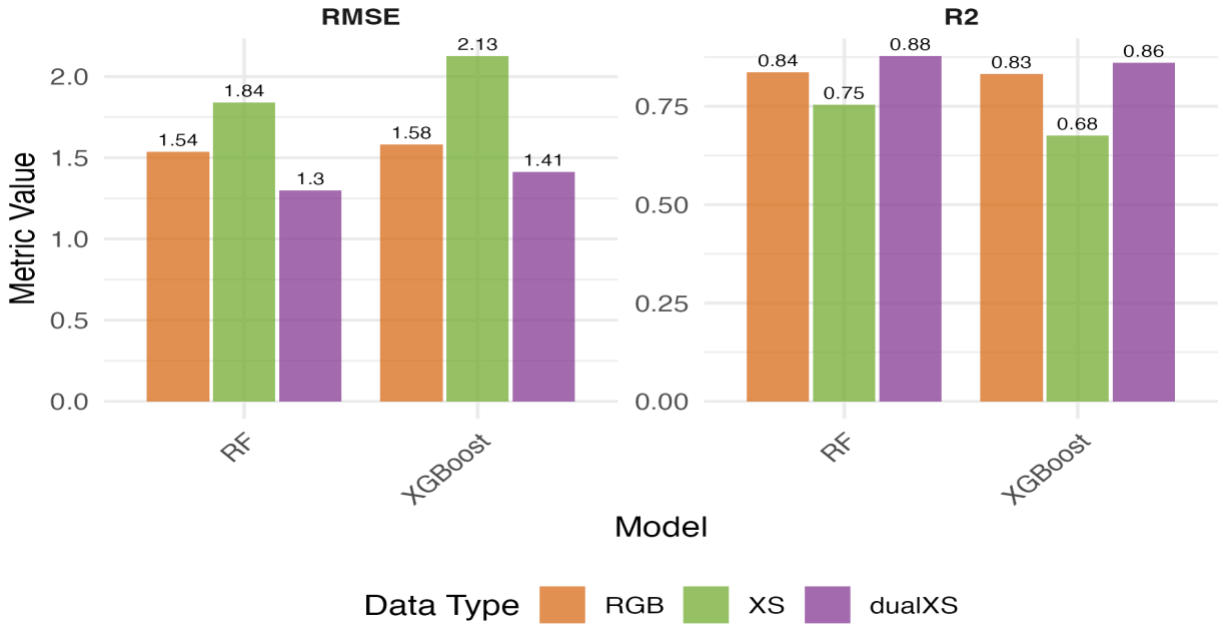

Figure 13. Random Forest and Extreme Gradient Boosting model performance in predicting Acid Detergent Fiber (ADF) across RGB, multispectral, and dual multispectral-derived sensors. RMSE

= Root Mean Square Error. R2 = Coefficient of Determination. RGB = Red, Green, Blue. XS = Multispectral. dualXS = Dual Multispectral.

Forage Quality: Neutral Detergent Fiber (NDF)

Summary Statistics

The summary statistics for neutral detergent fiber (NDF) show that the mean NDF values range from 34.67 on D2 to 43.85 on D3 (Table 17). The coefficient of variation (CV) indicates that D2 and D3 have relatively low variability, CV = 0.06 and 0.04, respectively. The standard deviation (SD) for both collecting dates is relatively low, with D1 having SD = 1.98 and D2 having SD = 1.94.

Table 17. Summary statistics of neutral detergent fiber (NDF) of alfalfa obtained from near-infrared spectroscopy.

Collecting date	Mean	Coefficent of Variation	Standard Deviation	Minimum	Maximum
D2	34.67	6 %	1.98	29.57	38.85
D3	43.85	4 %	1.94	39.90	50.05

Pearson Correlation Coefficient Between NDF and RGB Variables

The relationships between NDF and RGB variables show a similar pattern to the relationships between ADF and RGB variables (Figure 14). However, Pearson correlation coefficient values show stronger relationships of NDF with RGB than ADF. The vegetation indices, ExG (r = 0.89), GLI (r = 0.86), GRVI (r = 0.83), and VARI (r = 0.82), have very high positive correlations with NDF. Also, the green band (r = 0.87) has a high correlation with NDF, and the red (r = 0.48) and blue (r = 0.45) bands have moderate correlations.

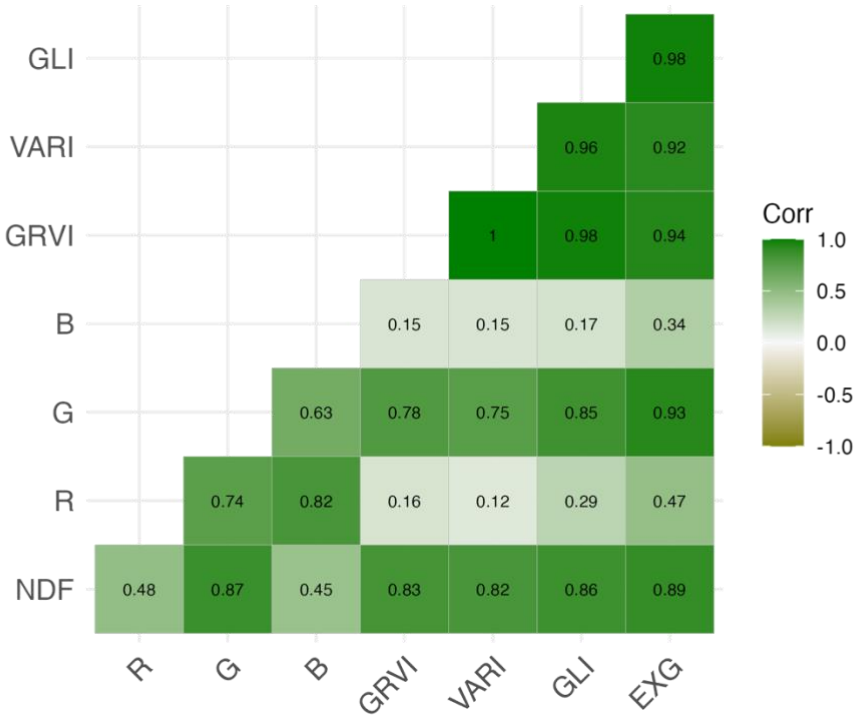

Figure 14. Relationships between Neutral Detergent Fiber (NDF) and RGB bands and vegetation indices. R = Red. G = Green. B = Blue. GRVI = Greed Red Vegetation Index. VARI = Visible Atmospherically Resistance Index. GLI = Green Lead Index. ExG = Excessive Green Index.

Pearson Correlation Coefficient Between NDF and XS Variables

The relationships between NDF and multispectral variables show that vegetation indices such as GRVI (r = 0.9) and NDVI (r = 0.9), SR (r = 0.87), and NDRE (r = 0.86) have very high positive correlations with NDF (Figure 15). The single bands, such as the NIR (r = 0.81), green (r = 0.71), and red edge (r = 0.62) bands, also exhibit a high to very high positive correlation with NDF. Notably, the red band (r = -0.91) has a very high negative correlation with NDF. Although a similar pattern of relationships can be seen in ADF, multispectral variables have stronger relationships with NDF than with ADF.

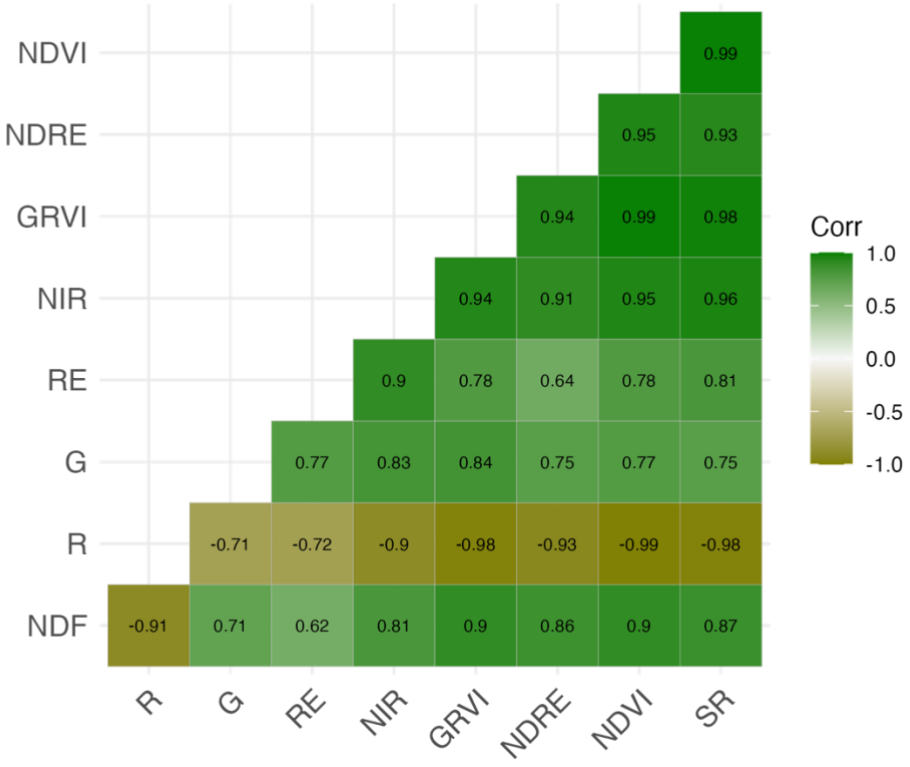

Figure 15. Relationships between Neutral Detergent Fiber (NDF) and multispectral bands and vegetation indices. R = Red. G = Green. RE = Red Edge. NIR = Near Infrared. GRVI = Green Red Vegeation Index. NDRE = Normalized Difference Red Edge. NDVI = Normalized Difference Vegetation Index. SR = Simple Ratio.

Pearson Correlation Coefficient Between NDF and Dual XS Variables

The relationships between NDF and single bands derived from dual multispectral cameras show moderate to very high negative correlations with NDF, except for the NIR band, which has a very low positive correlation with NDF (Figure 16). These results are comparable to the results of the relationships between ADF and dual XS variables.

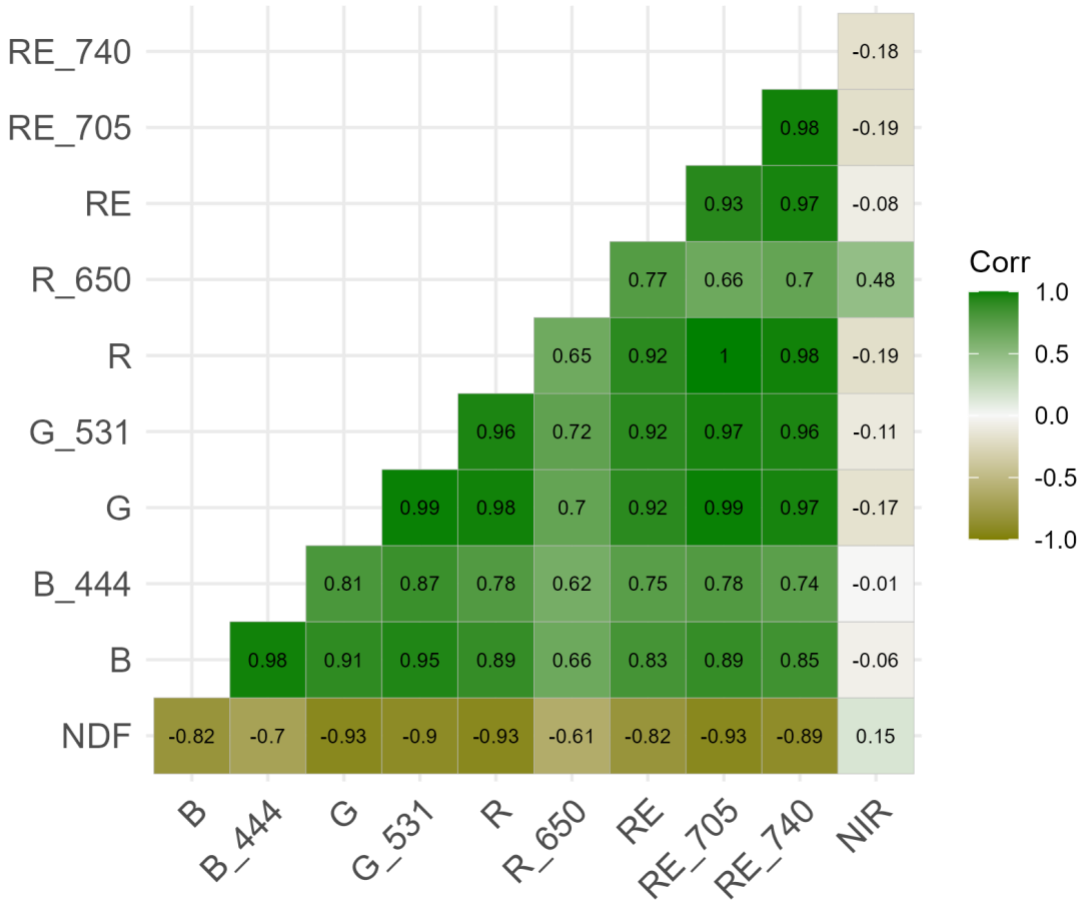

Figure 16. Correlation matrix showing the relationship between Neutral Detergent Fiber (NDF) and various multispectral bands derived from dual multispectral cameras. B = Blue. G = Green. R = Red. RE = Red Edge. NIR = Near Infrared.

The relationships between NDF and dual multispectral variables show that the vegetation indices derived from the 10 bands of the dual multispectral sensor have high to very high correlations with NDF. NDVI 1 (r = 0.92), NDRE 2 (r = 0.92), GNDVI 1 (r =0.92), GNDVI 2 (r =0.9), CHLRE 2 (0.9), SR 1(r=0.9), NDRE 3 (r = 0.86), CHLRE 3 (r = 0.81), and NDRE 1 (r = 0.8) have very high correlations with NDF (Figure 17). While NDVI 2 (r = 0.79), SR 2 (r = 0.79),

and CHLRE 1 (r=0.76) have high correlations with NDF. In contrast, the band combinations in MTCI have weak positive correlations and negative correlations with NDF.

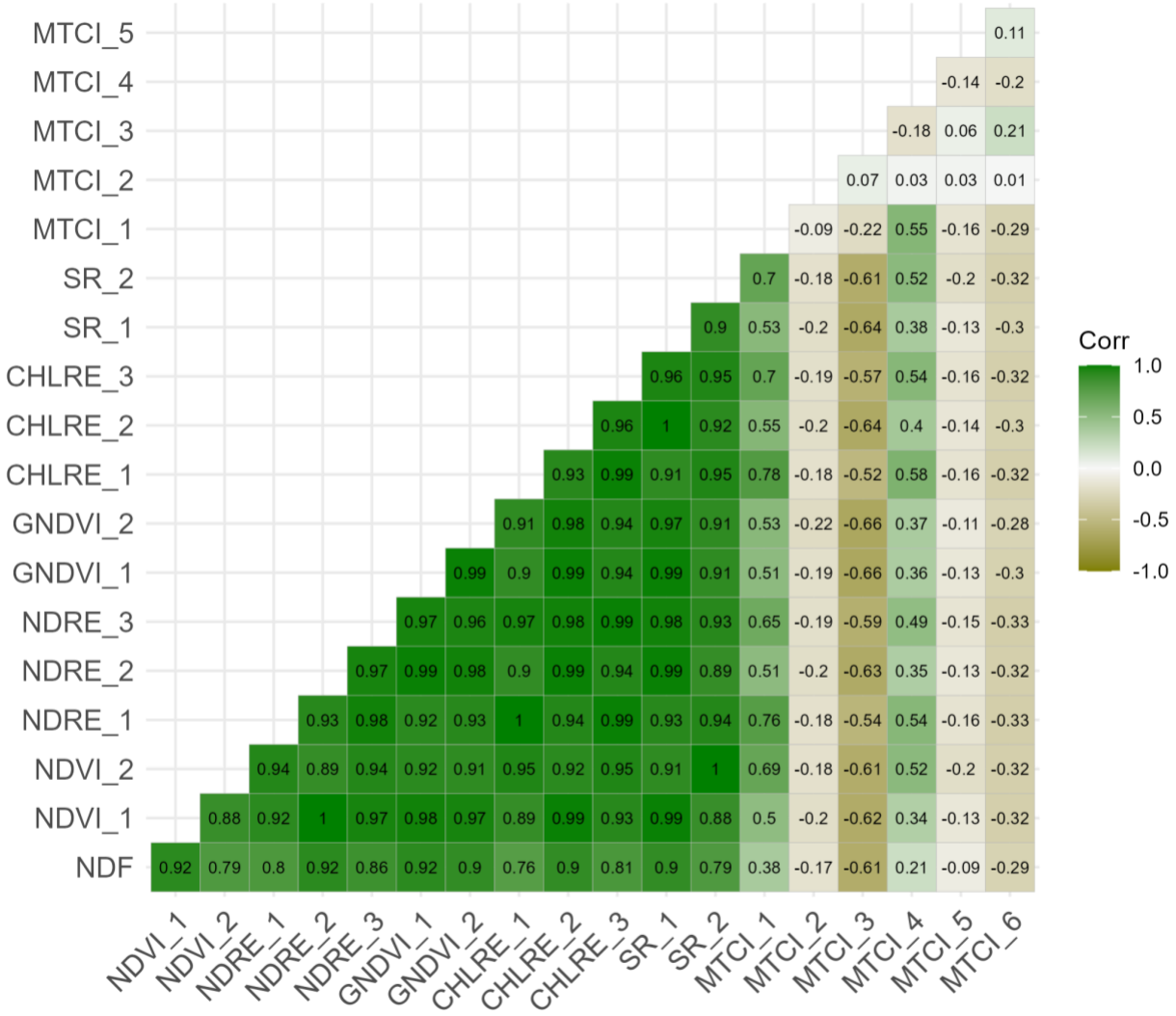

Figure 17. Correlation matrix showing the relationship between NDF and various vegetation indices from dual multispectral cameras. NDVI = Normalized Difference Vegetation Index. NDRE = Normalized Difference Red Edge Index. GNDVI = Green Normalized Difference Vegetation Index. CHLRE = Chlorophyll Red Edge Index. SR = Simple Ratio. MTCI = MERIS Terrestrial Chlorophyll Index.

The model performance of RF and XGBoost models in predicting NDF across three data types from RGB, XS, and dual XS sensors is shown in Figure (18). The dual XS data type has the best performance among the three data types in both models. The RF model has an RMSE of 1.86 and an R2 of 0.86, whereas the XGBoost model has an RMSE of 1.96 and an R2 of 0.85. This result displays a similar pattern to the performance of RF and XGBoost models with dual XS data types when predicting ADF. RGB data type outperformed XS data type with lower RMSE and higher R2 in both models. The RF model outperforms the XGBoost model with lower RMSE and higher R2 across all data types in predicting the NDF of alfalfa. Based on the variable importance analysis of the RF model with the dual XS data type, the most important variables are B 444, SR 2, NDVI, R, and CHLRE 2.

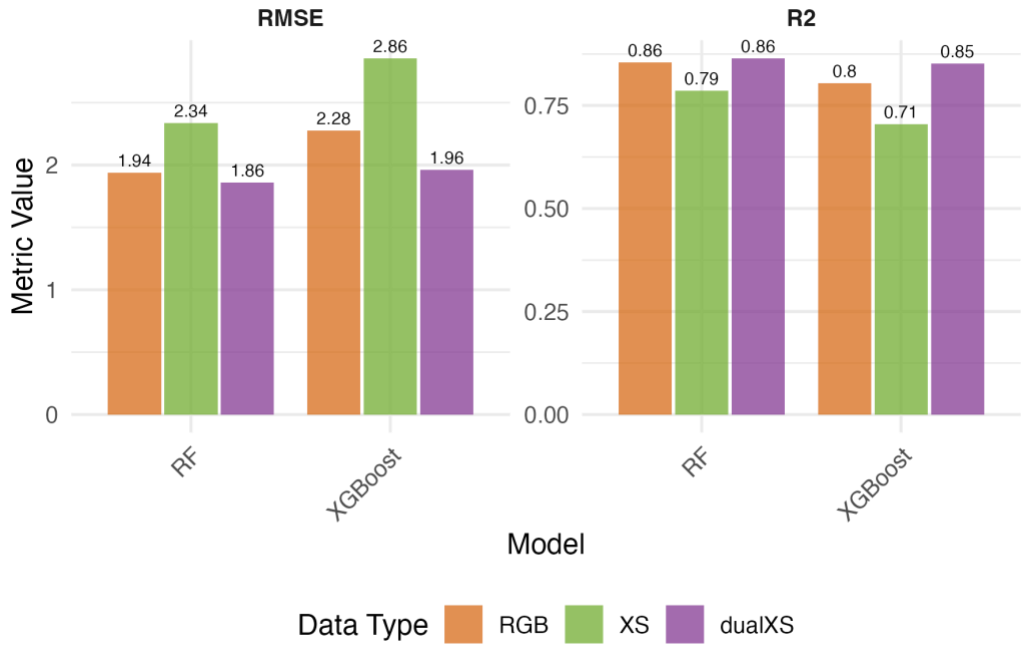

Figure 18. RF and XGBoost model performance in predicting NDF across RGB, multispectral, and dual multispectral-derived sensors. RMSE = Root Mean Square Error. R2 = Coefficient of Determination. RF = Random Forest. XGBoost = Extreme Gradient Boosting. RGB = Red, Green, Blue. XS = Multispectral. dualXS = Dual Multispectral.

Forage Quality: Crude Protein (CP)

Summary statistics

The crude protein (CP) content of alfalfa varied across the collection dates (Table 18). Higher mean CP content was observed on the second collection date (D2) at 24.05% than in D3 with 20.97%. The variability of CP content within each collection date was relatively low, with coefficients of variation (CV) of 4.5% for D2 and 6.5% for D3.

Table 18. Summary statistics of crude protein across two collecting dates.

Collection Date	Mean (cm)	Coefficient of Variation (%)	Standard Deviation	Minimum	Maximum
D2	24.05	4.5	1.09	20.75	27.23
D3	20.97	6.5	1.36	18.12	24.68

Pearson Correlation Coefficient Between CP and RGB Variables

The relationships between CP and RGB reveal that RGB variables have low to high negative correlations with CP (Figure 19). The vegetation indices, ExG (r = -0.76), GLI (r = -0.72), GRVI (r = -0.69), and VARI (r = -0.68), have high negative correlations with CP. The green band (r = -0.75) also has a high negative correlation. The red (r = -0.43) and blue (r = -0.37) have moderate and low correlations with CP, respectively. In contrast, the vegetation indices derived from the multispectral sensor exhibit high to very high positive correlations with ADF and NDF.

Pearson Correlation Coefficient Between CP and XS Variables

The relationships between CP and XS variables (Figure 20) show that the red band (r = 0.76) is the only band that has a high positive correlation with CP. The other bands and vegetation indices, G, RE, NIR, GRVI, NDVI, and SR, have high negative correlations with CP. These results are opposed to the results in ADF and NDF, wherein the red band derived from the multispectral sensor has a very high negative correlation with ADF and NDF.

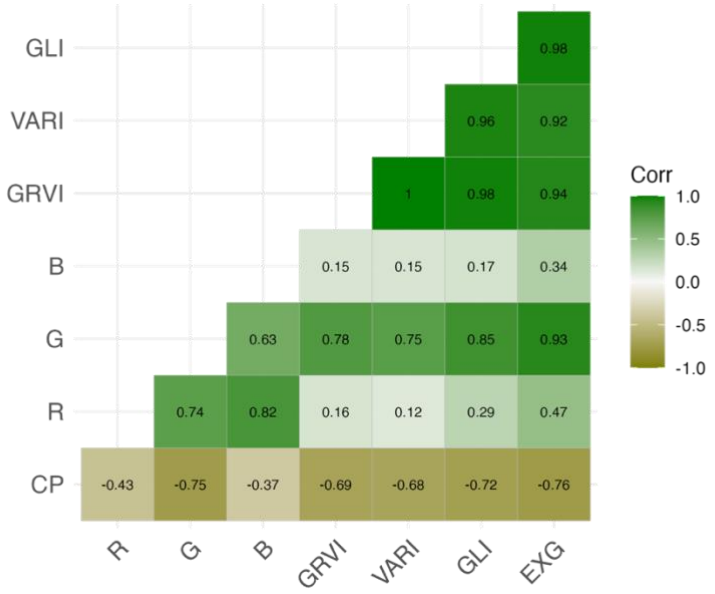

Figure 19. Relationships between Crude Protein (CP) and RGB bands and vegetation indices. R = Red. G = Green. B = Blue. GRVI = Greed Red Vegetation Index. VARI = Visible Atmospherically Resistance Index. GLI = Green Lead Index. ExG = Excessive Green Index.

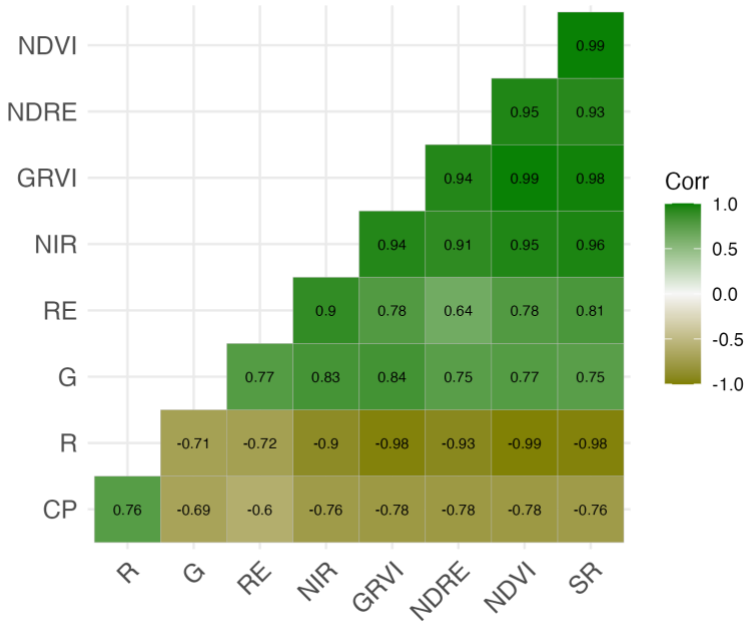

Figure 20. Relationships between Crude Protein (CP) and multispectral bands and vegetation indices. R = Red. G = Green. RE = Red Edge. NIR = Near Infrared. GRVI = Green Red Vegeation

Index. NDRE = Normalized Difference Red Edge. NDVI = Normalized Difference Vegetation Index. SR = Simple Ratio.

Pearson Correlation Coefficient Between CP and Dual XS Variables

The relationships between the CP and the single bands derived from the dual multispectral sensor are shown in Figure (21). The results show that only the NIR band has a low negative correlation with CP. The single bands with high positive correlations include G (r = 0.8), RE 705 (r = 0.78), RE 740 (r = 0.78), G 531 (0.77), R (r = 0.77), RE (r = 0.75), and B (r = 0.67). While B 444 and R 650, both have an r value of 0.58, display a moderate positive relationship with CP.

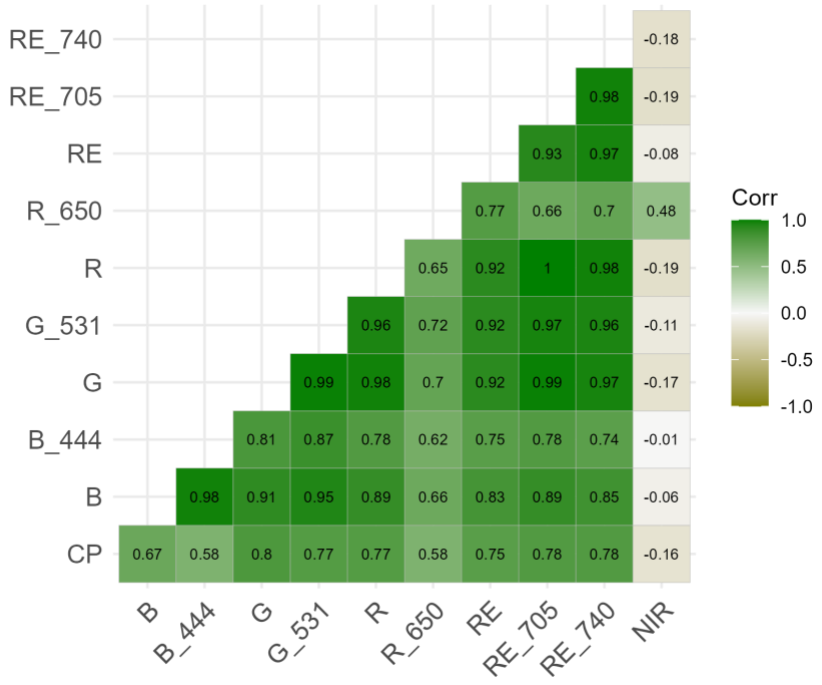

Figure 21. The correlation matrix shows the relationship between Crude Protein (CP) and various multispectral bands. B = Blue. G = Green. R = Red. RE = Red Edge. NIR = Near Infrared

The correlation matrix of the relationship between CP and vegetation indices derived from the dual multispectral sensor shows that MTCI 3 (r = 0.5) has a moderate positive correlation, MTCI 6 (r = 0.27) has a low positive correlation, MTCI 5 (r = 0.12) and MTCI 2 (r=0.09) have

very low positive correlations with CP. MTCI 1 (r=-0.46) and MTCI 2 (r=-0.39) have low to moderate negative correlation with CP (Figure 22). The other vegetation indices, NDVI (1,2,) , NDRE (1,2,3), GNDVI (1,2), CHLRE (1,2,3), SR (1,2) have high negative correlations with CP.

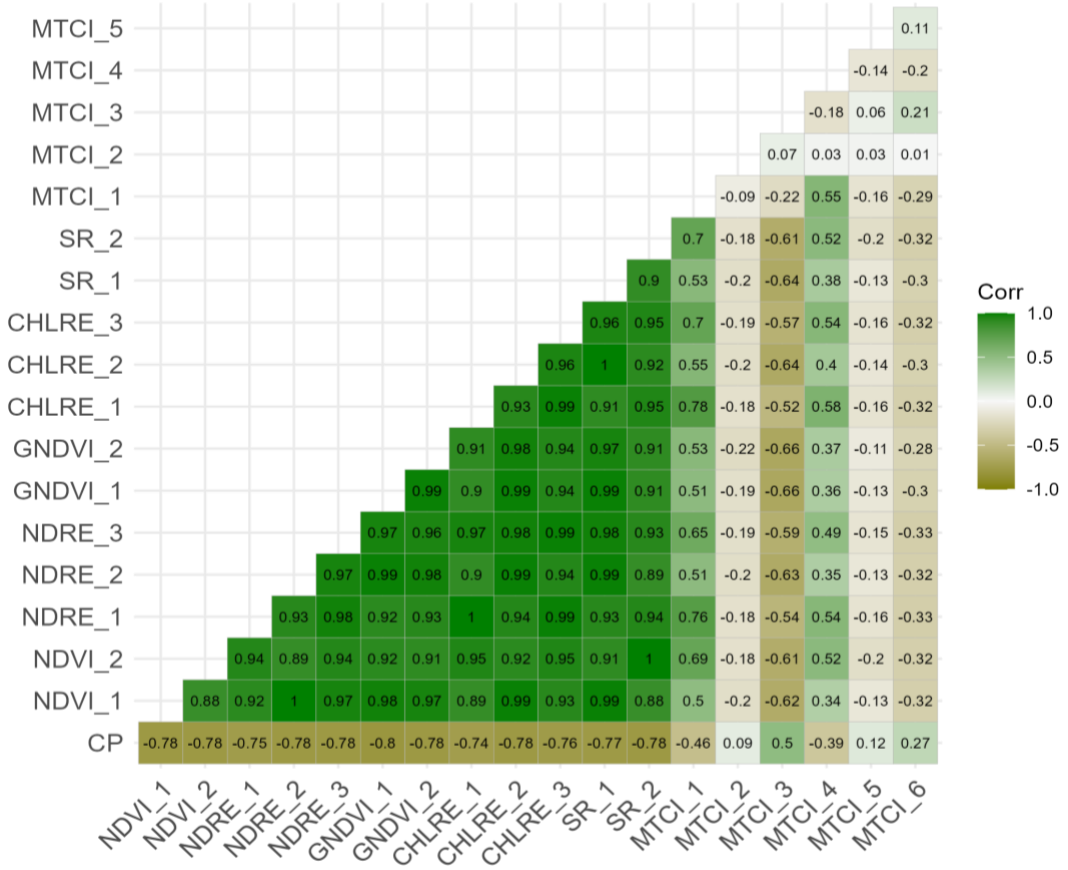

Figure 22. Correlation matrix showing the relationship between Crude Protein (CP) and various vegetation indices from dual multispectral cameras. NDVI = Normalized Difference Vegetation Index. NDRE = Normalized Difference Red Edge Index. GNDVI = Green Normalized Difference Vegetation Index. CHLRE = Chlorophyll Red Edge Index. SR = Simple Ratio. MTCI = MERIS Terrestrial Chlorophyll Index.

The performance of RF and XGBoost models in predicting CP with three data types, RGB, XS, and dualXS, reveals that the RF model outperformed the XGBoost model across all the data types (Figure 23). However, the results of the models with XS and dual XS data types are

comparable in both metrics, RMSE and R2, and both RF and XGBoost models. Both data types, XS and dual XS, have lower RMSE and higher R2 than the RGB data type. Based on the variable importance analysis, the key predictors for the RF model with dual XS data type are NDVI 2, SR 2, and GNDVI 1. For the RF model with XS data type, the key predictors are NDVI and GRVI. In contrast, the XGBoost model with dual XS data type identified B (444), GNDVI 1, and MTCI 6 as the important variables, while NDRE is the predominant predictor for the XGBoost model with XS data type.

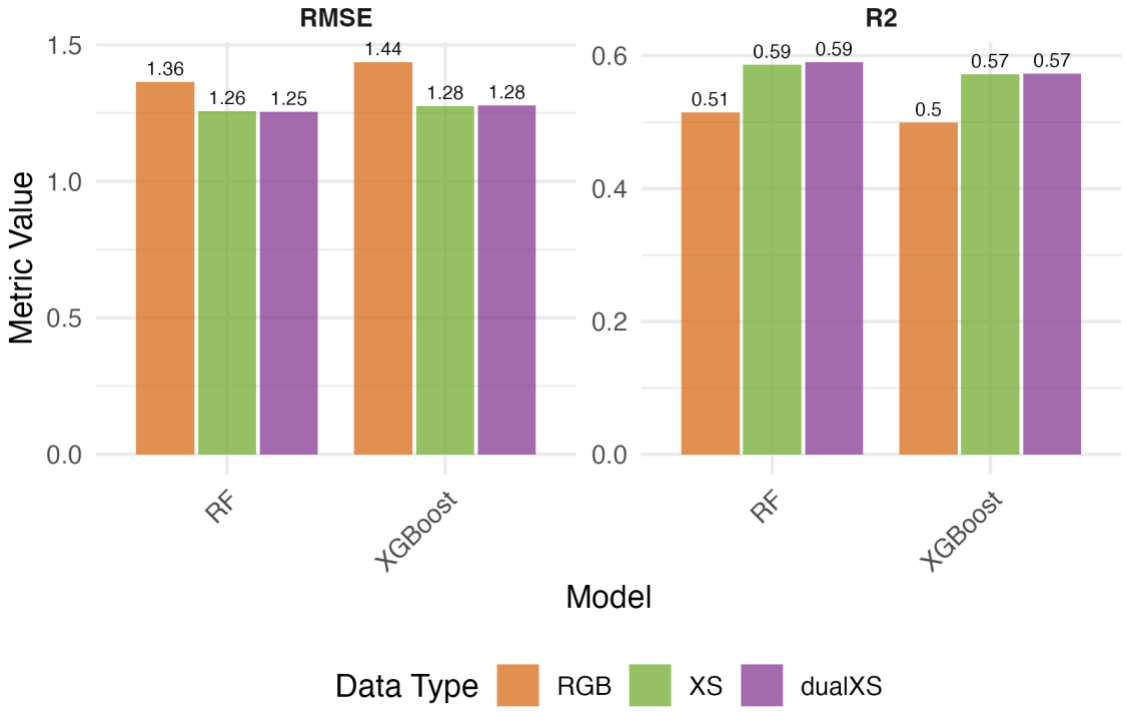

Figure 23. RF and XGBoost model performance in predicting CP across RGB, multispectral, and dual multispectral-derived sensors. RMSE = Root Mean Square Error. R2 = Coefficient of Determination. RF = Random Forest. XGBoost = Extreme Gradient Boosting. RGB = Red, Green, Blue. XS = Multispectral. dualXS = Dual Multispectral.

CHAPTER 4

DISCUSSIONS

Biomass Yield

Based on the Pearson correlation analysis, the findings suggest that RGB-based green (r = 0.57) and red (r = 0.53) bands have moderate correlations with yield. RGB-based vegetation indices such as GLI (r = 0.67) and ExG (r = 0.67) have high correlations with yield. Both vegetation indices use green, red, and blue wavelengths in their formula. While multispectral-based green band (r = 0.91) and GRVI (r = 0.86) have very strong correlations with yield. Biwas et al. (2021) found a high Pearson correlation coefficient with alfalfa herbage accumulation and NDVI, GNDVI, GRVI, and NDRE across four harvest dates. However, NDVI has a low correlation (r = 0.31) with alfalfa yield in this study. Chandel et al. (2021) also found a weak correlation of NDVI with alfalfa yield. NDVI was developed to characterize vegetation in low-biomass situations (Huete et al., 1997). It was reported to saturate at higher biomass or denser canopy coverage, which could result in reduced sensitivity at the harvest stage of alfalfa (Haboudane et al., 2004). The performance of vegetation indices varies across crop types and across different growth stages. In the case of alfalfa, the plant canopy changes across harvest dates, with denser canopy coverage corresponding to greater biomass yield. Furthermore, the biomass yield is highest on the first harvest date and decreases after succeeding harvests. The canopy structure is one of the determinants of the saturation effect of VIs (Gao et al., 2023).

Plant height is an important growth and development indicator of alfalfa yield (Jia et al., 2022). The results exhibited moderate correlations of plant height with alfalfa yield. Previous

studies by Islam et al. (2014) and Fathipoor et al. (2019) reported a high correlation of plant height with forage yield. Plant height has been integrated with vegetation indices in several studies to improve the biomass yield estimation (Bendig et al., 2015; Adak et al., 2021).

The Random Forest (RF) model outperforms XGBoost in predicting alfalfa yield. Combining red, green, blue (RGB), multispectral (XS), and plant height (PH) (RGB + XS + PH) data results in the lowest RMSE value for both RF (RMSE = 774.21) and XGBoost (RMSE = 768.2) models. Integrating plant height data with the RGB or XS data improves accuracy. These results align with those of Viljanen et al. (2018), who reported that the combination of height and RGB-based vegetation index features yielded the best estimation results for grass sward biomass yield using a Random Forest (RF) model. Similarly, Borra-Serrano et al. (2019) acquired the best estimations from combining canopy height, vegetation indices, and environmental data. Moreover, the inclusion of manually-measured plant height increased the predictive ability of the models. However, using conventional methods for measuring plant height limits the scalability and efficiency of the phenotyping process. Plant height estimation using UAS-based RGB and LiDAR sensors was done in this study to determine which sensor is more accurate in estimating alfalfa plant height.

Plant Height

Overall relationship between plant height and RGB and LiDAR metrics

The overall correlation analysis for four collecting dates and correlations for each of the 17 alfalfa entries revealed that RGB-based metrics are more effective than LiDAR-derived metrics for estimating alfalfa plant height.

For the overall correlations, RGB metrics, the 95th percentile (P95) showed the strongest correlation (r = 0.88), followed by other percentile-based height measures and vegetation indices

like GRVI, GLI, and VARI. In contrast, LiDAR metrics demonstrated moderate correlations, with the 99th percentile (P99) showing the highest correlation (r = 0.45). The 95th percentile height consistently emerged as a reliable indicator of plant height across both sensor types. Furthermore, the plant height extracted from the 95th percentile is more robust to outliers compared to the other metrics, such as the maximum height. Thus, this avoids overestimation of height due to outliers. These results suggest that both structural and spectral features extracted from RGB imagery are effective for estimating plant height in alfalfa.

The results for correlations across the 17 alfalfa entries revealed varying degrees of association between plant height and LiDAR and RGB metrics. High percentile metrics (P85-P95) for both LiDAR and RGB data exhibited moderate to very high correlations with plant height. Additionally, RGB-based vegetation indices, including GRVI, GLI, and VARI, showed high correlations with plant height across all entries, highlighting their potential utility in estimating plant height. These findings suggest that RGB metrics, particularly high percentile values and vegetation indices, can be effective in capturing plant height variability in alfalfa.

High-percentile metrics of RGB and LiDAR data have been consistent in having moderate to very high correlations with plant height across all collecting dates and across the alfalfa entries. These findings are consistent with prior studies. For example, Tirado et al. (2020) identified the 97th percentile as a suitable metric for maize plant height estimation using UAS remote sensing. They utilized SfM to obtain plant height from RGB cameras. Zhang et al. (2018) also demonstrated the usefulness of basic statistical features such as mean, median, minimum, maximum, and standard deviation derived from canopy surface models (CSMs) generated from RGB imagery.

The strong performance of high-percentile metrics in the current study supports their continued use in UAS-based plant height prediction.

Differences in sensor performance may also be related to the crop's growth stage. Magar et al. (2025) found that LiDAR sensors outperformed RGB cameras for plant height estimation during the early growth stages of soybean. However, RGB metrics were more accurate at physiological maturity. A similar pattern was observed in this study, which was conducted during the harvesting stage of alfalfa, where RGB-derived metrics showed stronger correlations with plant height than those from LiDAR. This suggests that RGB imagery may offer greater predictive accuracy during later stages of crop development, potentially due to increased canopy density and improved spectral signal.

In summary, the results highlight the superior performance of RGB-based metrics, particularly high-percentile height values and vegetation indices, for estimating alfalfa plant height at the harvest stage. These findings highlight the importance of selecting sensor types and features that are appropriate for the crop's growth stage to enhance the accuracy of UAS-based phenotyping.

SfM-derived RGB Metrics

SfM-derived RGB metrics have the highest correlations with plant height in D4. The mean, P99, P80, P85, and maximum RGB showed the highest correlations with r values of 0.9, 0.9, 0.89, 0.85, and 0.85, respectively. While SfM-derived RGB metrics showed the lowest correlations in D3, with very low and negative correlations with plant height. In D1, SfM-derived RGB metrics

such as P80, P85, P90, and P95 also showed very high correlations, while in D2, they showed low to moderate correlations.

The results show that the relationships of SfM-derived RGB metrics vary with the collecting date. Furthermore, RGB metrics in D4 have the highest correlations with plant height across all metrics among the collection dates. In D4, the canopy density is less dense as the growth of alfalfa is slower due to cooler temperatures than the other collecting dates. Negative correlations resulted from SfM-derived RGB metrics and plant height in D3. In D3, the plants have overgrown due to a larger gap in collecting date, resulting in a higher percentage of lodged plants. Additionally, the canopy is denser in D3. While D1 and D2 have moderately dense canopies. In D1, SfM-derived RGB metrics have high correlations with plant height in P80, P85, P90, and P95, while other metrics, such as mean, median, and P99 have low correlations. In D2, only maximum RGB, P95, and P99 have moderate correlations with plant height. Holman et al., (2016) calculated the average plot heights from the 99th percentile to isolate the upper photosynthetic tissue of each plant. Also, Watanabe et al. (2017) concluded that more accurate plant height estimation of sorghum could be achieved by using the 90th-99th percentile. The 90th -99th percentile is selected over the mean and median for plant height estimation in UAS-based remote sensing since they represent the tallest height of the plants and have less noise than the maximum plant height (Fujiwara et al., 2022).

RGB-based Vegetation Indices

RGB-based vegetation indices, including GRVI, VARI, GLI, and EXG, exhibit high correlation in D4 and D2, whereas they show low correlations in D1 and D3. Although in D3, RGB-based vegetation indices have better correlation with plant height than the SfM-derived RGB metrics. The high correlations observed in D4 and D2 may be attributed to the erect stature and

overall good health of the plants. Additionally, the plants are not overgrown. In contrast, D1 and D3 exhibit dense crop canopies, which could lead to spectral saturation and, consequently, misestimation of values. Correlating vegetation indices with plant height has been done by Ferraz et al. (2024) and they noted high correlations with maize plant height and vegetation indices derived from PlanetScope, NDVI (r = 0.80), NDRE (r = 0.78), and GNDVI (r = 0.81). Payero et al. (2004) used several vegetation indices to estimate the plant height of alfalfa. Although they mainly used NIR and red-based vegetation indices, they found that above 0.40 m, several vegetation indices become less sensitive to plant height.

LiDAR-derived Metrics

The highest correlation of LiDAR-derived metrics was observed in D1, followed by D4, then D2. While both RGB and LiDAR-based metrics have low correlations with plant height in D3, LiDAR metrics have better correlations with plant height. The LiDAR metrics, including mean, median, P80, P85, P90, and P95, have better correlations with plant height than maximum and P99 across all collecting dates. Sheffield et al. (2019) suggested that the optimum value for estimating alfalfa canopy height is the 95th percentile of LiDAR-measured height.

Machine learning models

For plant height estimation, the combination of spectral and structural data, RGB + LiDAR data type, has the lowest RMSE and the highest R2 among the three machine learning models, RF (RMSE = 4.22, R2 = 0.96), XGBoost (RMSE = 4.55, R2 = 0.95), and Elastic Net (RMSE = 6.23, R2 = 0.91). Vegetation indices have been used by several studies to estimate plant height (Payero et al., 2004). Integration of LiDAR and multispectral data by Barzafkan et al. (2025) enhanced plant height predictions in pulse crops.

Forage Quality

The Pearson correlation coefficient analysis reveals that ADF and NDF have high to very high correlation with the vegetation indices derived from RGB (GRVI, VARI, GLI, and ExG), multispectral (GRVI, NDRE, NDVI, and SR), and dual multispectral sensors (NDVI, NDRE, GNDVI, CHLRE, and SR). In contrast, single bands derived from the dual multispectral sensor have negative correlations with ADF and NDF, except for NIR. The dual XS data type outperformed the RGB and XS data types in predicting the ADF and NDF of alfalfa.

Vegetation indices from various remote sensing sensors and methods have been utilized to estimate and predict forage quality (Kawamura et al., 2005; Geipel, 2021; Kumar et al., 2022; Lo et al., 2024). Wejisingha (2020) reported that normalized difference spectral indices and spectral ratios performed better than single band models in a linear regression analysis with CP and ADF. In this study, Pearson correlation analysis between vegetation indices showed stronger relationships between vegetation indices and forage quality, CP, ADF, and NDF, than single bands. Also, the key predictors for crude protein (CP) estimation using the RF model were NDVI 2 and SR 2 with dual XS data, and NDVI and GRVI with XS data.

Zwick et al. (2024) evaluated several models to predict forage quantity and quality using multispectral sensors and vegetation indices, and their results showed that the RF model and XGBoost models are included in the best-performing algorithms. In this study, the RF model mostly outperformed the XGBoost model with lower RMSE and higher R2 across different data types and in predicting various forage quality parameters. Fernández-Habas et al. (2022) reported R2 of 0.70 and an RMSE of 2.95 in predicting CP using an RF model. Feng et al. (2021) used UAS-based hyperspectral imagery and developed a multitask learning (MTL) model to estimate CP, ADF, and ash-corrected NDF (aNDF), in alfalfa, and their results showed that MTL

outperformed the single task models, including RF. Although RF has better performance than the other single task models, SVR, ANN, and STL.

RGB variables have lower correlation with CP and lower RF, and XGBoost model performance compared to XS and dual XS data types. Askari et al. (2019) reported that the NIR range had the most effect on the estimation of CP in grass. XS and dual XS sensors have NIR wavelengths; therefore, they have better sensitivity to CP.

CHAPTER 5

CONCLUSIONS

Increasing the biomass yield is the primary target of plant breeding programs. Plant phenotyping is important to characterize and evaluate the yield trials. However, manual techniques are a bottleneck in developing novel and improved cultivars. Alfalfa, a perennial species, would need to be characterized several times per year, making the breeding program for this important crop labor-intensive and resource-consuming. This study aimed to explore the use of unmanned aerial systems (UAS) based high-throughput phenotyping (HTP) to overcome one of the major bottlenecks in breeding alfalfa. It has explored RGB, multispectral, and LiDAR sensors to predict and estimate yield, plant height, and forage quality. Furthermore, spectral and structural data have been extracted from the sensors to be correlated to the field data of biomass yield, plant height, and forage quality.

Pearson correlation analysis revealed that RGB-based GLI and ExG showed high correlations with yield, and multispectral-based G and GRVI showed very high correlations with alfalfa yield. Additionally, integrating RGB, multispectral, and plant height data resulted in higher prediction accuracy for yield. Between RGB and multispectral sensors, RGB is low-cost and can provide spectral and structural data. However, multispectral sensors capture more specific spectral data and extend beyond red, green, and blue wavelengths. Vegetation indices with red edge and near-infrared wavelengths have shown advantages in estimating different plant traits. Also, with radiometric calibration, multispectral sensors provide more accurate results since they account for radiance variations throughout the flight.

Plant height is an important yield component of many crops, as taller plants generally have higher yields. In this study, spectral and structural data from RGB were obtained. Also, RGB-based vegetation indices became important features in the prediction of alfalfa plant height. Point cloud data from LiDAR was also utilized in this study. Pearson correlation analysis revealed that RGB-based metrics have stronger correlations than LiDAR metrics. Also, higher percentile metrics, such as percentiles greater than 85, resulted in higher correlation and higher predictive accuracy of machine learning models. Random forest and XGBoost have superior performance in predicting alfalfa plant height across different data types of RGB and LiDAR metrics. The combination of spectral and structural data, RGB + LiDAR data type, has the superior performance across different machine learning models, with the lowest RMSE and the highest R2 among the three machine learning models, RF, XGBoost, and ElasticNet. Moreover, when considering UAS-based RGB or LiDAR sensors for plant height, the trade-offs between using different sensors are crucial for optimizing the performance and predictability. RGB-based sensors are low-cost and offer high-resolution images, wherein vegetation indices and using SfM, plant height data can be extracted. However, they are limited in capturing data beyond the red, green, and blue bands. LiDAR provides highly accurate 3D point clouds for plant height measurement, but it is high-cost and more complex to operate.

Forage quality, such as ADF, NDF, and CP, is an important characteristic of forage crops. Quantifying them would allow farmers to allocate feed rations and optimize profitability. However, studies on estimating the forage quality of alfalfa using UAS are very limited. The results of this study reveal a high correlation of vegetation indices derived from RGB, multispectral, and dual multispectral sensors. ADF and NDF have a high to very high correlation with the vegetation indices derived from RGB (GRVI, VARI, GLI, and ExG) multispectral (GRVI,

NDRE, NDVI, and SR) dual multispectral sensors (NDVI, NDRE, GNDVI, CHLRE, and SR). Single bands from the dual multispectral sensor exhibit negative correlations with ADF and NDF, except for the NIR band. RGB variables have lower correlations with CP compared to XS and dual XS data. The RF algorithm mostly outperformed the XGBoost model with different data types and in predicting various forage quality parameters. The best performing model across the forage quality parameters is the RF model with dual XS data type.

In predicting yield, plant height, and forage quality of alfalfa, this study shows that using a multimodal approach, which combines different sensors such as RGB, multispectral, and LiDAR in measuring different traits, and fusion of different data types from different sensors can provide more accurate results. Integrating RGB and multispectral data in estimating yield increased model accuracy. The combination of spectral and structural data, RGB + LiDAR data type, has the highest accuracy in predicting alfalfa height. The dual multispectral sensor showed the most accurate prediction of forage quality.

Various data types from different sensors were explored to predict alfalfa traits using multiple machine learning models. Among these models, Random Forest emerged as the most effective algorithm across different traits and data types, efficiently handling high-dimensional data and identifying key features.

The results of this study showed the potential of UAS-based sensors such as RGB, multispectral, and LiDAR in estimating biomass yield, plant height, and forage quality to increase the speed in alfalfa breeding. It has explored various metrics from different sensors and has also explored spectral and structural data. However, this is limited to one year of harvest data only and only limited to one location. The data could be extended to several years and locations to increase

scope, precision, and accuracy. Environmental data could be included to develop more accurate predictive models for different alfalfa traits. Future research can be expanded to integrate other sensors, such as hyperspectral, to increase correlations and model performance in estimating alfalfa traits.

REFERENCES

Askari, M. S., McCarthy, T., Magee, A., & Murphy, D. J. (2019). *Evaluation of grass quality under different soil management scenarios using remote sensing techniques. Remote Sens. 11, 1835*.

Barzin, R., Pathak, R., Lotfi, H., Varco, J., & Bora, G. C. (2020). Use of UAS multispectral imagery at different physiological stages for yield prediction and input resource optimization in corn. *Remote Sensing*, *12*(15), 2392.

Bendig, J., Yu, K., Aasen, H., Bolten, A., Bennertz, S., Broscheit, J., ... & Bareth, G. (2015). Combining UAV-based plant height from crop surface models, visible, and near infrared vegetation indices for biomass monitoring in barley. *International Journal of Applied Earth Observation and Geoinformation*, *39*, 79-87.

Biswas, A., Andrade, M. H. M. L., Acharya, J. P., de Souza, C. L., Lopez, Y., de Assis, G., ... & Rios, E. F. (2021). Phenomics-assisted selection for herbage accumulation in alfalfa (Medicago sativa L.). Frontiers in Plant Science, 2763.

Capstaff, N. M., & Miller, A. J. (2018). Improving the yield and nutritional quality of forage crops. *Frontiers in Plant Science*, *9*, 535.

Cates, A. M., Ruark, M. D., Hedtcke, J. L., & Posner, J. L. (2016). Long-term tillage, rotation and perennialization effects on particulate and aggregate soil organic matter. *Soil and Tillage Research*, *155*, 371-380

Cazenave, A. B., Shah, K., Trammell, T., Komp, M., Hoffman, J., Motes, C. M., & Monteros, M. J. (2019). High-Throughput Approaches for Phenotyping Alfalfa Germplasm under Abiotic Stress in the Field. The Plant Phenome Journal, 2(1), 1-13.

Chang, A., Jung, J., Maeda, M. M., Landivar, J. A., Carvalho, H. D., & Yeom, J. (2020). Measurement of cotton canopy temperature using radiometric thermal sensor mounted on the unmanned aerial vehicle (UAV). *Journal of Sensors*, *2020*.

Chang, A., Jung, J., Yeom, J., Maeda, M. M., Landivar, J. A., Enciso, J. M., ... & Anciso, J. R. (2021). Unmanned aircraft system-(UAS-) based high-throughput phenotyping (HTP) for tomato yield estimation. *Journal of Sensors*, *2021*, 1-14.

Chawade A., van Ham J., Blomquist H., Bagge O., Alexandersson E., Ortiz R. (2019). High-Throughput field-phenotyping tools for plant breeding and precision agriculture. *Agronomy* 9(5), 258. 10.3390/agronomy9050258

Creech, E., Yost, M., Cardon, G., Ransom, C., & Clark, J. (2020). Considerations for crop rotation from alfalfa to corn.

Dash, J., & Curran, P. J. (2004). The MERIS terrestrial chlorophyll index.

de Castro, A. I., Ehsani, R., Ploetz, R. C., Crane, J. H., & Buchanon, S. (2015). Detection of laurel wilt disease in avocado using low altitude aerial imaging. *PloS one*, *10*(4), e0124642.

De Swaef, T., Maes, W. H., Aper, J., Baert, J., Cougnon, M., Reheul, D., ... & Lootens, P. (2021). Applying RGB-and thermal-based vegetation indices from UAVs for high-throughput field phenotyping of drought tolerance in forage grasses. Remote Sensing, 13(1), 147.

Duan, B., Fang, S., Zhu, R., Wu, X., Wang, S., Gong, Y., & Peng, Y. (2019). Remote estimation of rice yield with unmanned aerial vehicle (UAV) data and spectral mixture analysis. *Frontiers in plant science*, *10*, 204.

Fan, J., Zhou, J., Wang, B., de Leon, N., Kaeppler, S. M., Lima, D. C., & Zhang, Z. (2022). Estimation of Maize Yield and Flowering Time Using Multi-Temporal UAV-Based Hyperspectral Data. *Remote Sensing*, *14*(13), 3052.

Feng, L., Zhang, Z., Ma, Y., Sun, Y., Du, Q., Williams, P., ... & Luck, B. (2021). Multitask learning of alfalfa nutritive value from UAV-based hyperspectral images. *IEEE Geoscience and Remote Sensing Letters*, *19*, 1-5.

Fernández-Habas, J., Cañada, M. C., Moreno, A. M. G., Leal-Murillo, J. R., González-Dugo, M. P., Oar, B. A., ... & Fernández-Rebollo, P. (2022). Estimating pasture quality of Mediterranean grasslands using hyperspectral narrow bands from field spectroscopy by Random Forest and PLS regressions. *Computers and Electronics in Agriculture*, *192*, 106614.

Ferraz, M. A. J., Barboza, T. O. C., Arantes, P. D. S., Von Pinho, R. G., & Santos, A. F. D. (2024). Integrating satellite and UAV technologies for maize plant height estimation using advanced machine learning. *AgriEngineering*, *6*(1), 20-33.

Fujiwara, R., Kikawada, T., Sato, H., & Akiyama, Y. (2022). Comparison of remote sensing methods for plant heights in agricultural fields using unmanned aerial vehicle-based structure from motion. *Frontiers in Plant Science*, *13*, 886804.

Geipel, J., Bakken, A. K., Jørgensen, M., & Korsaeth, A. (2021). Forage yield and quality estimation by means of UAV and hyperspectral imaging. *Precision Agriculture*, *22*, 1437-1463.

Genangeli, A., Avola, G., Bindi, M., Cantini, C., Cellini, F., Grillo, S., ... & Gioli, B. (2023). Low-Cost Hyperspectral Imaging to Detect Drought Stress in High-Throughput Phenotyping. *Plants*, *12*(8), 1730.

Gitelson, A. A., Kaufman, Y. J., & Merzlyak, M. N. (1996). Use of a green channel in remote sensing of global vegetation from EOS-MODIS. *Remote sensing of Environment*, *58*(3), 289-298.

Gitelson, A. A., Kaufman, Y. J., Stark, R., & Rundquist, D. (2002). Novel algorithms for remote estimation of vegetation fraction. *Remote sensing of Environment*, *80*(1), 76-87.

Gitelson, A. A., Keydan, G. P., & Merzlyak, M. N. (2006). Three-band model for noninvasive estimation of chlorophyll, carotenoids, and anthocyanin contents in higher plant leaves. *Geophysical research letters*, *33*(11).

Holman, F. H., Riche, A. B., Michalski, A., Castle, M., Wooster, M. J., & Hawkesford, M. J. (2016). High throughput field phenotyping of wheat plant height and growth rate in field plot trials using UAV based remote sensing. *Remote Sensing*, *8*(12), 1031.

Fu, Y. B. (2015). Understanding crop genetic diversity under modern plant breeding. *Theoretical and Applied Genetics*, *128*, 2131-2142.

Hojilla-Evangelista, M. P., Selling, G. W., Hatfield, R., & Digman, M. (2017). Extraction, composition, and functional properties of dried alfalfa (Medicago sativa L.) leaf protein. *Journal of the Science of Food and Agriculture*, *97*(3), 882-888.

Holman, F. H., Riche, A. B., Michalski, A., Castle, M., Wooster, M. J., & Hawkesford, M. J. (2016). High throughput field phenotyping of wheat plant height and growth rate in field plot trials using UAV based remote sensing. *Remote Sensing*, *8*(12), 1031.

Kawamura, K., Akiyama, T., Yokota, H. O., Tsutsumi, M., Yasuda, T., Watanabe, O., & Wang, S. (2005). Comparing MODIS vegetation indices with AVHRR NDVI for monitoring the forage quantity and quality in Inner Mongolia grassland, China. *Grassland Science*, *51*(1), 33-40.

Khuimphukhieo, I., Marconi, T., Enciso, J., & da Silva, J. A. (2023). The use of UAS-based high throughput phenotyping (HTP) to assess sugarcane yield. Journal of Agriculture and Food Research, 100501.

Kingston-Smith, A. H., Marshall, A. H., & Moorby, J. M. (2013). Breeding for genetic improvement of forage plants in relation to increasing animal production with reduced environmental footprint. *Animal*, *7*(s1), 79-88. Li, B., Xu, X., Han, J., Zhang, L., Bian, C., Jin, L., & Liu, J. (2019). The estimation of crop emergence in potatoes by UAV RGB imagery. *Plant Methods*, *15*(1), 1-13.

Li, F., Piasecki, C., Millwood, R. J., Wolfe, B., Mazarei, M., & Stewart Jr, C. N. (2020). High-throughput switchgrass phenotyping and biomass modeling by UAV. Frontiers in Plant Science, 11, 574073.

Lo, A., Diouf, A. A., Leroux, L., Tagesson, T., Fensholt, R., Mottet, A., ... & Diedhiou, I. (2024). Remote sensing-based assessment of dry-season forage quality for improved rangeland management in Sahelian ecosystems. *Rangeland Ecology & Management*, *96*, 94-104.

Louhaichi, M., Borman, M. M., & Johnson, D. E. (2001). Spatially located platform and aerial photography for documentation of grazing impacts on wheat. *Geocarto International*, *16*(1), 65-70.

Lu, J., Cheng, D., Geng, C., Zhang, Z., Xiang, Y., & Hu, T. (2021). Combining plant height, canopy coverage and vegetation index from UAV-based RGB images to estimate leaf nitrogen concentration of summer maize. *Biosystems Engineering*, *202*, 42-54.

Madec, S., Baret, F., De Solan, B., Thomas, S., Dutartre, D., Jezequel, S., ... & Comar, A. (2017). High-throughput phenotyping of plant height: comparing unmanned aerial vehicles and ground LiDAR estimates. *Frontiers in plant science*, *8*, 2002.

Ninomiya, S. (2022). High-throughput field crop phenotyping: current status and challenges. *Breeding Science*, *72*(1), 3-18. Niu, Y., Zhang, L., Zhang, H., Han, W., & Peng, X. (2019). Estimating above-ground biomass of maize using features derived from UAV-based RGB imagery. *Remote Sensing*, *11*(11), 1261.

Patrick, A., Pelham, S., Culbreath, A., Holbrook, C. C., De Godoy, I. J., & Li, C. (2017). High throughput phenotyping of tomato spot wilt disease in peanuts using unmanned aerial systems and multispectral imaging. *IEEE Instrumentation & Measurement Magazine*, *20*(3), 4-12.

Payero, J. O., Neale, C. M. U., & Wright, J. L. (2004). Comparison of eleven vegetation indices for estimating plant height of alfalfa and grass. *Applied Engineering in Agriculture*, *20*(3), 385-393.

Pittman, J. J., Arnall, D. B., Interrante, S. M., Wang, N., Raun, W. R., & Butler, T. J. (2016). Bermudagrass, wheat, and tall fescue crude protein forage estimation using mobile-platform, active-spectral and canopy-height data. Crop Science, 56(2), 870-881.

POWO (2023). "Plants of the World Online. Facilitated by the Royal Botanic Gardens, Kew. Published on the Internet; http://www.plantsoftheworldonline.org/

Sapkota, A., Haghverdi, A., & Montazar, A. (2023). Estimating fall-harvested alfalfa (Medicago sativa L.) yield using unmanned aerial vehicle–based multispectral and thermal images in southern California. *Agrosystems, Geosciences & Environment*, *6*(2), e20392.

Singh, A. K., Singh, A., Sarkar, S., Ganapathysubramanian, B., Schapaugh, W., Miguez, F. E., ... & Zhang, J. (2021). High-throughput phenotyping in soybean. *High-throughput crop phenotyping*, 129-163.

Qiu, R., Wei, S., Zhang, M., Li, H., Sun, H., Liu, G., & Li, M. (2018). Sensors for measuring plant phenotyping: A review. *International Journal of Agricultural and Biological Engineering*, *11*(2), 1-17.

Ruckle, M. E., Meier, M. A., Frey, L., Eicke, S., Kölliker, R., Zeeman, S. C., & Studer, B. (2017). Diurnal leaf starch content: an orphan trait in forage legumes. *Agronomy*, *7*(1), 16.

Rushing, J. B., Saha, U. K., Lemus, R., Sonon, L., & Baldwin, B. S. (2016). Analysis of some important forage quality attributes of Southeastern Wildrye (Elymus glabriflorus) using near-infrared reflectance spectroscopy. (9), 642-662.

Roy, E., Mahieu, S., Surault, F., Combes, D., Louarn, G., Frak, E., & Ghesquière, M. (2021). Using UAV-borne imagery for plant height measurements of perennial forage species by photogrammetry. *Sensing–New Insights into Grassland Science and Practice*, 68.

Samac, D. A., Jung, H. J. G., & Lamb, J. F. S. (2006). Alcoholic fuels.

Schaefer, M. T., & Lamb, D. W. (2016). A combination of plant NDVI and LiDAR measurements improve the estimation of pasture biomass in tall fescue (Festuca arundinacea var. Fletcher). Remote Sensing, 8(2), 109.

Sheffield, S. T. (2021). Assessing the Use of LiDAR and UAV Technology for Monitoring Growing Alfalfa.

Sheffield, S. T., Dvorak, J., Smith, B., Arnold, C., & Minch, C. (2021). Using LiDAR to measure alfalfa canopy height. *Transactions of the ASABE*, *64*(6), 1755-1761.

Singh, J., Koc, A. B., & Aguerre, M. J. (2023). Aboveground Biomass Estimation of Tall Fescue using Aerial and Ground-based Systems. In *2023 ASABE Annual International Meeting*(p. 1). American Society of Agricultural and Biological Engineers

Soil Survey Staff, Natural Resources Conservation Service and United States Department of Agriculture Web soil survey. Available at: https://websoilsurvey.sc. egov.usda.gov/App/WebSoilSurvey.aspx

Surault, F., Roy, E., Mahieu, S., Combes, D., Ghesquière, M., & Julier, B. (2021). UAV to measure canopy height and plot biomass in a lucerne variety trial. *Sensing–New Insights into Grassland Science and Practice*, 65.

Tang, Z., Parajuli, A., Chen, C. J., Hu, Y., Revolinski, S., Medina, C. A., ... & Yu, L. X. (2021). Validation of UAV-based alfalfa biomass predictability using photogrammetry with fully automatic plot segmentation. Scientific Reports, 11(1), 3336.

Thorp, K. R., Thompson, A. L., Harders, S. J., French, A. N., & Ward, R. W. (2018). High-throughput phenotyping of crop water use efficiency via multispectral drone imagery and a daily soil water balance model. *Remote Sensing*, *10*(11), 1682.

Tucker, C. J. (1979). Red and photographic infrared linear combinations for monitoring vegetation. *Remote sensing of Environment*, *8*(2), 127-150.

USDA (2025). Quick Stats 2.0. National Agricultural Statistics Service. https://quickstats.nass.usda.gov/

Viscarra Rossel, R. A., Taylor, H. J., & McBratney, A. B. (2007). Multivariate calibration of hyperspectral γ-ray energy spectra for proximal soil sensing. *European Journal of Soil Science*, *58*(1), 343-353.

Volpato, L., Pinto, F., González-Pérez, L., Thompson, I. G., Borém, A., Reynolds, M., ... & Rodrigues Jr, F. A. (2021). High throughput field phenotyping for plant height using UAV-based RGB imagery in wheat breeding lines: Feasibility and validation. *Frontiers in Plant Science*, *12*, 591587.

Wang, Z. Y., & Brummer, E. C. (2012). Is genetic engineering ever going to take off in forage, turf and bioenergy crop breeding?. *Annals of Botany*, *110*(6), 1317-1325.

Watanabe, K., Guo, W., Arai, K., Takanashi, H., Kajiya-Kanegae, H., Kobayashi, M., ... & Iwata, H. (2017). High-throughput phenotyping of sorghum plant height using an unmanned aerial vehicle and its application to genomic prediction modeling. *Frontiers in plant science*, *8*, 421.

Weiyuan, H., Ziqiu, L., Xiangqian, F., Jinhua, Q., Aidong, W., Shichao, J., ... & Song, C. (2024). Estimating key phenological dates of multiple rice accessions using unmanned aerial vehicle-based plant height dynamics for breeding. *Rice Science*, *31*(5), 617-628.

Wijesingha, J., Astor, T., Schulze-Brüninghoff, D., Wengert, M., & Wachendorf, M. (2020). Predicting forage quality of grasslands using UAV-borne imaging spectroscopy. *Remote Sensing*, *12*(1), 126.

Woebbecke, D. M., Meyer, G. E., Von Bargen, K., & Mortensen, D. A. (1995). Color indices for weed identification under various soil, residue, and lighting conditions. *Transactions of the ASAE*, *38*(1), 259-269.

Zwick, M., Cardoso, J. A., Gutiérrez-Zapata, D. M., Cerón-Muñoz, M., Gutiérrez, J. F., Raab, C., ... & Barrett, B. (2024). Pixels to pasture: Using machine learning and multispectral remote sensing to predict biomass and nutrient quality in tropical grasslands. *Remote Sensing Applications: Society and Environment*, *36*, 101282.

APPENDICES

Appendix A. Average yield (kg/ha) of each alfalfa entry per harvest date.

Entry ID	Entry name	Yield 1 (kg/ha)	Yield 2 (kg/ha)	Yield 3 (kg/ha)
1	GAMS1403FSH	5507.60	1370.67	2938.79
2	GAMS1405FSH	5459.15	1403.56	2848.10
3	GAMS1406FSH	6846.15	1300.55	2847.21
4	GAMS1433	5325.30	1648.85	2786.82
5	GAMS1434	7440.43	1275.31	2974.26
6	GAMS1406A35	6925.82	1155.26	2943.14
7	GAMS1438	6783.67	1322.71	2868.39
8	GAMS1439	7239.93	1140.12	3140.15
9	GAMS1548	7085.71	1071.69	2845.44
10	GAMS19100	7546.17	1400.80	3272.40
11	Bulldog 505	7297.74	1357.32	2861.31
12	Bulldog805	6552.15	1235.66	2575.82
13	GAMS1402FSH	5243.58	1379.13	2853.42
14	GAMS1401A35	6780.14	1238.63	3056.68
15	Alfagraze 600 RR	6381.00	1492.64	2718.53
16	GAMS1404FSH	5356.79	1332.74	2911.48
17	GAMS1436	5556.99	1356.08	2889.67
Total		6431.08	1322.45	2901.86

Appendix B. Figure showing proportions of yield (kg/ha) of each alfalfa entry per harvest date.

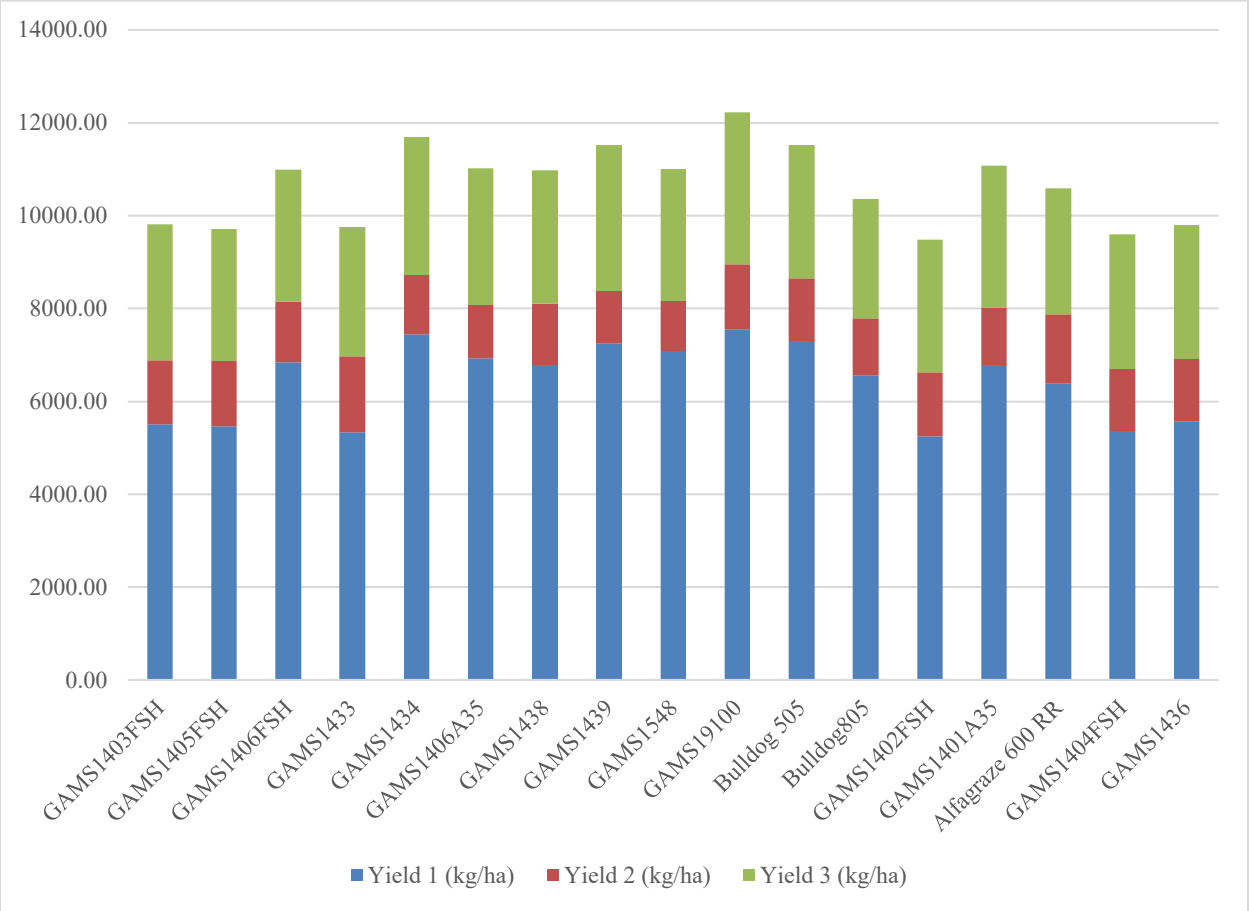

Appendix C. Random Forest model performance for predicting alfalfa yield.

Data Type	Test set metrics	Observed vs. Predicted Plot	Variable Importance
RGB	RMSE = 942.6463757 R2 = 0.8218536	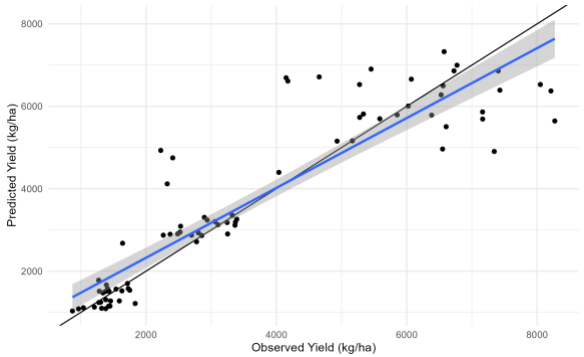	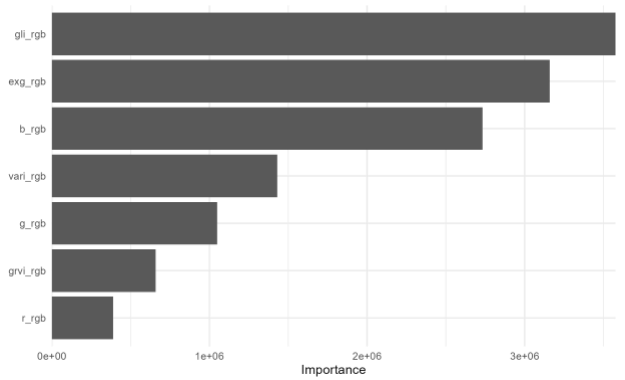
RGB + PH	RMSE = 927.1296199 R2 = 0.8266364	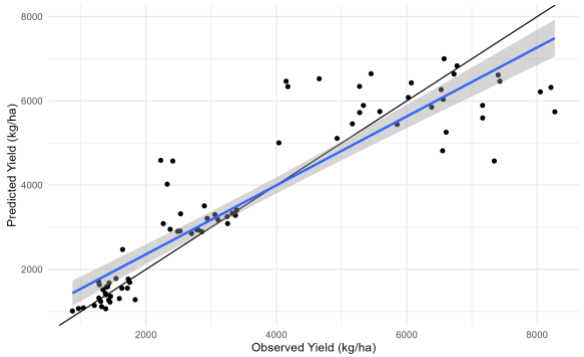	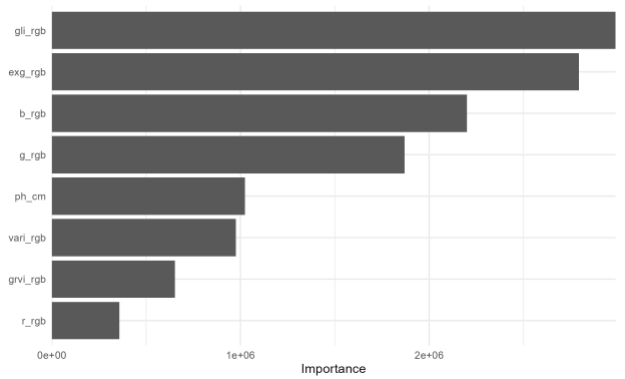

XS	RMSE = 784.8956648 R2 = 0.8798407	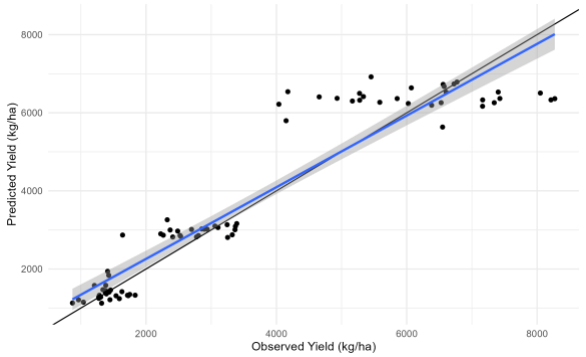	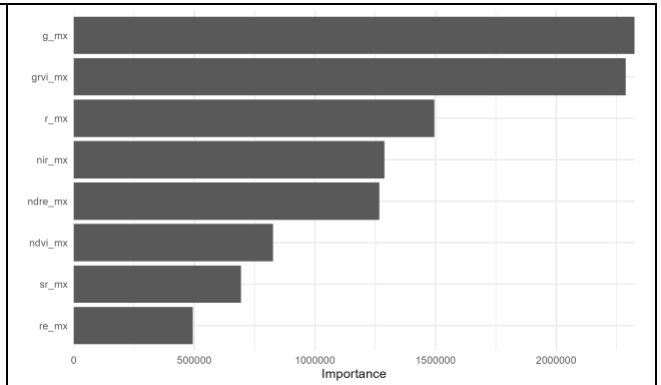
XS + PH	RMSE = 752.1682940 R2 =0.8998878	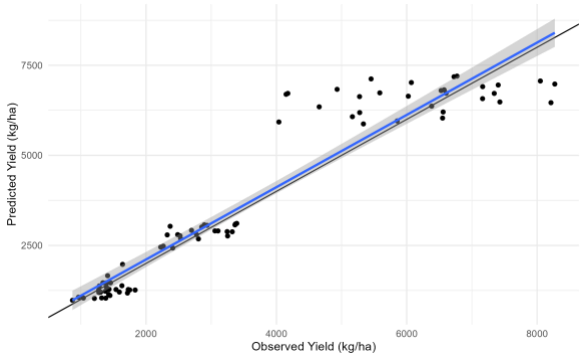	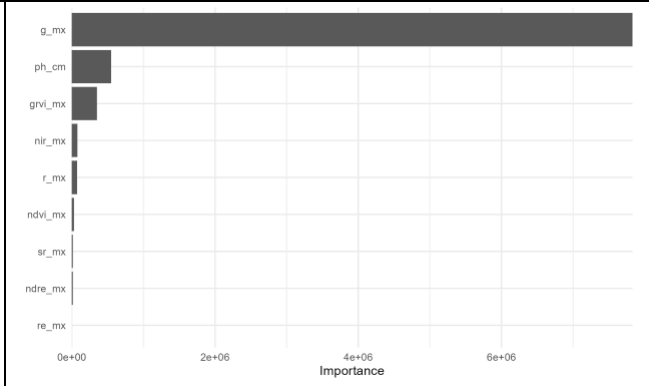
RGB + XS	RMSE = 799.8194512 R2 = 0.8784832	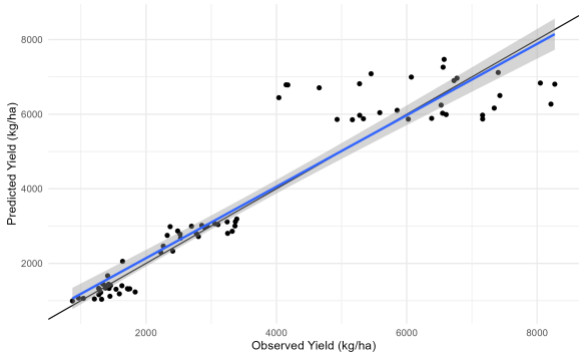	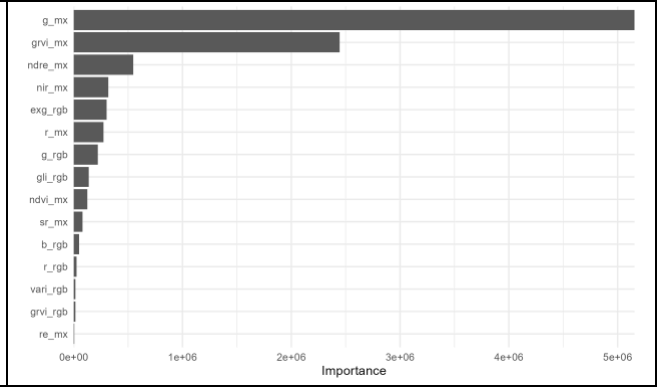

RGB+XS +PH	RMSE = 774.2118145 R2 = 0.8857663	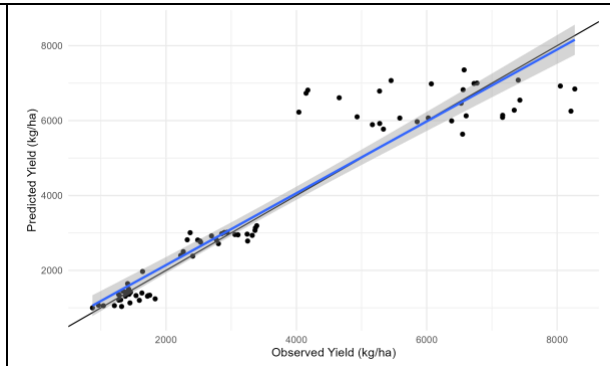	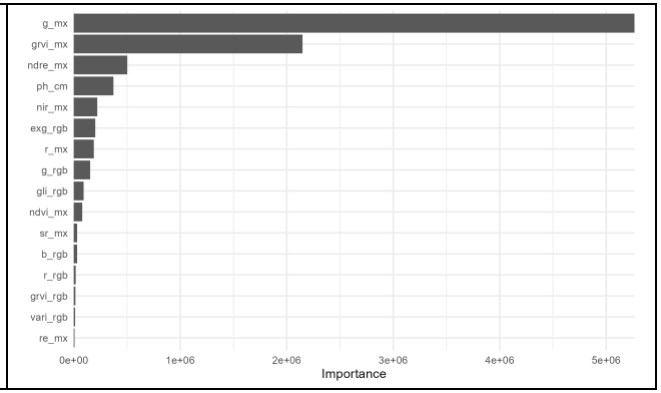

Appendix D. Extreme gradient boosting model performance in predicting alfalfa yield.

Data Type	Test set metrics	Observed vs. Predicted Plot	Variable Importance
RGB	RMSE = 1086.290137 R2 = 0.7767565	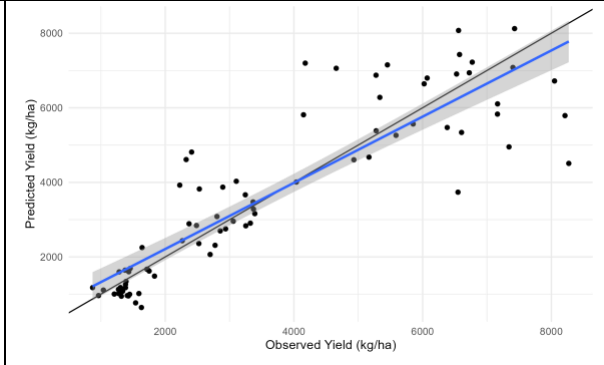	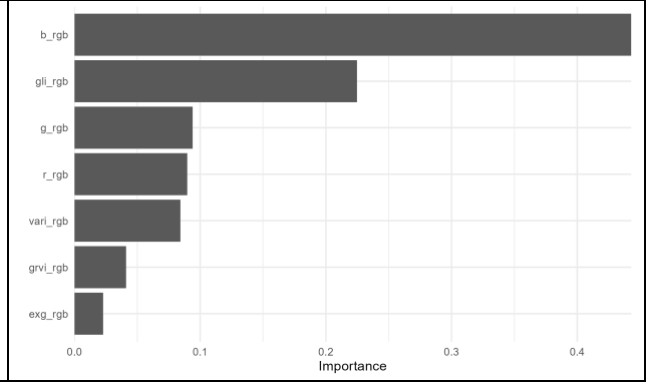

RGB + PH	RMSE = 1059.5573543 R2 = 0.7901803	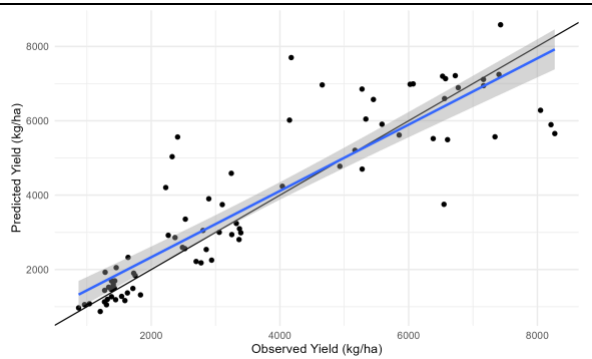	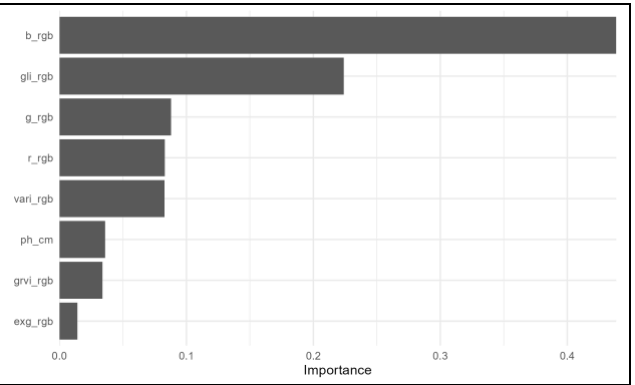
XS	RMSE = 810.9854 R2 = 0.8807441	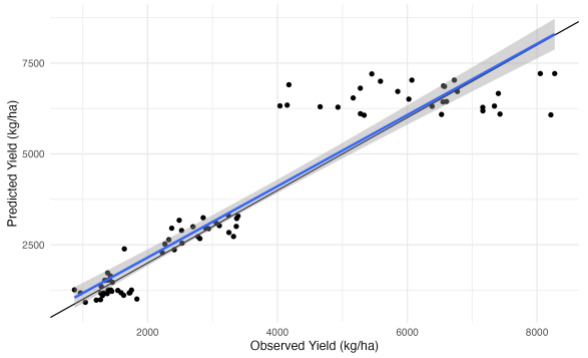	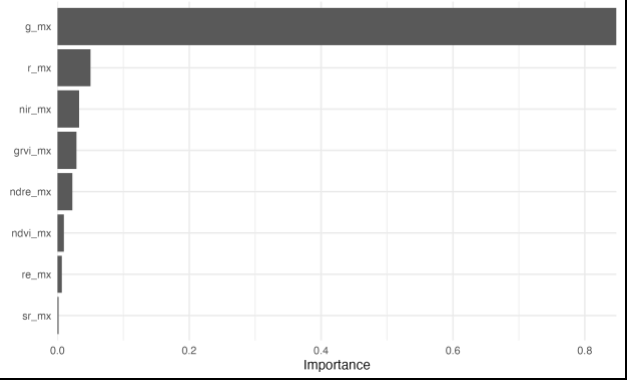
XS + PH	RMSE = 775.5307 R2 = 0.8898278	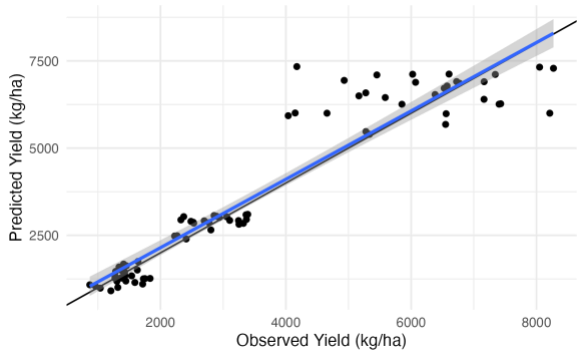	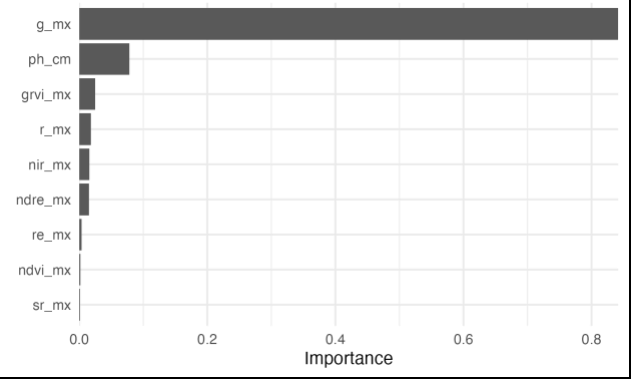

RGB + XS	RMSE = 891.6274 R2 = 0.8583248	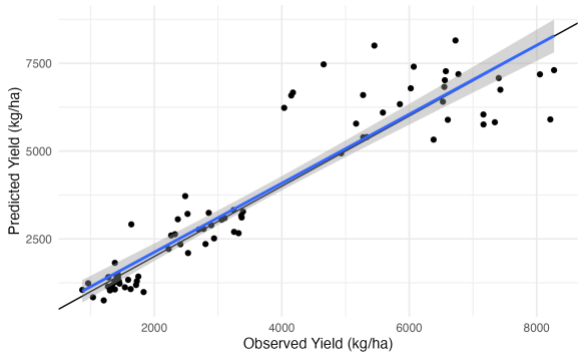	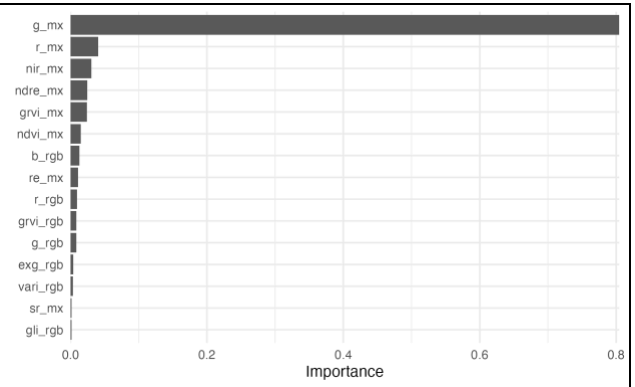
RGB+XS +PH	RMSE = 768.2015 R2 = 0.8899896	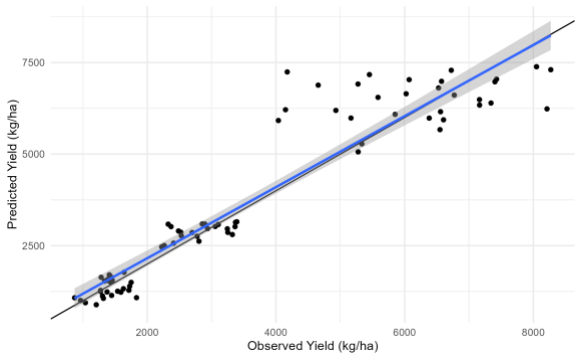	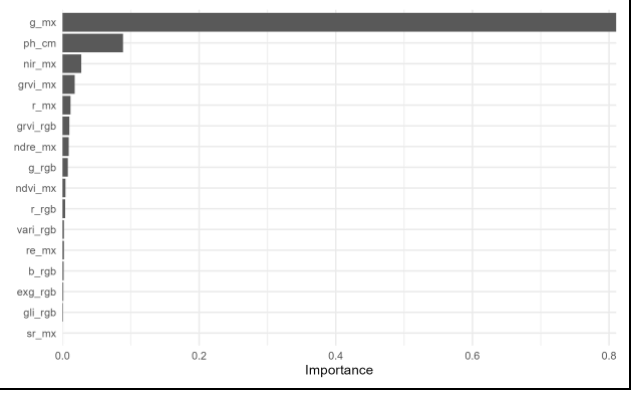

Appendix E. Random Forest model performance for predicting alfalfa forage yield.

	Test set metrics	Observed vs. Predicted Plot	Variable Importance
ADF_RGB	RMSE = 1.5370237 R2 = 0.8362107	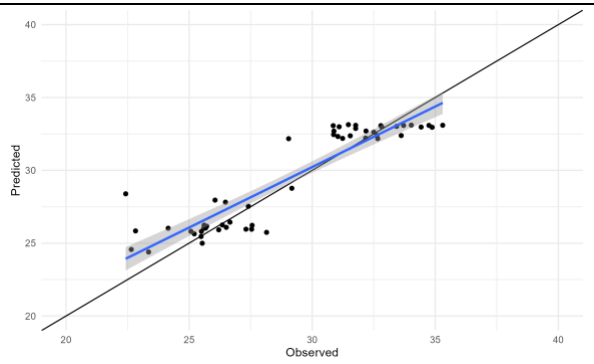	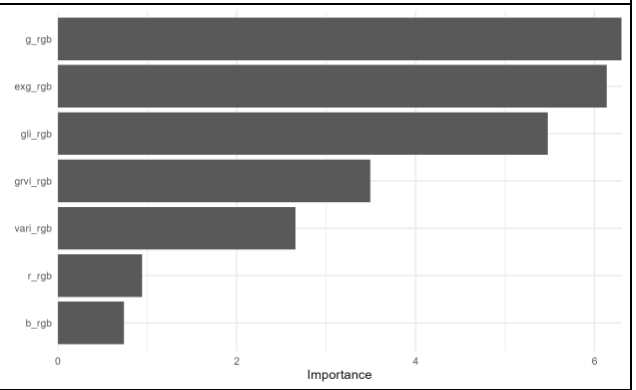
NDF_RGB	RMSE = 1.9361835 R2 = 0.8552206	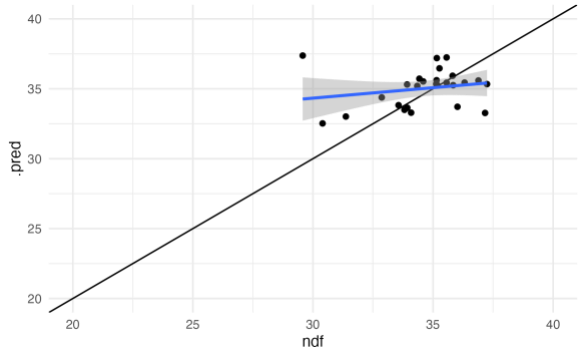	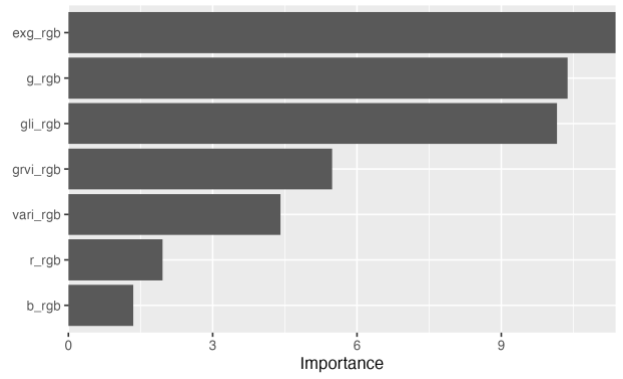

CP_RGB	RMSE = 1.3634690 R2 = 0.5141593	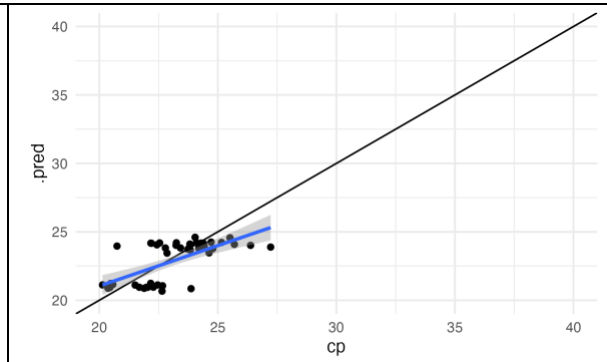	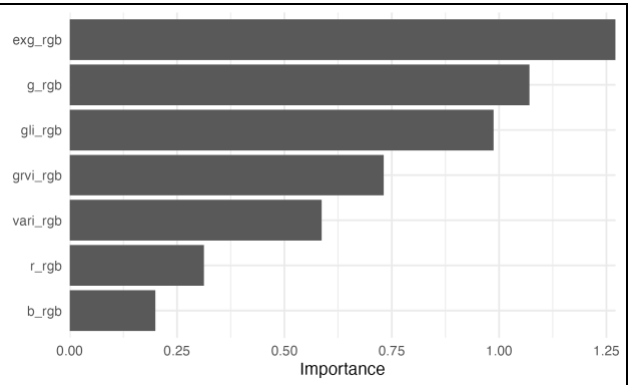
ADF_XS	RMSE = 1.8413679 R2 = 0.7543507	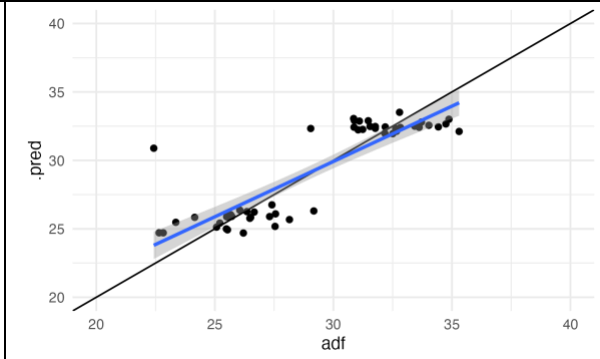	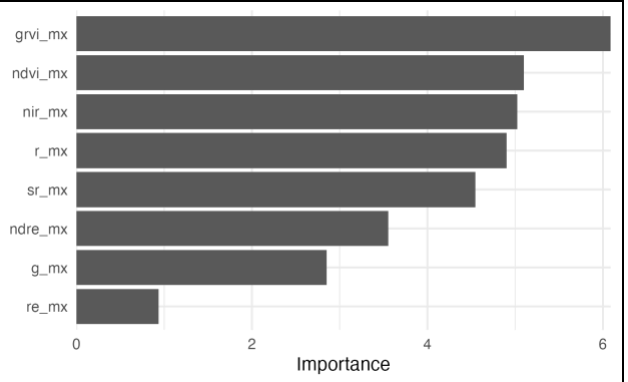
NDF_XS	RMSE = 2.3375407 R2 = 0.7866238	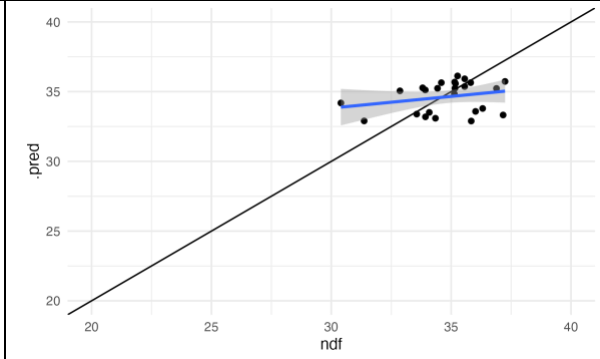	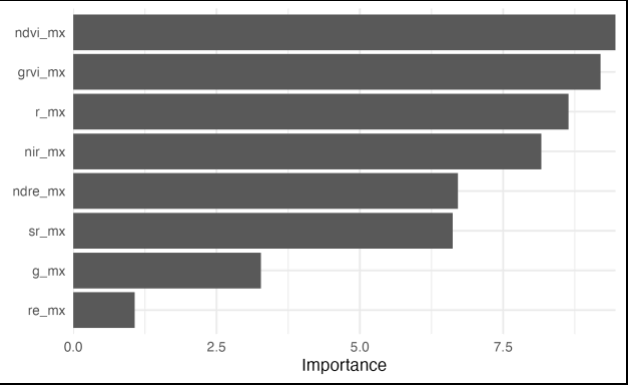

CP_XS	RMSE = 1.2571933 R2 = 0.5863815	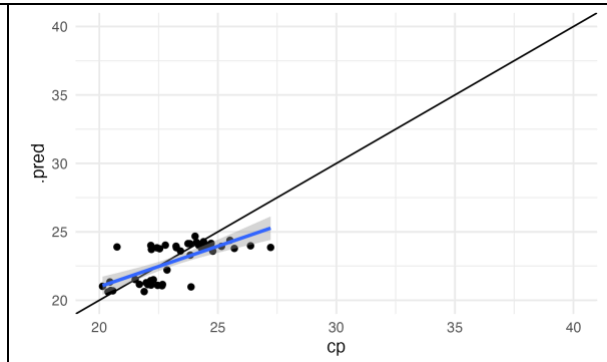	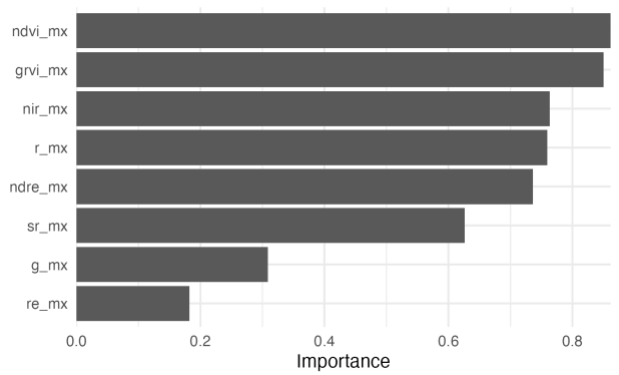
ADF_dualXS	RMSE = 1.2975310 R2 = 0.8782382	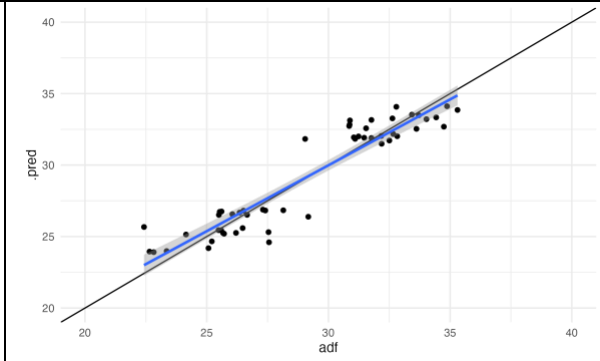	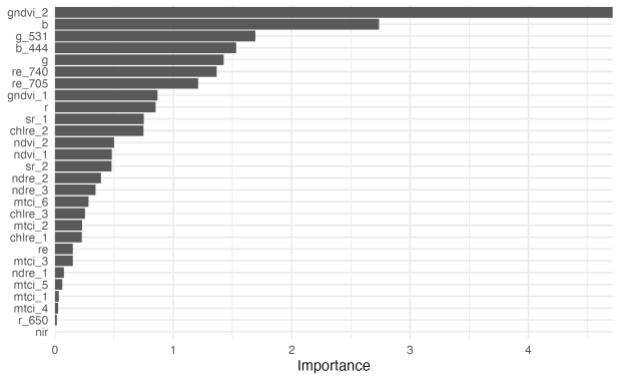
NDF_dualXS	RMSE = 1.8611533 R2 = 0.8649879	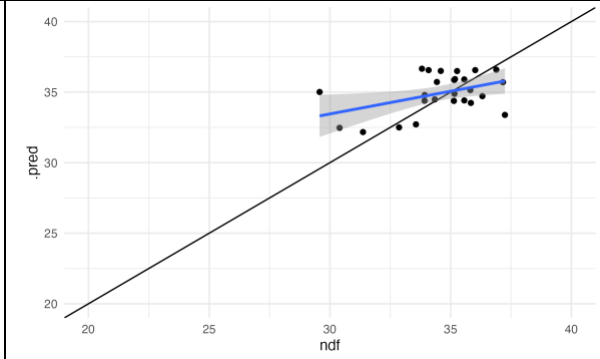	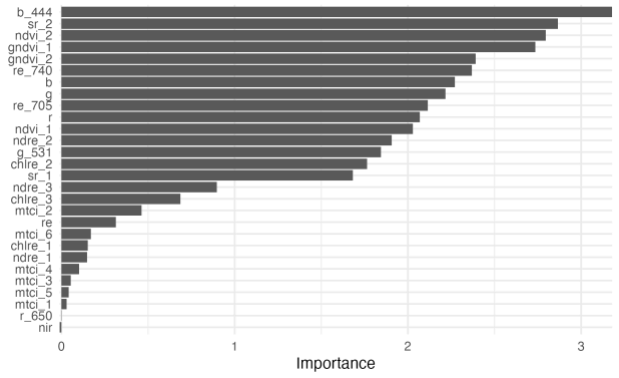

CP_dualXS	RMSE = 1.2548211 R2 = 0.5905924	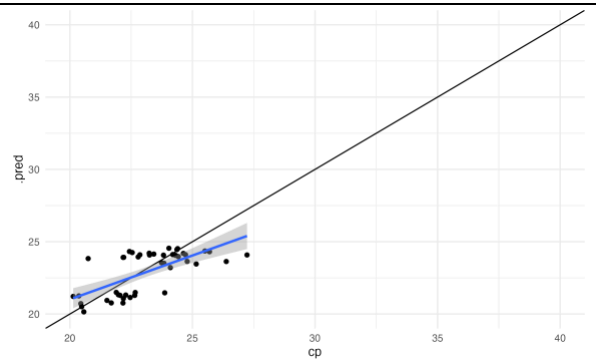	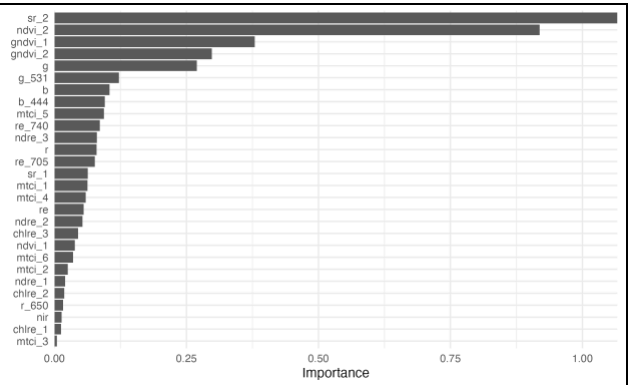

Appendix F. Extreme gradient boosting model performance in predicting alfalfa forage quality.

	Test set metrics	Observed vs. Predicted Plot	Variable Importance
ADF_RGB	RMSE = 1.5823769 R2 = 0.8315642	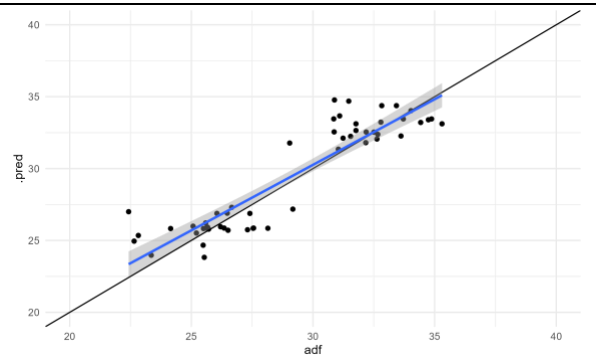	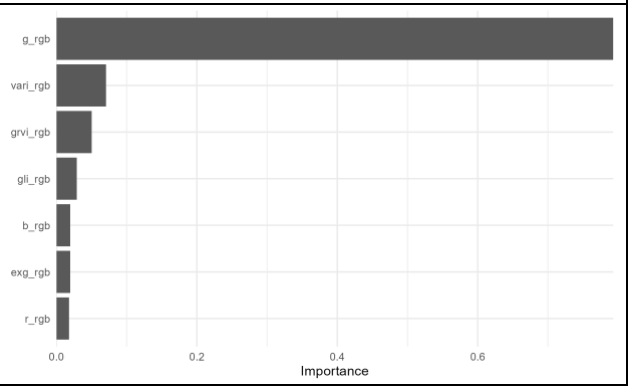

NDF_RGB	RMSE = 2.2777105 R2 = 0.8038429	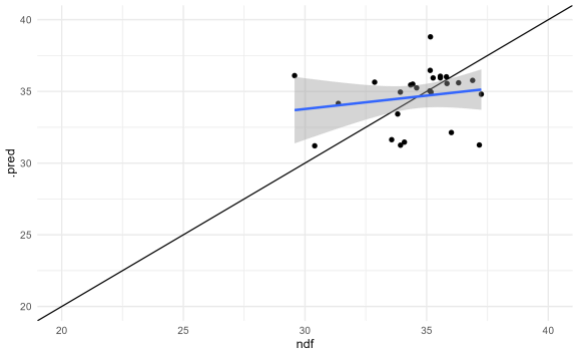	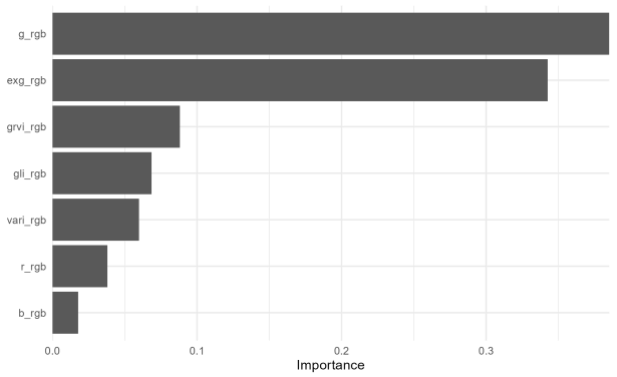
CP_RGB	RMSE = 1.4370495 R2 = 0.4994009	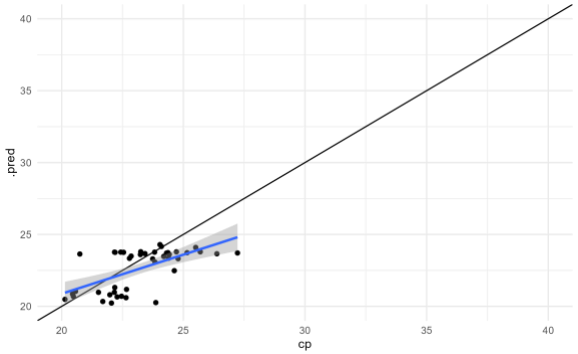	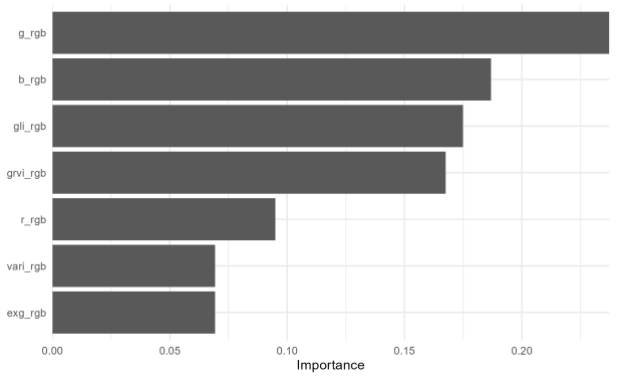
ADF_XS	RMSE = 2.1274996 R2 = 0.6754816	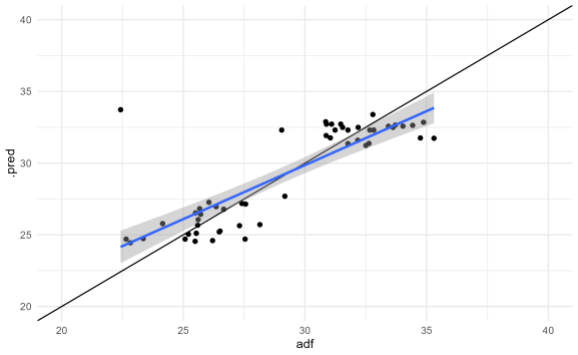	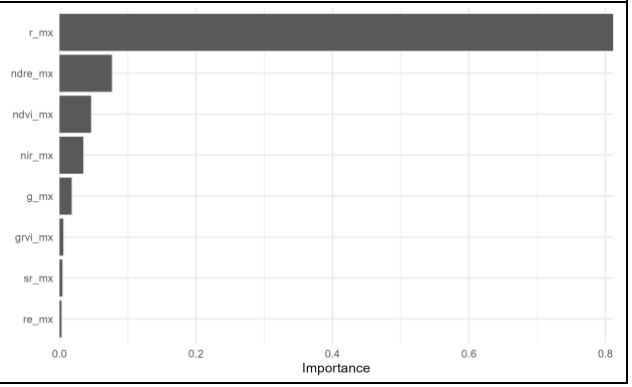

NDF_XS	RMSE = 2.8570067 R2 = 0.7051037	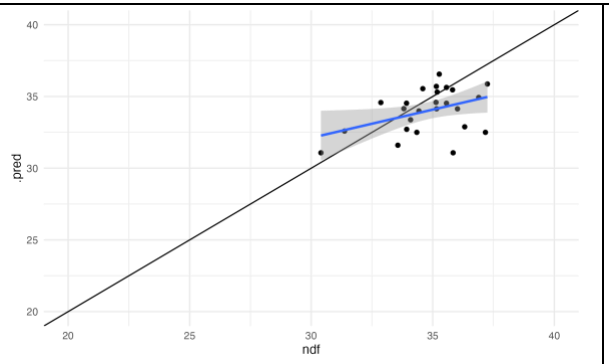	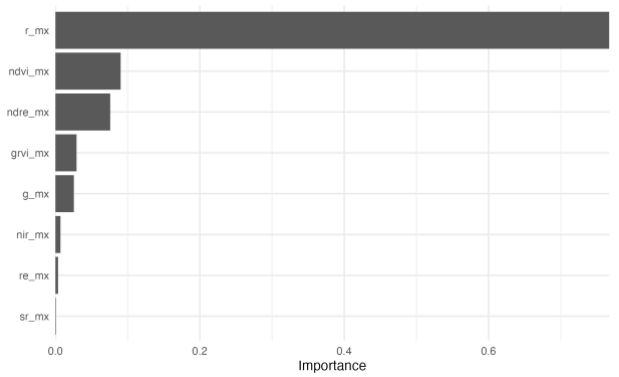
CP_XS	RMSE = 1.276423 R2 = 0.572248	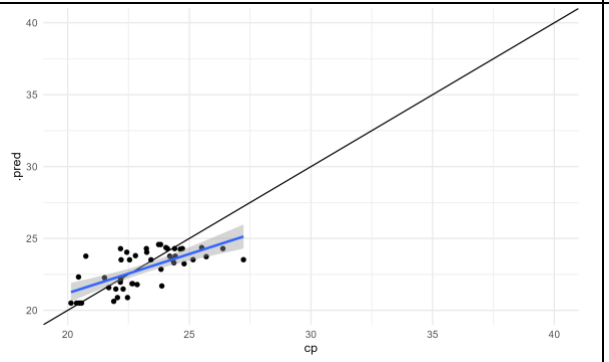	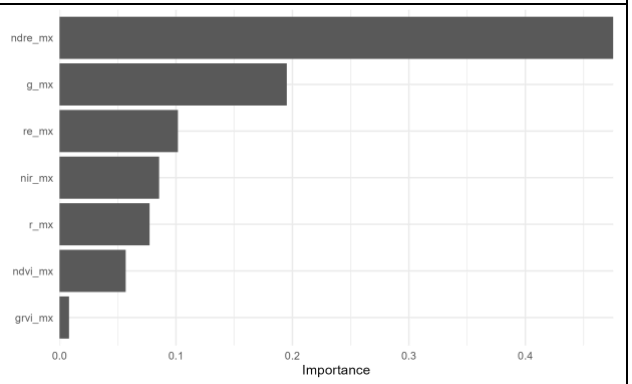
ADF_dualXS	RMSE = 1.4140109 R2 = 0.8612023	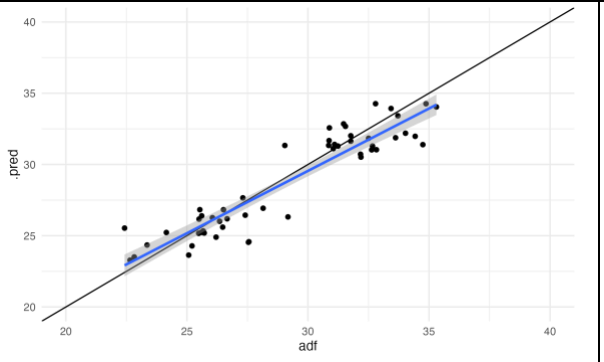	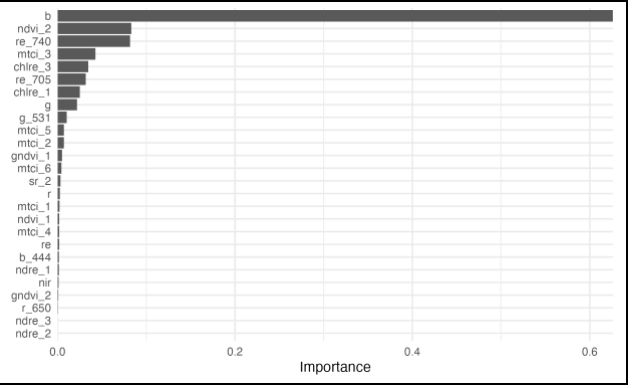

NDF_dualXS	RMSE = 1.9599187 R2 = 0.8513521	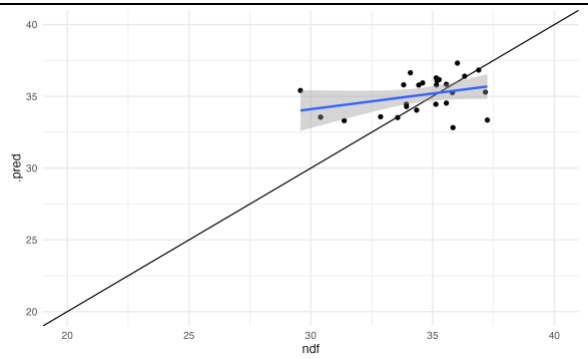	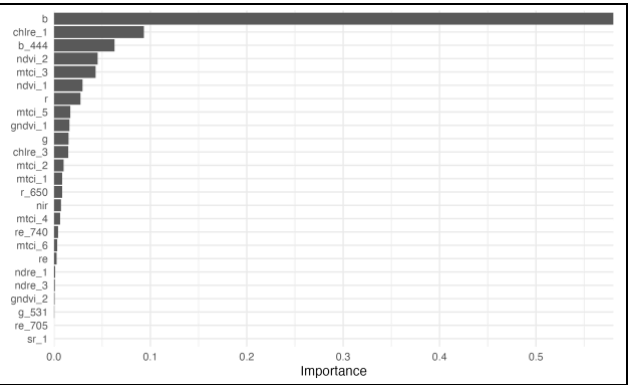
CP_dualXS	RMSE = 1.2779240 R2 = 0.5730066